

NASA Contractor Report 189594

P-165

MOM3D Method of Moments Code
Theory Manual

John F. Shaeffer

DENMAR, Inc.
Marietta, Georgia

LOCKHEED ADVANCED DEVELOPMENT COMPANY
Sunland, California

Contract NAS1-18603
March 1992



Langley Research Center
Hampton, Virginia 23665-5225

Review for general release March 31, 1994

(NASA-CR-189594) MOM3D METHOD OF
MOMENTS CODE THEORY MANUAL Final
Report (DENMAR) 165 p

N94-32897

Unclass

NASA Contractor Report 189594

**MOM3D Method of Moments Code
Theory Manual**

John F. Shaeffer

**DENMAR, Inc.
Marietta, Georgia**

**LOCKHEED ADVANCED DEVELOPMENT COMPANY
Sunland, California**

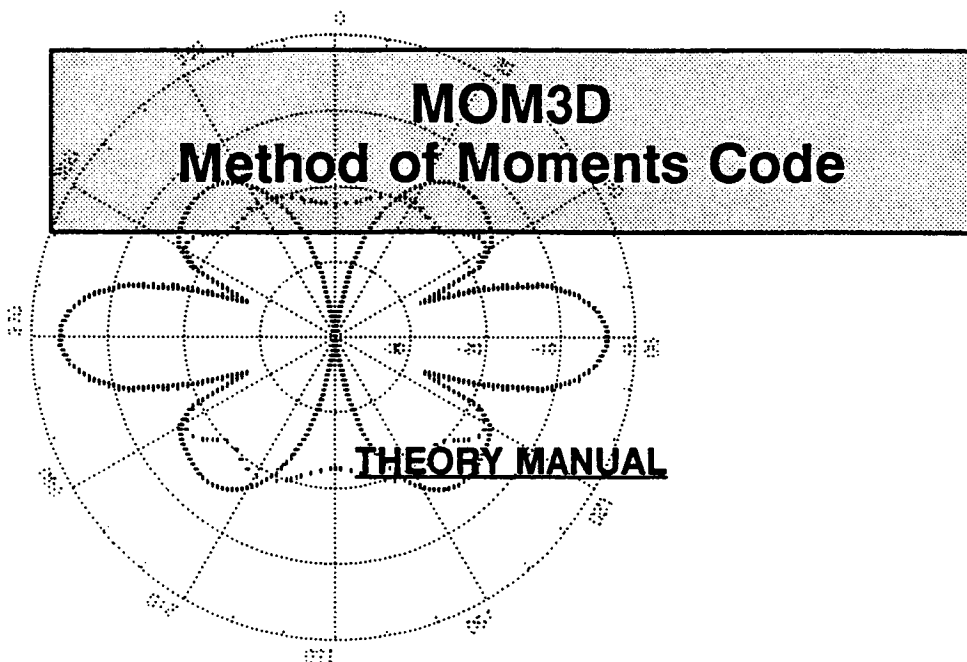
**Contract NAS1-18603
March 1992**



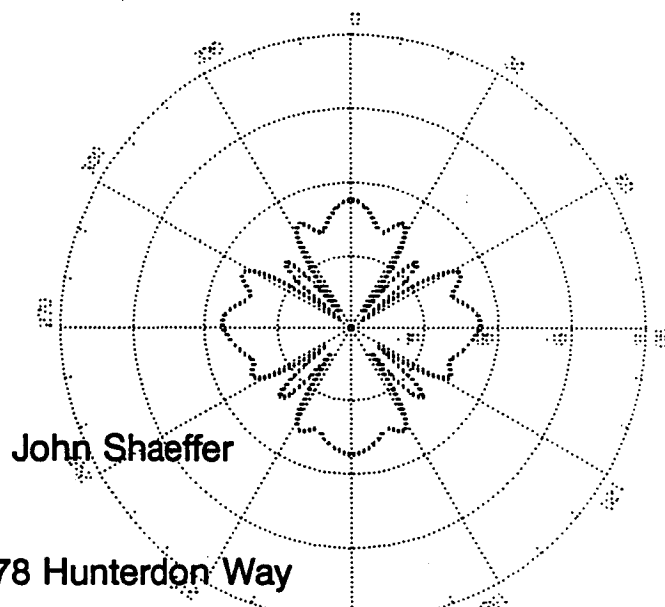
**National Aeronautics and
Space Administration**

**Langley Research Center
Hampton, Virginia 23665-5225**

Review for general release March 31, 1994



March 1992



John Shaeffer

3278 Hunterdon Way

Marietta, Georgia 30067

(404) 952-3678

PREFACE

This report summarizes the theory for a three dimensional method of moments triangular patch code for RCS and antenna analysis. Diagnostic capability includes scattering image analysis, current display, and near field computation. The algorithm was designed to be cpu time and memory efficient. Individual parts of this work have been documented previously as separate tasks. MOM3D now contains most of the original goals, thus it is time to bring together the appropriate theory in one report.

The FORTRAN code itself is described elsewhere. Computer codes are never static. They are continually changed by interested users. User manuals become dynamic documents compared to theory.

This work is in support of the Advanced Aircraft Branch of the NASA Langley Research Center. Mr. Noel Talcott is the NASA point of contact.

This report prepared by John Shaeffer, Denmar, Inc., Atlanta Office, 3278 Hunterdon Way, Marietta, Georgia 30067, (404) 952-3678.

TABLE OF CONTENTS

Section	Page
OVERVIEW and SUMMARY	1-1
What Is MOM3D ?	1-1
What Does MOM3D Compute ?	1-1
Why Is MOM3D Different ?	1-2
 GENERAL METHOD OF MOMENTS THEORY	 2-1
Which Integral Equation To Use?	2-1
Boundary Conditions	2-4
Matrix Solution of the Integral Equation	2-5
Voltage Vector	2-8
Matrix Elements	2-8
Scattered Field	2-9
Computer Resource Considerations	2-11
 MOM3D SURFACE PATCH FORMULATION	 3-1
Current Couple	3-2
Couple Basis Function Average (Moment)	3-4
Matrix Elements	3-4
Green's Function Computation and Approximations	3-7
Centroid Approximation	3-8
Self Term Approximation	3-9
Voltage Vector	3-10
Scattered Field	3-12
 GEOMETRY SYMMETRY CONSIDERATIONS	 4-1
Mirror Geometry Symmetry	4-2
System Matrix	4-2

Matrix element relationships	4-3
BISTATIC IMAGE ANALYSIS USING k SPACE CONCEPTS	5-1
Experimental Image Concepts	5-2
Bistatic k Space Image Background	5-3
Bistatic Image Theory	5-6
Approach	5-7
Cross Range Direction Rotation	5-10
Rotation Center	5-10
NEAR FIELD COMPUTATIONS	6-1
Scattered Electric Fields	6-2
Scattered Field Expression for MOM3D	6-5
Every Thing You Wanted to Know About Complex Vectors But Were Afraid to Ask	6-7
Formulation When the Field Point is Near Surface	6-11
MONOSTATIC and BISTATIC RADAR CROSS SECTION	7-1
Polarization Scattering Matrix	7-1
Radar Cross Section Definition	7-2
Monostatic Case	7-4
Bistatic Case	7-5
CURRENT COMPUTATION	8-1
Couple Spatial Averaged Current	8-1
Triangle Currents	8-2
Time Varying Vectors and Surface Current Animation	8-3
Time Average Currents	8-3
ANTENNA FORMULATION	9-1
Voltage Vector	9-1

Antenna Gain	9-3
Input Impedance and Admittance	9-5
RESISTIVE BOUNDARY CONDITIONS	10-1
Resistive Sheet Concepts	10-1
Dielectric Thin Sheet Impedance Concepts	10-3
Resistive Boundary Conditions	10-4
Impedance Boundary Condition Theory	10-6
Approximate Impedance Boundary Condition Theory	10-10
Summary	10-11
SYSTEM MATRIX SOLUTION	11-1
System Matrix	11-1
Matrix Condition Number	11-3
MODELING ISSUES	12-1
Surface Current Characteristics	12-1
Triangle Basis Function Considerations	12-2
EXAMPLE RESULTS	13-1
Coordinate System	13-1
Model Geometry	13-1
Backscatter RCS	13-2
Bistatic RCS	13-3
Current Computation	13-5
Downrange Images	13-6
Cross Range Images	13-7
Near Field Examples	13-10
E Total Field	13-10
E Scattered Field	13-11
Antenna Example	13-12

REFERENCES	R-1
APPENDIX A	A-1
NUMERICAL and ANALYTICAL MATRIX ELEMENT INTEGRATION	
Overview	A-1
Numerical Triangle Integration Formulas	A-4
Analytical Point to Plane Line Integral Approach	A-6
Singularity Removal and 1/R Formulas	A-7
Combined Numerical and Analytical Result	A-13
APPENDIX A REFERENCES	A-15

LIST OF FIGURES

Figure No.	Caption	Page
Figure 2-1	Far field distance approximation geometry	2-10
Figure 3-1	Arbitrary surface modeled by triangular patches	3-1
Figure 3-2	Triangle couple basis function	3-2
Figure 3-3	Net couple moment (current) is from triangle centroid to centroid	3-4
Figure 3-4	Matrix element interaction is between pairs of triangles (four terms)	3-5
Figure 3-5	Distance between triangles using centroid	3-8
Figure 3-6	Polarization unit vectors and incident field unit vector	3-13
Figure 4-1	Geometry example that has symmetry about the $X = 0$ (Y-Z) plane. . .	4-2
Figure 4-2	Reflected right couple has opposite direction so that $Z_{LS} = Z_{RS}$ and $Z_{LV} = -Z_{RV}$	4-3
Figure 4-5	Bistatic image k space	5-4
Figure 8-1	Triangle current can be considered as the sum of couple currents	8-2
Figure 10-1	Ohms per square concept	10-2
Figure 10-2	Ohms per square (OPS)	10-3
Figure 10-3	Dallenbach layer	10-7
Figure 12-1	Basis function currents are from triangle centroid to centroid (zig-zag)	12-2
Figure 12-2	Geometry symmetry alters basis vector orientation	12-3
Figure 13-1	MOM3D coordinate system is the standard spherical system	13-1
Figure 13-2	PLT-55.GEO Mesh Model, Symmetric about $Y = 0$ (X-Z) plane. . .	13-2
Figure 13-3	Backscatter RCS	13-3
Figure 13-4	Bistatic RCS	13-4
Figure 13-5	Current examples	13-5
Figure 13-6	Down range image of plate	13-7
Figure 13-7	Two dimensional range / cross range images	13-9
Figure 13-8	Near field computation grid	13-10
Figure 13-9	Total field	13-11

Figure 13-10 Scattered field	13-12
Figure 13-11 Half wave dipole strip antenna geometry	13-12
Figure 13-12 Half wave dipole antenna gain pattern	13-13
Figure A-1 Interaction distance R	A-1
Figure A-2 Matrix elements involve 4 triangle interactions	A-2
Figure A-3 Triangle function evaluation points	A-5
Figure A-4 Coordinate system for 1/R triangle integration	A-8
Figure A-5 Singularity removal depends on projection of field point r_f	A-10

SECTION 1

OVERVIEW and SUMMARY

What Is MOM3D ? : MOM3D is a FORTRAN algorithm that solves Maxwell's equations as expressed via the electric field integral equation for the electromagnetic response of open or closed three dimensional surfaces modeled with triangle patches. Two joined triangles (couples) form the vector current unknowns for the surface. Boundary conditions are for perfectly conducting or resistive surfaces. The impedance matrix represents the fundamental electromagnetic interaction of the body with itself. A variety of electromagnetic analysis options are possible once the impedance matrix is computed.

What Does MOM3D Compute ? : The following analysis options are available once the impedance matrix is computed for each frequency and solved:

- * **Backscatter radar cross section (RCS)** for two orthogonal linear polarizations as a function of user specified azimuth and / or elevation angles;
- * **Bistatic radar cross section** for two orthogonal linear polarization for user specified excitation angle and polarization. Bistatic RCS is computed over user specified azimuth and / or elevation angles;
- * **Antenna pattern prediction** for user specified body voltage excitation ports. Isotropic gain is computed for user specified polarization and azimuth and / or elevation angles along with antenna input impedance;

- * **RCS image prediction** shows RCS scattering center locations (mechanisms) for user specified plane wave excitation of the body (polarization and azimuth and elevation). Either down range or 2D range / cross range images may be specified for user specified spatial extent and resolution to $\lambda/2$;
- * **Surface currents** excited on the body as induced by specified plane wave excitation (polarization and azimuth and elevation);
- * **Near field computation** for the electric field on or near the body as produced by user specified incident plane wave (polarization and azimuth and elevation).

MOM3D allows users the ability not only to compute RCS or antenna patterns, but also has diagnostic capability to aide in understanding electromagnetic responses.

Why Is MOM3D Different ? : MOM3D is different from other surface patch codes based on the same basis expansion functions in the following respects:

- * A wider choice of analysis options: Backscatter RCS, Bistatic RCS, and Antenna gain;
- * Diagnostic capability for: 1) Image analysis in one or two dimensions, 2) Surface current display, and 3) Near surface electric fields;
- * Efficient formulation to reduce required computer resources. This means that a given set of computation resources may be applied to electrically larger bodies. Explicitly: 1) A symmetric matrix formulation is used to reduce the matrix solve time by $1/2$. This varies as N^3 where N is the number of unknowns and

thus represents a large part of the solution time; 2) The symmetric matrix formulation requires 1/2 less CPU time and memory to compute and store the matrix elements since only the upper half of the matrix is used. Memory requirements vary as N^2 and become the limiting factor for electrical problem size; 3) A user option for computing geometrically symmetric bodies. This reduces the matrix solution time by another factor of *four* and matrix memory storage by a factor of *two*; and 4) A centroid approach for computing matrix interaction elements for all triangle to triangle distances greater than ten triangle dimensions. For closer spacing the user has three options for matrix element integration: two numerical / analytical approaches or the centroid approach.

The major efficiency for applying MOM3D to electrically large bodies is for computing symmetric bodies. Then, compared to the patch code described in [1], MOM3D represents a factor of *EIGHT* less in matrix solution time and a factor of *FOUR* less in required memory to store matrix elements. Solution time and memory are always the limiting parameters for electromagnetic analysis codes. MOM3D is designed to use these resources in an efficient manner allowing larger bodies to be analyzed.

This report discusses the theory behind the analysis as the reader can figure out by looking at the Table of Contents.

SECTION 2

GENERAL METHOD OF MOMENTS THEORY

This section discusses the fundamental theory for solving Maxwell's equations as expressed in the electric field integral equation. This theory may then applied to any geometry, e.g., wires, 2D strips, bodies of revolution, and of course 3D triangle surface patches. References [2] through [7] contain more detail. The approach followed here is due to Mautz and Harrington [5] since they derive a very general purpose expression for matrix elements which then may be applied to many types of geometries and for many variations of basis expansion and weight functions.

Which Integral Equation To Use? Maxwell's four differential equations relate magnetic and electric fields to their electric and magnetic sources of currents and charges. These differential equations may be transformed to two integral equations for scattered electric and magnetic fields. They relate the scattered field to surface or volumetric source currents and charges. Green's vector theorem is used to derive the integral form of Maxwell's equations [7]. An alternative approach is to consider the scattered fields as derived from vector and scalar potentials.

The usual fashion for expressing fields when dealing with scattering problems is to express the total field, for which boundary conditions apply, as the sum of an incident field, which is what exists at a given location independent of the scattering body, and a scattered field that is caused by the currents and charges on the scattering body. Thus

$$\begin{aligned}\vec{E}^{Total} &= \vec{E}^{inc} + \vec{E}^{scat} \\ \vec{H}^{Total} &= \vec{H}^{inc} + \vec{H}^{scat}\end{aligned}\tag{2-1}$$

The incident fields are usually plane waves as specified by propagation direction, wavelength, and polarization. Spherical or cylindrical wave sources could just as easily be used. \mathbf{E}^{inc} is the mathematical approach of specifying the field due to outside sources. We do not know the source current distribution, just the resulting field.

The integral form of Maxwell's equations, called the Stratton Chu equations, use the surface parallel and perpendicular field components as source terms. These are defined as surface magnetic and electric currents and charges. The total surface fields are defined in terms of electric and magnetic surface currents and charge densities. If \hat{n} is the unit vector perpendicular to the surface, then:

$$\begin{aligned}\vec{J} &= \vec{H}_\parallel = \hat{n} \times \vec{H}; & \rho^e &= E_\perp = \hat{n} \cdot \vec{E} \\ \vec{M} &= \vec{E}_\parallel = \vec{E} \times \hat{n}; & \rho^m &= H_\perp = \hat{n} \cdot \vec{H}\end{aligned}\tag{2-2}$$

where J and M are the electric and magnetic currents while ρ is the corresponding charge density. Note that electric currents are proportional to tangential magnetic fields while magnetic currents are proportional to tangential electric fields. The field quantities are the total fields at the surface.

The Electric Field Integral Equation (EFIE) is the Stratton Chu integral equation for the scattered electric field:

$$\vec{E}^{\text{scat}}(\vec{r}) = - \int [j\omega \mu \vec{J}g - \vec{M} \times \nabla g - \frac{\rho^e}{\epsilon} \nabla g] dS\tag{2-3}$$

The source terms are the electric and magnetic currents and electric charge density.

The free space Green's function g relates source quantities to field quantities via phase (time delay) and $1/R$ spatial decay. It is

$$g = \frac{e^{-jk\cdot R}}{4\pi R} \quad (2-4)$$

where the wave number vector \mathbf{k} points from source to field points and has the magnitude $k = 2\pi/\lambda$. The distance R is from the source point to field point location

$$R = |\vec{r} - \vec{r}'| = \sqrt{(x-x')^2 + (y-y')^2 + (z-z')^2} \quad (2-5)$$

The Magnetic Field Integral Equation (MFIE) is the Stratton Chu integral equation for the scattered magnetic field:

$$\vec{H}^{scat}(\vec{r}_f) = \int [-j\omega \epsilon \vec{M} g + \vec{J} \times \nabla g + \frac{\rho^m}{\mu} \nabla g] dS \quad (2-6)$$

The source terms are the magnetic and electric currents and magnetic charge density ρ^m .

For perfect electrically conducting bodies the magnetic currents are identically zero since there can be no tangential electric field. Then either the EFIE or MFIE may be used. Typically the EFIE approach is used for open and / or closed surfaces while the MFIE is used only for closed surfaces (due to problems in numerically evaluating the Green's function).

MOM3D uses the EFIE approach with electric current unknowns.

Magnetic currents must be included for the more general case when considering magnetic materials, e.g., radar absorbing material. This doubles the number of unknowns, with matrix element memory increasing by *four* N^2 , and matrix solution time increasing by *eight* N^3 . We also must formulate the system matrix to include the magnetic sources. This requires additional analytical and computation effort.

For Perfect Electric Conductors, PEC, there are no magnetic source currents or charges since the tangential E field is zero. This greatly simplifies the EFIE and MFIE because now we only have to solve for the unknown surface currents J.

The astute reader will ask why we also do not explicitly solve for the charge density. The reason is that continuity relates current to surface charge density, i.e., when current flows into a region the charge density increases while when current flows out of a region the charge density decreases. Mathematically,

$$\nabla \cdot \vec{J} = -\frac{\partial \rho}{\partial t} = -j\omega \rho \quad (2-7)$$

where we have explicitly assumed time variation of $e^{j\omega t}$, i.e., we assume a time harmonic monochromatic frequency.

Boundary Conditions: The next major step is to specify the boundary conditions on the tangential electric field. For resistive boundary conditions the tangential electric field is equal to the surface impedance Z_{surf} times the current density J. If the surface is a perfect conductor, $Z_{surf} = 0$, then we have the requirement that the tangential E field vanish. When the field observation point is on the body surface we have

$$\hat{n} \times \vec{E}^{Total} = \hat{n} \times (\vec{E}^{inc} + \vec{E}^{scat}) = Z_{surf} \vec{J} \quad (2-8)$$

The known quantities are the incident field and surface impedance. The unknown is the current density \mathbf{J} (which also appears under the integral sign of the EFIE). The boundary conditions lead to a Fredholm integral equation. When Z_{surf} is zero, this is an integral equation of the first kind, i.e., the unknown \mathbf{J} appears only under the integral, or when non zero, an integral equation of the second kind since \mathbf{J} also appears outside the integral.

It is customary to rearrange the unknowns to the left and known quantities to the right:

$$-\hat{n} \times \vec{E}^{\text{scat}} + Z_{\text{surf}} \vec{J} = \hat{n} \times \vec{E}^{\text{inc}} \quad (2-9)$$

It is also customary to write the integral expression for \mathbf{E}^{scat} as a linear operator L operating on the current \mathbf{J} , as $L(\mathbf{J})$:

$$L(\vec{J}) = -\vec{E}^{\text{scat}} = jk\eta \int [\vec{J}g - \frac{\nabla_s \cdot \vec{J}}{k^2} \nabla_s g] dS \quad (2-10)$$

where $k\eta = \omega\mu$, $\omega\epsilon = k/\eta$ and have set the magnetic sources to zero.

Matrix Solution of the Integral Equation: The formal solution of the integral equation yields a matrix or set of simultaneous equations. Sub domain basis functions with unknown coefficients j represent the unknown surface current:

$$\vec{J} = \sum_{i=1}^N j_i \vec{f}_i(t) \quad (2-11)$$

The sub-domain basis function $\mathbf{f}(t)$ contains the vector and functional characteristics for the local surface current expansion function. This representation of a function is a generalization of other types of series expansions such as Taylor or Fourier.

The boundary conditions are enforced at each point or region on the body to determine the unknown currents. The boundary conditions, where we know the solution, are enforced at N unique locations on the body, i.e., the tangential field *must* be equal to $Z_{\text{surf}} \mathbf{J}$. At each location on the body the total field is the sum of the incident field plus the field caused (scattered) by currents located on *every other part of the body*. This leads to a coupled system of equations by which every part of the body affects every other part (Maxwell's equations are elliptic).

Impedance matrix elements express mutual body coupling. When enforcing the BC at specified locations on the body, we sample the region surrounding the BC location. Mathematically we obtain an *average* value by using a weight function for each BC enforcement location. Explicitly we multiply the boundary condition equation by a surface tangential vector weight function \mathbf{W} and use an inner product integral defined as

$$\langle \vec{W}_p, L(\vec{f}) \rangle = \int \vec{W}_p \cdot L(\vec{f}) \, dS_p \quad (2-12)$$

where the integration is over the p th surface area which surrounds the p th BC match point.

The current series expansion is inserted into EFIE expression for scattered field and the boundary conditions applied to obtain the matrix form of the integral equation.

The inner product is a linear operation which slides over the integrals. A set of N equations for N unknown current coefficients results:

$$\sum_{q=1}^N \langle \vec{W}_p, L(\vec{f}_q) \rangle j_q + Z_{\text{surf}} \langle \vec{W}_p, \vec{f}_p \rangle j_p = \langle \vec{W}_p, \vec{E}^{\text{inc}} \rangle \quad \text{for } p = 1 \text{ to } N \quad (2-13)$$

for N unique locations on the body. A matrix, i.e., set of simultaneous equations, represents the original elliptic integral equation.

The matrix element interaction between body surface patch areas p and q is the inner product $\langle W_p, L(f_q) \rangle = Z_{pq}$. The voltage vector solution forcing function is the right hand side inner product, $V_q = \langle W_q, E^{\text{inc}} \rangle$.

With this notation, the original integral equation becomes a matrix equation:

$$\begin{bmatrix} z_{11} & z_{12} & \dots & z_{1N} \\ \vdots & \ddots & & \vdots \\ \vdots & \vdots & & \vdots \\ z_{N1} & z_{N2} & \dots & z_{NN} \end{bmatrix} \begin{bmatrix} j_1 \\ j_2 \\ \vdots \\ j_N \end{bmatrix} = \begin{bmatrix} v_1 \\ v_2 \\ \vdots \\ v_N \end{bmatrix} \quad (2-14)$$

or in compact matrix notation

$$\bar{Z} \bar{J} = \bar{V} \quad (2-15)$$

where Z is a N by N square matrix, J is the unknown current vector, and V is the voltage vector forcing function. J and V are column vectors with N rows.

The solution is obtained by computing the matrix elements Z_{pq} and solving for the currents J for various body excitations forcing functions V , e.g., plane waves or antenna voltage ports:

$$\vec{J} = \vec{Z}^{-1} \vec{V} \quad (2-16)$$

Voltage Vector: The forcing function for scattering problems is usually specified as an incident plane wave. The tangential component of the incident field is automatically obtained from the surface vector weight function W which is defined tangent to the body surface. The excitation for RCS computations is usually a plane wave:

$$\vec{E}^{inc} = E_0 \hat{u}^* e^{-j\vec{k}^{inc} \cdot \vec{R}} \quad (2-17)$$

where E_0 is the wave amplitude, \hat{u} is the polarization unit vector, \vec{k}^{inc} is the vector direction of the plane wave, and \vec{R} is any coordinate location vector. Planes of constant phase are perpendicular to \vec{k}^{inc} . The components of \vec{V} for plane wave incidence are then:

$$v_q^* = \langle \vec{W}_q, \vec{E}^{inc} \rangle = \int (\vec{W}_q \cdot \hat{u}^*) e^{-j\vec{k}^{inc} \cdot \vec{R}_q} dS_q \quad (2-18)$$

where $\hat{u}^* = \hat{e}_0 \text{ or } \hat{e}_9$ is the polarization unit vector, \vec{k}^{inc} is the wave number in the direction of propagation of the incident wave, and \vec{R}_q the local coordinates of the q th sub-domain.

Matrix Elements: Mautz and Harrington, [5], derived a universal formula for computing matrix elements. This recipe is applicable to any geometry for arbitrary choice of expansion functions f and weight functions W . The expression for matrix elements is:

$$Z_{pq} = \langle \vec{W}_p, L(\vec{f}_q) \rangle = +jk\eta \int \int [(\vec{W}_p \cdot \vec{f}_q) g + \frac{\nabla \cdot \vec{f}_q}{k^2} \vec{W}_p \cdot \nabla g] dS_p dS_q \quad (2-19)$$

which for three dimensional surfaces becomes a four fold integral, i.e., surface to surface. Reference [5] used the 2D surface divergence theorem on a closed surface to convert the second term dot product:

$$\int \vec{W} \cdot \nabla g dS = - \int g \nabla \cdot \vec{W} dS \quad (2-20)$$

to arrive at the universal matrix element interaction expression:

$$Z_{pq} = +jk\eta \int dS_p \int dS_q [\vec{W}_p \cdot \vec{f}_q - \frac{(\nabla \cdot \vec{W}_p)(\nabla \cdot \vec{f}_q)}{k^2}] \frac{e^{-jk\vec{R}}}{4\pi R} \quad (2-21)$$

This expression is the "mother of all matrix element formulas." It applies to all geometries and to all types of expansion functions f and weight functions W . It applies to bodies of revolution (BOR's), wires, 2-d strips, 3-D patch, wires attached to BOR's or patches, BOR's coupled with 3-D patches, etc..

Scattered Field: The heart of the MOM solution is to solve for the current distribution on the body. From these currents one is then often interested in computing the resulting radiation pattern, \mathbf{E}^{rad} , from which we obtain radar cross section or antenna gain patterns. Far field radiation is given by the transverse components of the electromagnetic vector potential \mathbf{A} :

$$E^{\alpha, \text{scat}}(\theta, \phi) = -j\omega(\hat{n}^\alpha \cdot \vec{A}) = -j\omega\mu \int (\hat{n}^\alpha \cdot \vec{J}) g dS \quad (2-22)$$

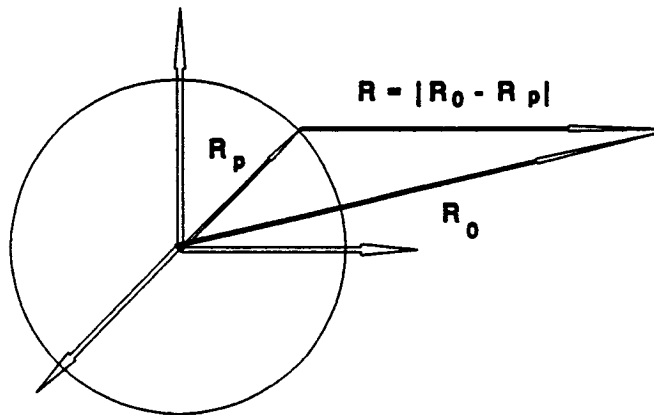


Figure 2-1 Far field distance approximation geometry

where $\alpha = \theta$ or ϕ polarization. The standard approximation for the distance from source to field point is then made using the law of Cosines, Figure 2-1, which is valid whenever the field point distance is much greater than the local body dimensions:

$$\begin{aligned} R &= |\vec{R}_0 - \vec{R}_p| = R_0 \left[1 - \frac{2\hat{R}_0 \cdot \vec{R}_p}{R_0} + \left(\frac{R_p}{R_0} \right)^2 \right]^{1/2} \\ &\approx R_0 - \hat{R}_0 \cdot \vec{R}_p \end{aligned} \quad (2-23)$$

where R_0 is the distance to the far field point, R_p is a local source point on the body, and \vec{R}_0 points in the same direction as k^{ext} . The distance R in the Green's function is approximated by R_0 in the denominator (amplitude) and by the two term approximation for the phase term. The series current basis function expansion is used for the current J . The

final expression for scattered field then becomes a complex dot product of the row measurement vector \mathbf{R} and the solution column vector \mathbf{j} :

$$E^{e, \text{scat}}(\theta, \phi) = \frac{-jk\eta}{4\pi R_0} e^{-jkr_0} \vec{R}^e \cdot \vec{j} \quad (2-24)$$

where the row vector \mathbf{R} is

$$R_p^e(\theta, \phi) = \int (\hat{n}^e \cdot \vec{f}_p) e^{jk^{\text{ext}} \cdot \vec{R}_p} dS_p \quad (2-25)$$

where the f_p is the current expansion function for the p th sub-domain, $n^e = \theta$ or ϕ is the polarization, k^{ext} is in the direction of the scattered field, and R_p is the local coordinates of the p th sub-domain. Harrington [6] derives the same formulation using reciprocity.

For backscatter $k^{\text{ext}} = -k^{\text{inc}}$ therefore the expression for scattered field is the same as the voltage vector expression. If $\mathbf{f} = \mathbf{W}$, the same computation routine may be used to compute either.

Computer Resource Considerations: The number of unknowns in a moment solution is proportional to the body size as measured in wavelengths since the currents must be sampled on a wavelength scale, typically 7 to 10 per wavelength. Computer resources of memory and available cpu time limits the body size which one may compute.

Surface currents require vector unknowns. Each sub-domain area requires two scalar unknowns, one for each basis vector direction. Let us characterize a body by dimension L and area L^2 . If we require n unknowns per linear dimension, then a surface with area A would require $2n^2$ unknowns per square-wave length (98 to 200 unknowns) of area. Matrix

storage then would be proportional to $(nL^2)^2 = n^4 L^4$. Matrix solution time, which varies as N^3 , would be proportional to $(nL^2)^3 = n^6 L^6$. Thus as the body grows in electrical size, required memory grows as (linear size)⁴ and matrix solution time grows as (linear size)⁶.

Linear sample density n should be as small as practical and still yield a satisfactory solution. This will reduce memory requirements (proportional to n^4) and matrix solution time (proportional to n^6). Computer resource requirements grow very rapidly with linear body size L and sample density n . We thus see the importance of optimizing the algorithm to conserve computer memory and time.

It should be noted that a fundamental reformulation of the analysis will be required if we are to compute very large electrical bodies. Alternately parallel computer architecture will be required.

The impedance matrix is of rank N^2 , i.e., N unknowns. This means that at least N^2 memory locations be available to store the complex matrix elements. This is the dominant requirement for memory storage. Matrix fill cpu time will also be proportional to N^2 .

Matrix solution time is proportional to N^3 . Matrix inversion (or equivalent process) dominates the solution time for large problems. Various approaches can change the proportionality constant (as optimized in MOM3D). For a given geometry and frequency, the impedance matrix may be computed, solved, and then saved to disk storage. Then various analysis options may later be performed using the saved LU decomposed matrix.

Matrix solution may be obtained in principle by a variety of approaches: inverse, Gaussian elimination, Crammer's rule, LU decomposition, iterative solutions, etc.. As discussed in [2], [8], and [9], LU matrix factorization requires 1/3 the time of direct matrix inversion. Therefore MOM3D utilized the LU factorization approach.

The LINPAK [9] library of matrix routines for LU decomposition and back solution was used. The matrix formulation was specifically made symmetric by choosing Galerkin weight functions, i.e., $f = W$ and the LINPAK library routines for symmetric matrices was used. This required 1/2 less matrix storage and computation time, and, more important, reduced the LU decomposition time by 1/2, which for large problems is significant.

Future adaptations could take advantage of parallel processor architectures using matrix libraries specific to these machines, such as the LAPACK library now under development, reference [10].

When using LU decomposition, the back solution time to compute the currents is proportional to N^2 . For backscatter RCS problems, a new voltage vector and current solution is required for each excitation angle. Therefore the solution time becomes proportional to $M_{\text{angles}} N^2$. Since we typically compute backscatter every degree, M may equal 181 to 361 depending on the angle range. Thus for small bodies, if N is less than M , the back solution time may become greater than the LU decomposition time.

The time to compute the voltage or row vectors is proportional to the number of unknowns N . This is not a significant time requirement compared to back solution time. Other computation overhead is required to compute the required geometry parameters from the input geometry description.

SECTION 3

MOM3D SURFACE PATCH FORMULATION

The theory developed in Section 2 is completely general. This section will apply the theory to the surface triangle basis functions introduced by Rao, Wilton, and Glisson [1]. Matrix and body symmetries are used in MOM3D to create a computational efficient code compared to [1]. MOM3D has diagnostic capabilities for imaging, near fields, and currents, as well as for backscatter & bistatic RCS and antenna gain pattern computations.

Surface patch basis functions must: 1) model two independent surface vector directions; 2) have desirable derivative properties since the second term in the matrix element formula requires the divergence of \mathbf{J} ; and 3) model arbitrary curved or planar surfaces. A

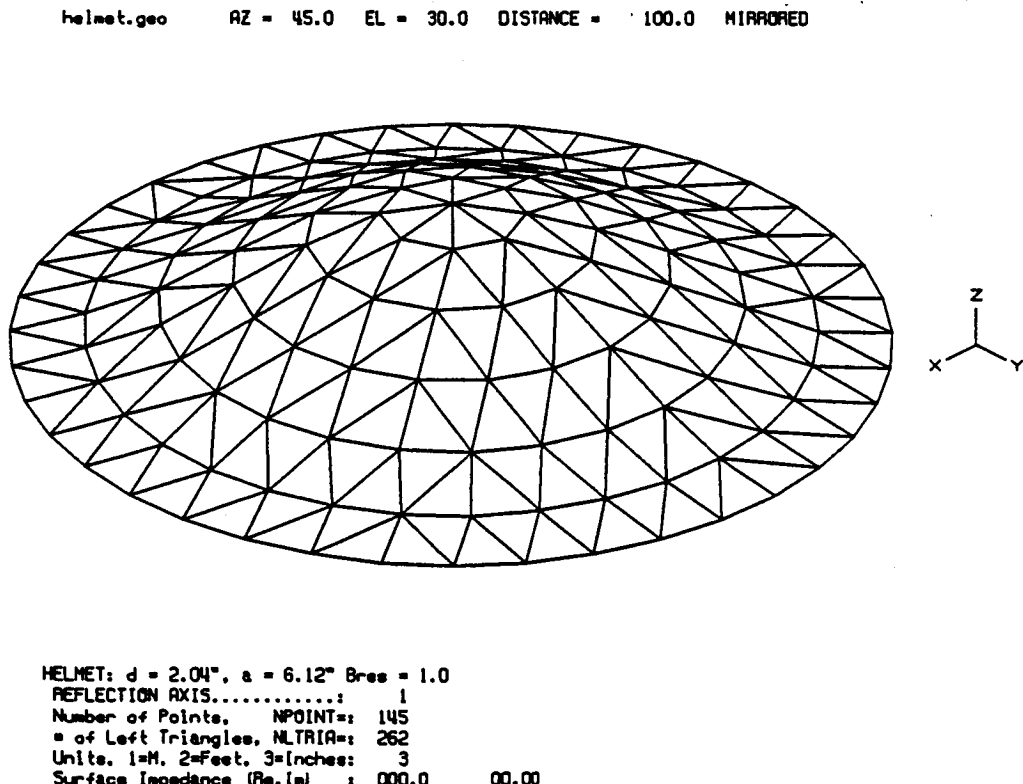


Figure 3-1 Arbitrary surface modeled by triangular patches

rectangular surface patch basis function code is reported in [11] but it has obvious problems when modeling arbitrary curved surfaces. These three criteria were used by [1] to develop the surface triangle basis functions. They can model a wide range of geometries as illustrated in Figure 3-1. Both open and closed geometries can be modeled.

Current Couple: A pair of coupled triangles that share a common edge were introduced by [1] as the fundamental vector basis function, Figure 3-2. The vector current flow is from one vertex flowing across the common edge toward the opposite vertex. Each triangle pair is a *couple* and is the fundamental unknown quantity in the analysis. This basis function is such that its magnitude is like a triangular hat function.

It has the value zero when r is at the vertex, unity when r is anywhere on the common edge, and zero when r is at the opposite vertex. The vector basis function associated with the q th edge is then

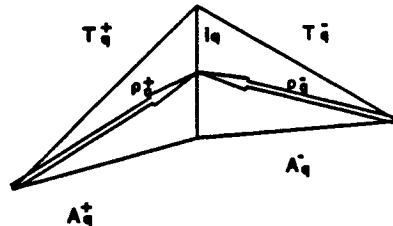


Figure 3-2 Triangle couple basis function

$$\vec{f}_q(\vec{r}) = \begin{cases} \frac{S_q^+ l_q}{2A_q^+} \vec{p}_q^+ & ; S_q^+ = +1 \\ \frac{S_q^- l_q}{2A_q^-} \vec{p}_q^- & ; S_q^- = -1 \end{cases} \quad (3-1)$$

By arbitrary definition, current flow is from the first triangle of area A^+ to the second triangle of area A^- . The length of the common edge is l_q , \vec{p}_q^\pm is a vector from either vertex toward the common edge, and S is a unity sign showing current flow direction. This definition is slightly different from that in [1] in that $S = \pm 1$ is explicitly used. This

simplifies the following analysis and resulting computer code since the vector ρ can always have a common definition regardless of whether a triangle is + or -. This basis function is the surface version of triangle basis functions used for wire or 2D analysis. It has the value of zero when ρ is at either vertex and a value of unity when ρ is on the common edge. The slope or derivative (divergence) is positive constant in the + triangle and negative constant in the - triangle. This derivative feature is such that the triangular hat current yields a pulse doublet charge distribution.

The surface divergence operator for triangular patch geometry is

$$\nabla_s \cdot \vec{f} = \frac{1}{\rho} \frac{\partial(\rho f_q)}{\partial \rho} \quad (3-2)$$

which results in the following expression for the surface divergence of the vector basis function (charge density)

$$\nabla_s \cdot \vec{f}_q = \begin{cases} \frac{S_q^+ l_q}{A_q^+} ; & S_q^+ = +1 \\ \frac{S_q^- l_q}{A_q^-} ; & S_q^- = -1 \end{cases} \quad (3-3)$$

These vector basis functions are used to represent (approximate) the surface currents. Since a triangle has three sides, and if each side has a common neighbor, then it contributes up to three basis functions (couples). The current in the q th patch is represented by up to three basis vectors. These are not orthogonal as is the case of usual basis vectors, however, they are independent and "span the space" to represent any physical direction of current required by the solution of Maxwell's equations.

Couple Basis Function Average (Moment): The fundamental current vector unknown is between two adjacent common triangles and *not* a single triangle by itself. It is convenient to describe the location of the couple centroid. The average or moment over the two triangles of the couple basis function is [1]:

$$\begin{aligned} \vec{f}_q^{\text{average}} &= \frac{\int \vec{f}_q^+ dS_q^+ + \int \vec{f}_q^- dS_q^-}{(A_q^+ + A_q^-)} = \frac{l_q}{2} \frac{(\bar{r}_q^{c+} - \bar{r}_q^{c-})}{(A_q^+ + A_q^-)} \\ &= l_q \frac{(\bar{r}_q^{c+} - \bar{r}_q^{c-})}{(A_q^+ + A_q^-)} \end{aligned} \quad (3-4)$$

where $\rho^{c\pm}$ is the vector from the free vertex to the centroid and $r^{c\pm}$ is the position vector of the triangle centroid, Figure 3-3. We see that the average of the basis function over the triangle couple pair is equal to the common edge length times the vector between the centroid of each triangle. The center of this vector is the center of the vector basis function f^{average} .

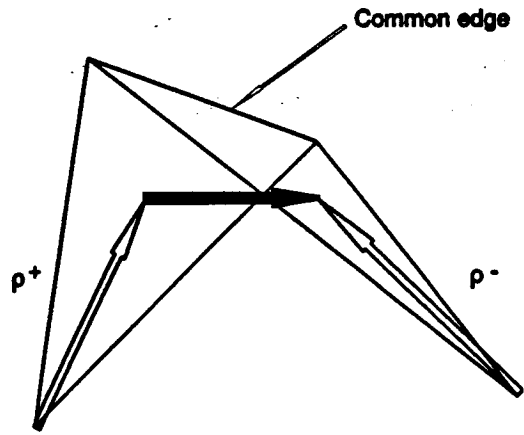


Figure 3-3 Net couple moment (current) is from triangle centroid to centroid

Matrix Elements: The development of expressions for matrix element interaction requires one to choose a specific weight function W and to consider if a symmetric matrix is to be obtained, i.e., $Z_{pq} = Z_{qp}$. Various options are possible as discussed by [2] and [7]. The general expression of matrix elements for three dimensional surfaces, Section 2, shows that Z_{pq} is a four fold integral, i.e., the E field integrated over surface patch p (with averaging weight function W) as caused by currents located on surface patch q with basis function f. Reference [1] simplified the computation by choosing delta or point matching weight functions so that a two fold integral resulted

(point to surface), however a symmetric matrix did not result. To obtain matrix symmetry, the weight functions must be of the same form as the current expansion functions, $\mathbf{W}_q = \mathbf{f}_q$, which is called the Galerkin choice for \mathbf{W} . The penalty paid to achieve matrix symmetry (with resultant reduction in LU decomposition and memory storage) is the requirement for four fold integration. As we shall shortly see, the centroid integration approximation eliminates this integration requirement. (We can have our cake and eat it too?)

The reader can easily see from Section 2 matrix element expression that a Galerkin choice for weights yields a symmetric matrix. This will be our choice. All we have to do is to insert the appropriate values to obtain the required expression. In doing this we must remember that the integrations are from one pair (couple) of triangles to another pair (couple), Figure 3-4. The result is:

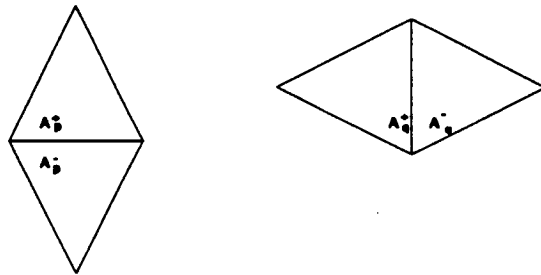


Figure 3-4 Matrix element interaction is between pairs of triangles (four terms)

$$Z_{pq} = jk\eta \int dS_p \int dS_q [\vec{f}_p \cdot \vec{f}_q - \frac{\nabla \cdot \vec{f}_p \nabla \cdot \vec{f}_q}{k^2}] \frac{e^{-jkR}}{4\pi R} \quad (3-5)$$

Since each couple has two triangles, each matrix element has four terms, i.e., each triangle interacting with the others, (+,+), (+,-), (-,+), and (-,-) :

$$\begin{aligned}
 Z_{pq} = jk\eta & \{ \int dS_p^+ \int dS_q^+ [\vec{f}_p^+ \cdot \vec{f}_q^+ - \frac{\nabla \cdot \vec{f}_p^+ \nabla \cdot \vec{f}_q^+}{k^2}] g + \\
 & \int dS_p^+ \int dS_q^- [\vec{f}_p^+ \cdot \vec{f}_q^- - \frac{\nabla \cdot \vec{f}_p^+ \nabla \cdot \vec{f}_q^-}{k^2}] g + \\
 & \int dS_p^- \int dS_q^+ [\vec{f}_p^- \cdot \vec{f}_q^+ - \frac{\nabla \cdot \vec{f}_p^- \nabla \cdot \vec{f}_q^+}{k^2}] g + \\
 & \int dS_p^- \int dS_q^- [\vec{f}_p^- \cdot \vec{f}_q^- - \frac{\nabla \cdot \vec{f}_p^- \nabla \cdot \vec{f}_q^-}{k^2}] g \}
 \end{aligned} \tag{3-6}$$

The next step is to pull out of the indicated integration the constant parameters and to define the major Green's function integrals. We define $G_{pq}^{(1)}$ and $G_{pq}^{(0)}$ normalized to triangle patch areas:

$$\begin{aligned}
 G_{pq}^{(1)} &= \frac{1}{A_p A_q} \int dS_p \int dS_q (\vec{p}_p \cdot \vec{p}_q) g \\
 G_{pq}^{(0)} &= \frac{1}{A_p A_q} \int dS_p \int dS_q g
 \end{aligned} \tag{3-7}$$

We then arrive at the required expression for the matrix elements by using the appropriate expressions for \mathbf{f} and divergence \mathbf{f} :

$$\begin{aligned}
 Z_{pq} = jk\eta l_p l_q & \{ S_p \cdot S_q \cdot [1/4 G_{p,q}^{(1)} - 1/k^2 G_{p,q}^{(0)}] + \\
 & S_p \cdot S_q \cdot [1/4 G_{p,q}^{(1)} - 1/k^2 G_{p,q}^{(0)}] + \\
 & S_p \cdot S_q \cdot [1/4 G_{p,q}^{(1)} - 1/k^2 G_{p,q}^{(0)}] + \\
 & S_p \cdot S_q \cdot [1/4 G_{p,q}^{(1)} - 1/k^2 G_{p,q}^{(0)}] \}
 \end{aligned} \tag{3-8}$$

This is our exact (numerically) desired expression. No approximations are made at this point other than the choice for the current expansion functions \mathbf{f} and weights $\mathbf{W} = \mathbf{f}$.

Green's Function Computation and Approximations: The principal task is now to compute $G^{(1)}$ and $G^{(0)}$ that integrate the free space Greens's functions over each pair of triangles. This of course is a four fold surface to surface interaction. $G^{(1)}$ and $G^{(0)}$ are related to the electromagnetic vector and scalar potentials. We start by estimating the dominate term in the matrix element computation. We assume that the surface is sampled such that $\rho < \lambda/10$ so that the ratio of the first term in Z (vector potential) to the second term (scalar potential) is approximately:

$$\frac{\text{Vector}}{\text{Scalar}} = \frac{0.25 \vec{p} \cdot \vec{p}}{1/k^2} < \frac{\pi^2}{100} \approx 0.1 \tag{3-9}$$

which shows that the dominant interaction between surface patches is from the scalar electrostatic term. Based on this observation, we approximate the $G^{(1)}$ integral as:

$$G_{pq}^{(1)} \approx (\bar{p}_p^c \cdot \bar{p}_q^c) G_{pq}^{(0)} \quad (3-10)$$

where ρ_p^c or ρ_q^c is the vector from the free vertex to the triangle centroid, i.e., we have used a centroid approximation for the vector dot product portion of the integrand in $G^{(1)}$.

Centroid Approximation: The computation of $G^{(0)}$ remains. This is still a surface to surface four fold integration involving the free space Green's function as the integrand. The appendix discusses a combination analytical / numerical integration approach, i.e., one surface integration is done analytically and the second surface integration is done with either a three or one point numerical integration. This section discusses the centroid approach.

The integrand has a $1/R$ intensity decay and phase (time) delay.

The surface patches have linear dimensions less than $\lambda/10$.

Therefore the stationary part of the phase involves the distance between triangle centroids,

Figure 3-5, while the varying portion has at most a $2(\lambda/20) = \lambda/10 = 36^\circ$ variation in phase. If

we recall the typical approximation used in plane wave EM analysis, a 22.5° variation is considered constant. Thus the phase part of the integrand is relatively constant centered on the centroid value.

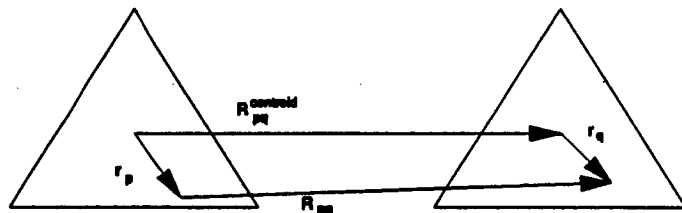


Figure 3-5 Distance between triangles using centroid

The $1/R$ amplitude portion of the integrand is dominated by the distance between triangle centroids that is just the leading term of a Taylor series (expanded about the centroid value).

Consider Figure 3-5 where the distance between source and field points, R_{pq} is expressed in terms of the vector from triangle centroids, R_{pq}^c and two local vectors in each triangle, r_p and r_q . Then we have

$$\begin{aligned} |\vec{R}_{pq}| &= |\vec{R}_{pq}^c + \vec{r}_q - \vec{r}_p| \\ &\approx |\vec{R}_{pq}^c| \end{aligned} \quad (3-11)$$

With this centroid approximation, $G^{(0)}$ becomes a very simple expression, i.e., just the free space Green's function evaluated at the centroid distance:

$$G_{pq}^{(0)} = \frac{1}{A_p A_q} \int dS_p \int dS_q \frac{e^{-jkR_{pq}}}{4\pi R_{pq}} \approx \frac{e^{-jkR_{pq}^c}}{4\pi R_{pq}^c} \quad (3-12)$$

Notice that no integrations are required.

Self Term Approximation: Self term matrix elements represent the field at a couple due to its own currents, Z_{pp} . Self term quantities also have four terms, two self triangles, (+,+) and (-,-) and two adjacent triangles, (+,-) and (-,+). When evaluating the self triangle, the centroid distance is zero and clearly an alternative expression is required to prevent the non-physical case of division by zero. The approach we will use is that by Harrington [6] who simply integrated the free space Green's function over a patch that he took to be circular with a radius defined such that the circular patch had the equivalent area to the actual (triangle) patch under consideration. The main contribution to the integral is from the region surrounding the centroid thus the result does not change appreciably provided the triangle aspect ratio is not extreme, i.e., the height to width ratio remains near unity. The self term approximation starts by writing the self term as:

$$G_{pp}^{self} = \frac{1}{A} \int dS \frac{e^{-jkR}}{4\pi R} \quad (3-13)$$

The integrand is then expanded about the center of the triangle, $R = 0$, and only the first two terms retained (remember that $R \ll \lambda$):

$$\frac{e^{-jkR}}{R} = \frac{1}{R} [1 - jkR + \dots] \approx \frac{1}{R} - jk \quad (3-14)$$

The self term then becomes

$$G^{self} = \frac{1}{4\pi A} \int [\frac{1}{R} - jk] dS ; \quad dS = 2\pi R dR, \text{ then} \quad (3-15)$$

$$G^{self} = \left[\frac{3.545}{\sqrt{A}} - jk \right] \frac{1}{4\pi}$$

This self term approximation along with the centroid approximation is used whenever MOM3D users specify centroid integration for all couples. The analytical / numerical approaches discussed in the appendix yield approximately the same result for self terms.

Voltage Vector: The right hand side forcing function of the matrix equation is the voltage vector. When computing either backscatter or bistatic radar cross section the voltage vector is due to the specified incident plane wave:

$$\vec{E}^{inc} = \hat{u}^\alpha = 0 \text{ or } \phi \quad E_0 e^{-j\vec{k}^{inc} \cdot \vec{R}} \quad (3-16)$$

where the polarization reference is to a spherical coordinate system and may be either θ or ϕ , the direction of propagation is \vec{k}^{inc} , and E_0 is the amplitude taken as either 1 volt / meter or in MOM3D as $\eta = 377$ volt / meter to reference currents to a unit incident magnetic field.

The voltage vector for our Galerkin weight functions, $\mathbf{W} = \mathbf{f}$, is then

$$V_p = \langle \vec{f}_p, \vec{E}^{inc} \rangle = \frac{S_p^+ l_p}{2 A_p^+} \int \vec{\rho}_p^+ \cdot \vec{E}^{inc} dS_p^+ + \frac{S_p^- l_p}{2 A_p^-} \int \vec{\rho}_p^- \cdot \vec{E}^{inc} dS_p^- \quad (3-17)$$

The centroid approximation is used to compute the two fold surface integral:

$$V_p = \frac{l_p}{2} \{ S_p^+ (\vec{\rho}_{p+}^c \cdot \hat{u}^\alpha) e^{-j\vec{k}^{inc} \cdot \vec{R}_p^c} + S_p^- (\vec{\rho}_{p-}^c \cdot \hat{u}^\alpha) e^{-j\vec{k}^{inc} \cdot \vec{R}_p^-} \} E_0 \quad (3-18)$$

In MOM3D, each row of the column voltage vector is computed by this expression.

Another approach for evaluating the voltage vector is to use \mathbf{f}^{ave} for the integration over the two triangles forming the couple:

$$\begin{aligned} V_p &= \langle \vec{f}_p, \vec{E}^{inc} \rangle \approx \langle \vec{f}_p^{ave}, \vec{E}^{inc} \rangle \\ &= l_p [(\vec{r}_p^{c+} - \vec{r}_p^{c-}) \cdot \hat{u}^\alpha] e^{-j\vec{k}^{inc} \cdot (\vec{r}_p^{c+} + \vec{r}_p^{c-})/2} E_0 \end{aligned} \quad (3-19)$$

where the specific form for \mathbf{f}^{scat} is used and the incident field phase is evaluated at the midpoint between triangle centroids.

Scattered Field: The field radiated by the currents on the body is computed using the general expression developed in Section 2. The radiation integral is evaluated as a complex dot product of a row measurement vector with the column current vector. The elements of the row measurement vector, when Galerkin weight functions are used, $\mathbf{W} = \mathbf{f}$, has identically the same form as the expression for the voltage vector. The astute reader will notice that the elements of the row vector are defined for \mathbf{k}^{scat} pointing away from the local origin while the voltage vector elements are defined for \mathbf{k}^{inc} pointing toward the local origin. This change of sign is what makes the row and voltage vectors have equivalent form.

The reader is cautioned that while the voltage vector subroutine may be used to compute the row vector, \mathbf{V}_r , is *not* equal to \mathbf{R}^p unless we are computing the backscatter case when $\mathbf{k}^{\text{scat}} = -\mathbf{k}^{\text{inc}}$. The elements of \mathbf{k} , as expressed in rectangular coordinates in terms of the polar angle θ and azimuth angle ϕ for an incident wave toward the origin, are

$$\bar{\mathbf{k}}^{\text{inc}} = \frac{2\pi}{\lambda} (-\cos\phi \sin\theta, -\sin\phi \sin\theta, -\cos\theta) \quad (3-20)$$

This is a radial vector pointed toward the origin. The two polarization unit vectors are orthogonal to \mathbf{k} . The usual choice is to pick the θ and ϕ directions, tangent to a sphere, as

$$\begin{aligned} \bar{\mathbf{u}}^\theta &= (\cos\theta \cos\phi, \cos\theta \sin\phi, -\sin\theta) \\ \bar{\mathbf{u}}^\phi &= (-\sin\phi, \cos\phi, 0) \end{aligned} \quad (3-21)$$

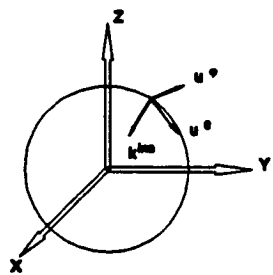


Figure 3-6 Polarization unit vectors and incident field unit vector

SECTION 4

GEOMETRY SYMMETRY CONSIDERATIONS

Considerable reduction in computer resources can occur if the geometry has symmetry (see Miller [2]). Examples of body symmetry would be bodies of revolution, bodies with planes of symmetry such as aircraft, and bodies such as hexagons with multiple symmetry planes. Body symmetry reduces solution resources because:

- * The impedance matrix represents the interaction of each part of the body with another, therefore symmetry implies that the coupling between similar body parts is equivalent. This means we do not need to recompute those elements of the impedance matrix. This implies a reduction in matrix element storage and compute time, an N^2 dependence.
- * The solution of the impedance matrix can take advantage of equivalent sub matrices to reduce the solution time N^3 dependence for LU decomposition.

Body symmetry does not automatically reduce computer resources. The solution algorithm must be specifically designed to incorporate symmetry.

Body symmetry is a completely different concept than matrix symmetry obtained by using Galerkin weight functions.

MOM3D solves body geometries with either no symmetry or with a plane of mirror symmetry about the X, Y, or Z axis.

With body symmetry the impedance matrix splits into two smaller matrices, each with approximate rank $N/2$ where N is the total number of unknowns on the body. The following efficiencies result:

- * Matrix storage reduced by *two*. We have two matrices of approximate rank $N/2$, therefore matrix fill time and memory storage is: $2(N/2)^2 = N^2 / 2$.
- * Matrix LU decomposition solution time reduced by *four*. Two matrices of rank $N/2$ require a solution time of: $2(N/2)^3 = N^3 / 4$.

The savings in computer resources becomes very significant for large electrical bodies when N is large.

Mirror Geometry Symmetry: MOM3D has incorporated mirror symmetry about either the x , y , or z axes if specified by the user. The geometry is described somewhat arbitrary as left side, right side, spine, and reflection plane, Figure 4-1. The left and right sides are those couples that are *all* either on the left or right. The spine couple unknowns bridge between left and right sides, i.e., they have one triangle on the left and the other on the right side.

The reflection plane couple unknowns are not reflected since they are on the symmetry plane.

We make use of specific relationships between these four type of unknowns to express the system impedance matrix as two separate matrices called Z_{even} and Z_{odd} .

System Matrix: The system impedance matrix is written in terms of these four types of unknowns: Z_{LL} and Z_{RR} the left and right side unknowns; Z_{SS} the spine unknowns; and Z_{VV} the reflection plane unknowns. With this breakdown the system matrix equation becomes

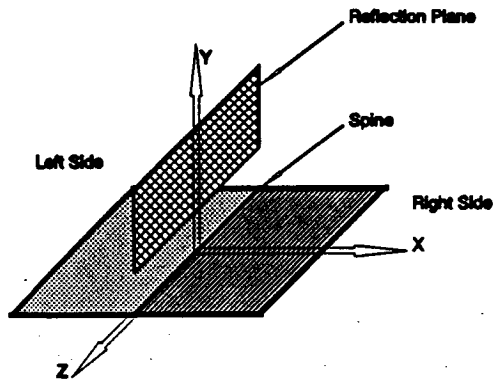


Figure 4-1 Geometry example that has symmetry about the $X = 0$ ($Y-Z$) plane.

$$\begin{bmatrix} Z_{LL} & Z_{LR} & Z_{LS} & Z_{LV} \\ Z_{RL} & Z_{RR} & Z_{RS} & Z_{RV} \\ Z_{SL} & Z_{SR} & Z_{SS} & Z_{SV} \\ Z_{VL} & Z_{VR} & Z_{VS} & Z_{VV} \end{bmatrix} \begin{bmatrix} I_L \\ I_R \\ I_S \\ I_V \end{bmatrix} = \begin{bmatrix} V_L \\ V_R \\ V_S \\ V_V \end{bmatrix} \quad (4-1)$$

Matrix element relationships: Geometry
 symmetry means that matrix elements are the same for left-left and right-right sides, i.e., the interaction of the left side of the body with itself is the same as the right side of the body with itself, $Z_{LL} = Z_{RR}$. The reflected couples are defined to have an opposite direction, Figure 4-2, so that the interaction of the spine with the left side is the same as the interaction of the spine with the right side, $Z_{LS} = Z_{RS}$ and the interaction of the left side with the reflection plane couples is the negative of the interaction of the right side, $Z_{LV} = -Z_{RV}$. The interaction of the spine couples, which are perpendicular to the reflection plane couples, is zero, $Z_{SV} = Z_{VS} = 0$. Due to matrix symmetry the following are equivalent: $Z_{LR} = Z_{RL}$, $Z_{LS} = Z_{SL}$, $Z_{LV} = Z_{VL}$, $Z_{RS} = Z_{SR}$, and $Z_{RV} = Z_{VR}$. The proof of these assertions is left to the reader.

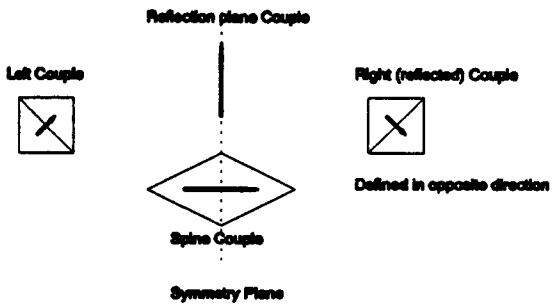


Figure 4-2 Reflected right couple has opposite direction so that $Z_{LS} = Z_{RS}$ and $Z_{LV} = -Z_{RV}$.

We develop the even and odd impedance matrices by multiplying out the system matrix equation, adding and subtracting various rows, and then use the sub-matrix equivalences. Multiplying out yields:

$$Z_{LL} I_L + Z_{LR} I_R + Z_{LS} I_S + Z_{LV} I_V = V_L \quad (1)$$

$$Z_{RL} I_L + Z_{RR} I_R + Z_{RS} I_S + Z_{RV} I_V = V_R \quad (2)$$

$$Z_{SL} I_L + Z_{SR} I_R + Z_{SS} I_S + Z_{SV} I_V = V_S \quad (3)$$

$$Z_{VL} I_L + Z_{VR} I_R + Z_{VS} I_S + Z_{VV} I_V = V_V \quad (4)$$

(4-2)

We define even and odd as follows: matrices Z_{even} and Z_{odd} ; unknown current vectors j_{even} and j_{odd} ; and voltage vectors V_{even} and V_{odd} .

We then start by adding and then subtracting (1) and (2) to obtain:

$$(Z_{LL} + Z_{LR})(I_L + I_R) + 2Z_{LS} I_S = (V_L + V_R) \quad (5)$$

(4-3)

$$(Z_{LL} - Z_{LR})(I_L - I_R) + 2Z_{LV} I_V = (V_L - V_R) \quad (6)$$

The even system of equations is defined as the set (5) and the spine set (3) with a factor of 2 incorporated to simplify later equations:

$$\begin{bmatrix} 2(Z_{LL} + Z_{LR}) & 2Z_{LS} \\ 2Z_{SL} & Z_{SS} \end{bmatrix} \begin{bmatrix} (I_L + I_R)/2 \\ I_S \end{bmatrix} = \begin{bmatrix} V_L + V_R \\ V_S \end{bmatrix} \quad (4-4)$$

The odd system of equations is defined as the set (6) and the reflection plane set (4) along with the factor of 2:

$$\begin{bmatrix} 2(Z_{LL} - Z_{LR}) & 2Z_{LV} \\ 2Z_{VL} & Z_{WW} \end{bmatrix} \begin{bmatrix} (I_L - I_R)/2 \\ I_V \end{bmatrix} = \begin{bmatrix} V_L - V_R \\ V_V \end{bmatrix} \quad (4-5)$$

If the original system matrix is symmetric due to Galerkin choice of weight functions, then the even and odd matrices are also symmetric.

The explicit even matrix and column vectors are:

$$\begin{aligned} Z^{\text{even}} &= \begin{bmatrix} 2(Z_{LL} + Z_{LR}) & 2Z_{LS} \\ 2Z_{SL} & Z_{SS} \end{bmatrix} \\ I^{\text{even}} &= \begin{bmatrix} (I_L + I_R)/2 \\ I_S \end{bmatrix} \\ V^{\text{even}} &= \begin{bmatrix} V_L + V_R \\ V_S \end{bmatrix} \end{aligned} \quad (4-6)$$

while the odd matrix and column vectors are:

$$\begin{aligned} Z^{\text{odd}} &= \begin{bmatrix} 2(Z_{LL} - Z_{LR}) & 2Z_{LV} \\ 2Z_{VL} & Z_{WW} \end{bmatrix} \\ I^{\text{odd}} &= \begin{bmatrix} (I_L - I_R)/2 \\ I_V \end{bmatrix} \\ V^{\text{odd}} &= \begin{bmatrix} V_L - V_R \\ V_V \end{bmatrix} \end{aligned} \quad (4-7)$$

MOM3D computes Z and V in normal fashion to create Z even/odd which are then solved via LU matrix decomposition. The even/odd voltage vector is computed from the normal V and the resulting even/odd currents are computed. Finally, the left and right side currents are obtained for scattered field analysis from the even/odd currents:

$$I_L = (I_{\text{even}} + I_{\text{odd}}) / 2 \quad (4-8)$$

$$I_R = (I_{\text{even}} - I_{\text{odd}}) / 2$$

For bodies that have a plane of symmetry, this algorithm approximately reduces matrix solution time by four and matrix fill and storage requirements by two.

Body symmetry and matrix symmetry form the cornerstone concepts for making MOM3D a computation efficient algorithm.

SECTION 5

BISTATIC IMAGE ANALYSIS USING k SPACE CONCEPTS

The experimental development of microwave images as pioneered by Dean Mensa [12] is one of the most powerful tools used to understand the scattering from various geometries. Imaging may be in one dimension, i.e., down range; or in two dimensions, i.e., down and cross range. This capability allows one to understand the scattering process in terms of specific scattering centers and mechanisms. Image development has been mostly experimental. While one could apply the same methods to predictive scattering algorithms, the computation burden has always been considered to great. This occurs because, experimentally, down range information is obtained by illuminating the target over a bandwidth of frequencies typically numbering 16, 32, 64, 128 or even 512. To do this with a method of moments analysis, one would have to recompute and solve the system matrix for each frequency. This computation burden is so great for large problems that the swept frequency approach is seldom pursued.

B. A. Cooper developed a new approach that requires only one computation of induced currents and therefore only one MOM matrix computation for down range images. A formal bistatic k space image theory was then developed by the author. This formulation computed cross range images without smear. The bistatic k space analytical image technique does not require a MOM code matrix solution for each frequency. Only one current distribution (matrix computation) is computed at the frequency of interest. The image is the Fourier transform of the k space bistatic scattered radiation for values of k^{scat} that correspond to downrange and cross range. The natural Fourier transform variables are wave number k and spatial position R . If we compute a bistatic field as a function of $k^{\text{scat}} = (k^{\text{downrange}}, k^{\text{cross range}})$ then the Fourier transform of the scattered field is naturally a function of the transformed spatial coordinates, $R^{\text{scat}} = (R^{\text{downrange}}, R^{\text{cross range}})$. The computation of the scattered field in k space is a generalization of the standard bistatic radiation integral. The difference is that E^{scat} is computed in term of k^{scat} for down and/or down/cross range rather

than in terms of the usual bistatic angles (θ, ϕ). Body currents are computed only once at the user specified incident angle and polarization.

Experimental Image Concepts: We start the discussion by looking at how experimentalist's obtain microwave images. This will form a background for the k space analytical image development.

The fundamental requirement for imaging is to obtain a scattering response that is a function of body location. This is done by causing the relative phase to change in both down and cross range. Down range phase is accomplished by sweeping the frequency which changes the relative downrange position (phase) of the scattering centers. Cross range phase is accomplished by rotating the body. In an electromagnetic sense, we rubber band or stretch the body in phase (time delay) so that we can reconstruct the physical scattering locations via the Fourier transform. Experimentally, the only way to move scattering centers in down range is to vary the number of wavelengths in a down range direction, i.e., change the frequency. Greater detail may be found in [12] and [13] and the author's section of Chapter 8 [18] taken from RADAR REFLECTIVITY, 2nd edition.

The limitations of experimental imaging are resolution and image smear or focus. Resolution increases with bandwidth:

$$\Delta r = \frac{c}{2\Delta f} = \frac{\lambda}{2} \frac{1}{(\Delta f/f)} \quad (4-5)$$

Typical experimental systems are usually bandwidth limited although a few experimentalists have pieced together body responses over several waveguide bands. A 10% bandwidth yields approximately a 5 wavelength resolution. At X band this is usually satisfactory, while at L band or VHF this clearly is not very practical.

Cross range resolution is increased by increasing the angular extent over which the model is rotated. The small angle approximation, $\cos \theta \approx 1$ and $\sin \theta \approx \theta$, however, limits resolution. Large angle extent causes the image to smear and become de-focused. It is possible to refocus the image with an appropriate algorithm, but this becomes a difficult image processing factor.

Additional concerns with experimental images are: 1) at what frequency does the image represent (since the image must be obtained over a bandwidth of frequencies)?; 2) what angle does the image represent for cross range since the model must be rotated through a finite angular extent?; and 3) what physical scattering mechanisms are we not observing or interpreting incorrectly due to the frequency and angular rotation sweep?

Bistatic k Space Image Background: The initial concept was explored by Cooper who developed the technique for down range images for a body of revolution MOM code using the experimental image approach with a synthetic frequency sweep in the radiation integral. It was soon apparent that high resolution images in down range were possible leading to spatial resolutions approaching $\lambda/2$ and most important, requiring only one MOM code matrix computation and inversion to compute the body currents. Very useful diagnostic information could be analytically computed with any MOM code for a very small additional computation cost.

When this technique was applied by the author to compute two dimensional images using the synthetic approach with frequency sweep and body rotation as described in [18], the wide bandwidth and angular rotation extent violated the small angle approximation. The result was a de-focusing (smear) of the 2D images and scattering amplitudes. Clearly one could have restricted the technique to small angular sweeps; but this would have negated the desirable high resolution.

To achieve high resolution in both range and cross range without image de-focus, the author reformulated the image mathematics from the experimental approach where frequency and angle are the primary variables to an analytical bistatic k space approach where the primary

variables are the bistatic wave number in down and cross range directions and the corresponding transform spatial position variables in down and cross range.

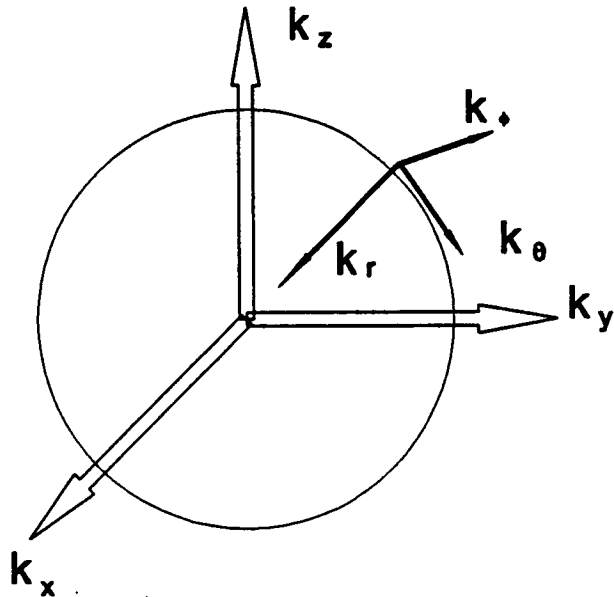


Figure 4-5 Bistatic image k space

A natural bistatic \mathbf{k} vector for down and cross range corresponds to the spherical coordinates of (k_r, k_θ, k_ϕ) , Figure 5-1. The downrange direction is radial, k_r , while the cross range direction is in a plane perpendicular to the radial down range direction, i.e., either k_θ or k_ϕ . A *full three dimensional image could be computed using this approach*. The present implementation is limited to either downrange or down / cross range.

The bistatic \mathbf{k} space image technique has the potential for the following (not all are presently implemented in MOM3D):

- * Resolution up to $\lambda/2$ unlimited by the usual experimental frequency and angle extent bandwidth concerns;

- * Image focus / smear does not occur due to the formulation of the approach;
- * Images are computed at the frequency and angle of body excitation. The body currents are computed only for this k^{inc} . In contrast to the experimental approach, the currents do not change with changes in the bistatic k^{ext} vector sweep;
- * One, two, or three dimensional images may be obtained. The limiting feature for obtaining 3D images is the display of the solution since multidimensional FFT algorithms are available;
- * The scattering body is imaged in a bistatic sense from the same direction as the excitation, i.e., a backscatter image. However, a more general bistatic approach is entirely possible since the center of k^{ext} is not required to be the negative of k^{inc} ;
- * A co-polarized image is implemented, but a cross polarized image could easily be computed.

The above list of possibilities shows that *the bistatic analytical approach to imaging can potentially yield substantially more information than experimental images. The bistatic image approach can be applied to any predictive algorithm for electromagnetic scattering or antenna radiation, e.g., Physical Optics.*

We can expect to see similarities and differences for a given target as imaged experimentally with swept frequency versus the analytical bistatic image. The analytical image is obtained from body currents that are excited only at one frequency and one excitation angle while the experimental image is a response over a bandwidth of frequencies and angle sector illumination. Experience must show how the two approaches will differ. One could argue that the bistatic image is a truer representation of the physical scattering mechanisms since

the body is truly excited at one frequency and angle. Thus line source radiation mechanisms such as reflected edge or surface traveling waves should image as radiative sources over the entire edge or surface as compared to the experimental approach where these mechanisms always show as emanating from an aft edge or tip vertex (because the swept frequency stationary phase point here is only at the fixed geometry end region).

Bistatic Image Theory: The key breakthrough in developing this approach for multiple dimensions was to abandon the experimental frequency and body rotation approach. The new concept falls naturally out of standard FFT theory [14]. We start by writing the bistatic scattered field as a function of three spatial coordinates that naturally constitute an image, i.e., down range and in a plane perpendicular to down range:

$$E^{a,p}(r_r, r_\theta, r_\phi) = \int \int \int W(\vec{k}^s) E^{a,p}(\vec{k}^{inc}, \vec{k}^{scat}) e^{j\vec{k}^{scat} \cdot \vec{R}} dk_r^s dk_\theta^s dk_\phi^s \quad (4-6)$$

This is the Fourier transform for the bistatic scattered field computed in \mathbf{k}^{scat} space, i.e., the square magnitude of this quantity converted to RCS is the image, i.e., intensity as a function of spatial position.

The variables are:

$|E^{a,p}(r_r, r_\theta, r_\phi)|^2$ is proportional to the amplitude of the desired image, e.g., RCS;

$\mathbf{k}^{scat} = \mathbf{k}^{(downrange, cross range)} = (k_r, k_\theta, k_\phi)$ is the wave number in spherical coordinates corresponding to down range and / or the two cross range directions;

$E^{a,p}(\mathbf{k}^{inc}, \mathbf{k}^{scat})$ is the scattered field in k^{scat} space computed from the radiation integral based on body currents excited on the body due to any form of

voltage vector excitation. For scattering problems this excitation is \mathbf{k}^{inc} . The received (image) and transmitted polarizations correspond to $\alpha, \beta = \theta$ or ϕ ;

$W(\mathbf{k}^{\text{scat}})$ is a standard FFT window weight function such as Hamming, Hanning, etc..

The downrange $k^{\text{scat}} = k_r$ vector component is centered on the free space value of k ,

$$k_r = \frac{2\pi}{\lambda_0} \pm \Delta k_r \quad (4-7)$$

Once we have computed the scattered field $E^{\alpha,\beta}(\mathbf{k}^{\text{inc}}, \mathbf{k}^{\text{scat}})$ in bistatic k space, equation 5-2 is the Fourier transform of the k space scattered field. The key is to compute the scattered field in terms of \mathbf{k}^{scat} vector components that naturally correspond to transformed image spatial coordinates.

The bistatic k space scattered field is computed from the standard radiation integral once body currents have been obtained for any given excitation:

$$E^{\alpha,\beta}(\bar{k}^{\text{inc}}, \bar{k}^{\text{scat}}) = \int \{ \hat{n}^\alpha \cdot \bar{J}^\beta(\bar{k}^{\text{inc}}) \} e^{j\bar{k}^{\text{scat}} \cdot \bar{R}} dS \quad (4-8)$$

where $\hat{n}^\alpha = \theta \text{ or } \phi$ is the receiver polarization unit vector, $\bar{J}^\beta = \theta \text{ or } \phi$ are the body currents resulting from plane wave excitation at the angle corresponding to \mathbf{k}^{inc} and polarization β .

Approach: The steps required to obtain an image are: 1) Compute body currents due to desired excitation, e.g., plane wave for scattering or port voltages for antenna radiation; 2) Specify image extent centered over the body; 3) Specify the approximate resolution desired; 4) Compute the scattered electric field in $\mathbf{k}^{\text{scat}} = (k_r^{\text{down}}, k^{\text{cross}})$ space; 5) Pad the data array

with zeros to obtain an array (linear or square) that is a power of 2 in length and perform the FFT; and 6) Resort the data and display the one, two, or three dimensional image.

Image extent, resolution, k space bandwidth, and number of steps in a Fourier transform are interrelated. Image resolution and bandwidth are inversely related such that fine resolution requires large bandwidth:

$$\Delta r = \frac{2\pi}{\Delta k} \quad (4-9)$$

Window extent (centered over the body) is an integral number of resolution cells M:

$$\text{Window extent} = M \Delta R \quad (4-10)$$

M is also the order of the Fourier transform, not necessarily a power of 2. The user then arbitrarily establishes desired independent parameters and computes the others from the above two equations.

Two factors limit resolution. The first is the number of basis functions per wavelength used to represent the current distribution. If too great a resolution is requested, then one images the individual basis functions. This is not physical. The second consideration is more fundamental. Since the spatial current behavior is inherently on a wavelength scale, it makes little sense to specify resolutions greater than $\lambda/2$.

In MOM3D the user specifies an *exact* window extent and an approximate resolution to compute the number of increments M in k^* space. The actual resolution is then recomputed using M. The bistatic electric field produced from the currents excited on the body is computed at these M k space locations in down range or at M by M k space

locations for 2-D down/cross range images. The Fourier transform is then done using a Fast Fourier Transform algorithm. Since the FFT requires data arrays that are powers of two, the data are padded with zeros to the next largest 2^N . Zero padding smooths the resulting transformed image data, however, the original resolution remains unchanged.

The radiation integral used to evaluate E^* requires that \mathbf{k}^{ext} be input in terms of rectangular coordinates. The fundamental variation for \mathbf{k}^{ext} is (k_r, k_θ, k_ϕ) . We must transform this representation back into a rectangular form. If we are computing an image from angular location (θ, ϕ) , then the rectangular form for \mathbf{k} is just the usual vector sum of components. Two cases occur. The first is for an "azimuth" or ϕ directed cross range direction where (k_r, k_θ) are transformed:

$$\begin{aligned} k_x^s &= k_r \sin\theta \cos\phi - k_\theta \sin\phi \\ k_y^s &= k_r \sin\theta \sin\phi + k_\theta \cos\phi \\ k_z^s &= k_r \cos\theta \end{aligned} \quad (4-11)$$

while for an "elevation" or θ directed cross range direction the transform of (k_r, k_θ) becomes

$$\begin{aligned} k_x^s &= k_r \sin\theta \cos\phi - k_\theta \cos\phi \cos\theta \\ k_y^s &= k_r \sin\theta \sin\phi + k_\theta \sin\phi \cos\theta \\ k_z^s &= k_r \cos\theta - k_\theta \sin\theta \end{aligned} \quad (4-12)$$

Lastly, the form for the windowing weight function W is unity at the array center and tapers to zero at the array ends. A radial hat function may be used, [14], or a dual weight function with a separate function for rows and columns may be used.

Cross Range Direction Rotation: For two dimensional images one may choose the cross range direction in either the ϕ or θ directions. The ϕ cross range direction corresponds to an azimuth rotation about the Z axis. This would be the typical case for an aircraft geometry coordinate system in which the Z axis is vertical. The θ cross range direction corresponds to a polar angle (elevation) rotation about an axis in the X-Y plane that is perpendicular to the specified azimuth direction ϕ .

Rotation Center: The image is computed by varying the down and cross range values of \mathbf{k}^{ext} . Down range direction implies that the corresponding radial direction *points* toward the origin of the coordinate system. This origin is then the center of the image window extent for the resulting image. Often, however, the coordinate system for the body geometry has an origin that is not necessarily where one wishes the center of the window extent. For example, most aircraft coordinate systems define an origin at or near the vehicle nose. For imaging, one would like to place the origin midway down the body so that the resulting image fills the window extent. To accomplish this translation shift of coordinates, a user could change all the vehicle coordinates in the geometry model file. A simpler approach is to introduce a phase shift that corresponds to the desired coordinate translation.

The \mathbf{k} space scattered field for the original or "old" bistatic scattered field radiation integral is :

$$\vec{E}_{\text{old}}^{\text{scat}}(\vec{k}^s) = \int \vec{J}(\vec{k}') e^{-j\vec{k}' \cdot \vec{R}} dS \quad (4-13)$$

When a new reference origin, $\mathbf{R}_{\text{new origin}}$, is defined relative to the previous body origin, then the new image transform becomes:

$$\begin{aligned}\vec{E}_{\text{new}}^{\text{scat}}(\vec{k}^s) &= \int \vec{J}(\vec{k}^i) e^{-j\vec{k}^s \cdot (\vec{R} - \vec{R}_{\text{new}})} dS \\ \vec{E}_{\text{new}}^{\text{scat}}(\vec{k}^s) &= e^{-j\vec{k}^s \cdot \vec{R}_{\text{new}}} \int \vec{J}(\vec{k}^i) e^{-j\vec{k}^s \cdot \vec{R}} dS \quad (4-14) \\ \vec{E}_{\text{new}}^{\text{scat}} &= e^{-j\vec{k}^s \cdot \vec{R}_{\text{new}}} \vec{E}_{\text{old}}^{\text{scat}}\end{aligned}$$

Therefore a coordinate shift is implemented as a phase shift at each k space scattered field value prior to Fourier transforming the data. We do need to remember that the coordinate rotation matrix then applies for a given viewing angle:

$$\begin{bmatrix} x_{\text{rot}} \\ y_{\text{rot}} \end{bmatrix} = \begin{bmatrix} \cos(\theta) & -\sin(\theta) \\ \sin(\theta) & \cos(\theta) \end{bmatrix} \begin{bmatrix} x \\ y \end{bmatrix} \quad (4-15)$$

Example results for down and down / cross range are shown in the example results section.

SECTION 6

NEAR FIELD COMPUTATIONS

The theory for computing near zone electric fields is presented. Near fields are computed from body current distributions that result from a specified voltage vector excitation and system impedance matrix. The theory applies for electric current sources and therefore applies for boundary conditions corresponding to a perfect electric conductor or to resistive surfaces. When compared to far zone fields, the near zone field computation requires the addition of the scalar potential term to the formulation.

Near surface electric fields are of interest to understand the scattering process and to evaluate E field magnitude, phase, and direction on or near a surface. Quantities involved are the total field, the incident field, and the scattered field. The computation of surface E fields is the first step in computing surface power flow.

Far field radiation is usually of interest and is computed by most all algorithms (including MOM3D). The far field is directly proportional to the transverse components of the vector potential and is used to compute radar cross section or antenna gain patterns.

The near field, in contrast, involves both the scalar and vector potential (conservative and solenoidal sources). While the near field expression is perfectly valid for the far field, one seldom goes to the trouble to compute the more complicated expression if only the far field is of interest.

Far field scattered radiation field lines are solenoidal, i.e., they close back on themselves without ending on a charge source while near fields have both solenoidal and conservative vector components. On a perfect electric conductor (PEC) surface the field lines originate on the induced surface charges. Near a PEC surface the field is dominated by the scalar rather than the vector potential and the field can be represented as a quasi static. As the field point moves away from the surface, the vector potential term increases its contribution.

In the far field the radial field from the scalar potential identically subtracts from the radial vector potential component leaving only the transverse components of the vector potential as the final contributor to the far field radiation.

Far field radiation usually involves the scattered field, i.e., that radiated by the surface currents. Near field radiation, in contrast, must consider the total, incident, and scattered fields, $\mathbf{E}^t = \mathbf{E}^i + \mathbf{E}^s$.

Boundary conditions for a perfect electric conductor (PEC) require zero tangential total electric field, i.e., a PEC surface is a short circuit that does not support a tangential electric field. Only a perpendicular field can exist at the surface of a PEC. \mathbf{E}^t is composed of the incident field \mathbf{E}^i and the field scattered by the body, \mathbf{E}^s . The physical process by which the boundary condition is satisfied is by induced surface charge and current. The scattered field caused by these sources, \mathbf{E}^s , is equal in magnitude but opposite in direction to the incident field \mathbf{E}^i on the body surface (tangential component). The total tangential field is zero, $\mathbf{E}_{tan}^t = [\mathbf{E}^i + \mathbf{E}^s]_{tan} = 0$ and thus $\mathbf{E}_{tan}^s = -\mathbf{E}_{tan}^i$.

Scattered Electric Fields: The fundamental theory for near zone scattered field is reviewed and the expressions for incorporation into MOM3D are derived. A discussion of the various field types and their physical meaning is then discussed.

Currents and charges induced on a scattering body radiate both electric and magnetic fields. A far field EM wave is composed of transverse components of \mathbf{E} and \mathbf{H} whose magnitudes are related by the impedance of free space, $Z = E / H = [\mu_0 / \epsilon_0]^{1/2} = 377 \approx 120 \pi$ Ohms. In the far field, \mathbf{E} and \mathbf{H} are not independent quantities, we may compute either.

In the near field, \mathbf{E} and \mathbf{H} are not related and must be computed separately. In this work we compute only the scattered electric field.

The time and frequency dependence of the fields have been assumed to be time harmonic and monochromatic, $e^{i\omega t}$.

Electromagnetic theory tells us that the scattered electric field is composed of vector and scalar potential terms for the solenoidal and conservative components of the vector field. When dealing with PEC or RBC boundary conditions, only electric current and charges are sources of the scattered field. In the more generalized case where magnetic currents and charges are required, additional terms are needed.

The expression for the scattered field at spatial position \mathbf{r}_f is:

$$\vec{E}^{scat}(\vec{r}_f) = -j\omega \vec{A} - \nabla_f \Phi \quad (6-1)$$

where j is the square root of -1 , ω is the radian frequency $2\pi f$, \mathbf{A} is the vector potential and Φ is the scalar potential with the gradient taken with respect to the field coordinates.

The vector potential \mathbf{A} is an integral over the vector surface currents:

$$\vec{A} = \mu_0 \int \vec{J} g dS \quad (6-2)$$

where μ is the permeability and \mathbf{J} the surface current. The Green's function is

$$g(\vec{r}_f, \vec{r}_s) = \frac{e^{-jk(\vec{r}_f - \vec{r}_s)}}{4\pi |\vec{r}_f - \vec{r}_s|} \quad (6-3)$$

where \mathbf{k} points in the direction of the scattered field and has magnitude of $2\pi/\lambda$, and the vector \mathbf{R} is from the source coordinate \mathbf{r}_s to the field coordinate \mathbf{r}_f , i.e., \mathbf{R} points away from the source point.

The scalar potential has electric charge as its source:

$$\Phi(\vec{r}_f) = \frac{1}{\epsilon_0} \int \sigma g dS \quad (6-4)$$

where σ is the electric surface charge density.

Surface current \mathbf{J} and charge density σ are not independent quantities. They are related by the requirement of charge continuity as expressed by:

$$\nabla_s \cdot \vec{J} = -j\omega \sigma \quad (6-5)$$

where the surface divergence (derivative) is with respect to source coordinates. Thus we can rewrite the expression for the scattered field entirely in terms of the surface current \mathbf{J} :

$$\bar{\mathbf{E}}^{scat}(\vec{r}_f) = -jk\eta \int [\vec{J}g + (\nabla_s \cdot \vec{J}) \nabla_f g / k^2] dS \quad (6-6)$$

where we have used $k\eta = \omega\mu$ and $\omega\epsilon = k/\eta$ where $\eta (=377)$ is the impedance of free space. ∇_f is a derivative operator on the field coordinates and slides through to $g(\mathbf{r}_b, \mathbf{r}_s)$. The last step is to use the relationship that $\nabla_f = -\nabla_s$ and that the gradient of the Green's function on the source coordinates is expressed as:

$$\nabla_s g(\vec{r}_f, \vec{r}_s) = -(1 + jkR) \frac{\vec{R}}{|\vec{R}|^2} g \quad (6-7)$$

where the vector $\mathbf{R} = \mathbf{r}_f - \mathbf{r}_s$ is from the source to field point.

Finally, we combine the above to arrive at the expression for the scattered field:

$$\bar{\mathbf{E}}^{\text{scat}}(\vec{r}_f) = -jk\eta \int [\bar{\mathbf{J}} - (\nabla_s \cdot \bar{\mathbf{J}})(1 + jkR)(\vec{r}_f - \vec{r}_s)/(kR)^2] g dS \quad (6-8)$$

This is our desired result which is a function of the surface current \mathbf{J} . It is evident that this expression involves additional computation when compared to that required for only the far field. Once \mathbf{J} is computed for a specific frequency and excitation the near zone electric field is computed with this expression.

Scattered Field Expression for MOM3D: All that remains now is to express the current vector \mathbf{J} in the basis function representation used in the surface patch model of MOM3D. The triangular couple sub-domain basis function expansion is:

$$\bar{\mathbf{J}} \approx \sum_{i=1}^N j_i \bar{f}_i(\bar{\rho}) \quad (6-9)$$

where j_i is the complex current coefficient determined from the solution and $f(\rho)$ is the vector basis function:

$$\bar{f}_q(\vec{r}) = \begin{cases} \frac{S_q^+ l_q}{2A_q^+} \bar{\rho}_q^+ & ; S_q^+ = +1 ; \text{ for } \vec{r} \in A^+ \\ \frac{S_q^- l_q}{2A_q^-} \bar{\rho}_q^- & ; S_q^- = -1 ; \text{ for } \vec{r} \in A^- \end{cases} \quad (6-10)$$

where ρ is the vector from the triangle vertex to any point in the triangle, l_q is the length of the qth edge, and A_q is the area of the qth triangle. This basis function has the property that its magnitude is unity any time ρ lies on the edge l . The surface divergence of the basis function has the form:

$$\nabla_s \cdot \vec{f}_q = \begin{cases} \frac{S_q^+ l_q}{A_q^+} & ; \quad S_q^+ = +1 \\ \frac{S_q^- l_q}{A_q^-} & ; \quad S_q^- = -1 \end{cases} \quad (6-11)$$

We note that the vector ρ points from the vertex to the opposite edge of the basis triangle. Current flows from the + triangle of the couple to the - triangle (by definition). MOM3D geometry defines ρ as pointing away from the vertex, despite whether the triangle is + or -. Thus we introduce a unity sign term that is either + or - depending on which triangle of the couple is being considered (or zero if the triangle edge does not have a common neighbor).

Combining the above expression for \mathbf{J} and $\nabla \cdot \mathbf{J}$ into the expression for scattered field, and replacing the integral with a sum over couples, we obtain the expression used in MOM3D to compute the scattered near field:

$$\vec{E}^{scat}(\vec{r}_f) = -jk\eta \sum_{i=1}^N \sum_{v=1}^3 \frac{l_v}{A_i} j_v S_v \int [\frac{\vec{\rho}_v}{2} - \frac{(1+jkR)}{(kR)^2} \vec{R}] g(\vec{r}_f, \vec{r}_s) dS \quad (6-12)$$

where the first summation is over all the triangles and the second summation is over each vertex. This sum is over all the current couples.

The integral over the triangle is approximated using the centroid approximation (similar to MOM3D matrix elements), i.e., the integrand is approximated by its value at the triangle centroid:

$$\frac{1}{A} \int F(\vec{r}) dS \approx F(\vec{r}_c) \quad (6-13)$$

where \mathbf{r}_c is the centroid. Using centroid evaluation for the integrand yields the desired expression for the scattered field:

$$\vec{E}^{scat}(\vec{r}_f) = -jk\eta \sum_{i=1}^N \sum_{v=1}^3 l_v j_v S_v \left[\frac{\vec{\rho}_{v,c}}{2} - \frac{(1 + jkR_c)}{(kR_c)^2} \vec{R}_c \right] g(\vec{r}_f, \vec{r}_{s,c}) \quad (6-14)$$

where $\mathbf{R}_c = \mathbf{r}_f - \mathbf{r}_{s,c}$ and $\mathbf{r}_{s,c}$ is the centroid of the source triangle.

Every Thing You Wanted to Know About Complex Vectors But Were Afraid to Ask: The vector quantities have components that are complex numbers. Each spatial vector component has its own magnitude and phase. Each vector is understood to be multiplied by the time dependence factor $e^{j\omega t}$.

Real world physical quantities, however, are not complex. Complex notation is the formal process by which the time delay due to the finite speed of propagation is expressed by phase (delay). The physical quantity is always understood to be the REAL part of the complex number. For an arbitrary complex vector \mathbf{E} with $e^{j\omega t}$ time dependence, the physical value is the REAL part:

$$\vec{E}_{\text{physical}} = \Re(\vec{E}e^{j\omega t}) = \sum_{i=1}^3 |\vec{E}_i| \Re(e^{j(\phi_i + \omega t)}) \hat{e}_i \quad (6-15)$$

where $|\vec{E}_i|$ and ϕ_i are the magnitude and phase of each vector component of \vec{E} and the sum is over the three vector components with unit direction \hat{e}_i . The physical vector quantity can then be written in rectangular coordinates as:

$$\vec{E}_{\text{physical}} = |E_x| \cos(\phi_x + \omega t) \hat{x} + |E_y| \cos(\phi_y + \omega t) \hat{y} + |E_z| \cos(\phi_z + \omega t) \hat{z} \quad (6-16)$$

where we have used the identity $e^{ix} = \cos(x) + j \sin(x)$ and where (x,y,z) are the standard unit vectors for an orthogonal representation.

We see that this complex time harmonic vector changes direction in space as a function of time. We could display this time dependent behavior by adding ωt time increments between $[0, 2\pi]$ to create a dynamic moving display of the solution.

However we also can investigate the two principal directions of the vector by taking the REAL or IMAG parts of the complex vector. To illustrate, we first set time to zero, $\omega t = 0$, obtaining:

$$\begin{aligned} \vec{E}_{\text{physical}}(\vec{r}, \omega t = 0^\circ) &= |E_x| \cos(\phi_x + 0) \hat{x} + |E_y| \cos(\phi_y + 0) \hat{y} + |E_z| \cos(\phi_z + 0) \hat{z} \\ &= \Re E_x \hat{x} + \Re E_y \hat{y} + \Re E_z \hat{z} \\ &= \Re \vec{E}(\vec{r}) \end{aligned} \quad (6-17)$$

while if we set time to - 90 degrees, $\omega t = -\pi/2$, we obtain:

$$\begin{aligned}
 \vec{E}_{\text{physical}}(\vec{r}, \omega t = -90^\circ) &= |E_x| \cos(\phi_x - 90) \hat{x} + |E_y| \cos(\phi_y - 90) \hat{y} + |E_z| \cos(\phi_z - 90) \hat{z} \\
 &= |E_x| \sin(\phi_x) \hat{x} + |E_y| \sin(\phi_y) \hat{y} + |E_z| \sin(\phi_z) \hat{z} \\
 &= \Re E_x \hat{x} + \Re E_y \hat{y} + \Re E_z \hat{z} \\
 &= \Re \vec{E}(\vec{r})
 \end{aligned} \tag{6-18}$$

The REAL and IMAG components of the vector E represent the two basis vectors (magnitude and direction) that describe the time varying vector. The IMAG part lags the REAL part by 90 degrees. A plot of REAL(E) and IMAG(E) will show two snapshots in time of how the time varying vector behaves. *Every other point in time will be linear combination of these two vectors.*

We now review the idea of time average quantities. Sensors seldom measure actual time variation, rather a time average value is "sensed." The scalar root mean square (RMS) time average of a vector quantity is obtained by averaging the real components:

$$E_{\text{ave}} = \langle \Re(\vec{E} e^{j\omega t}) \cdot \Re(\vec{E} e^{j\omega t}) \rangle^{1/2} \tag{6-19}$$

where $\langle \rangle$ indicates an average (integral) over $\omega t = 0$ to 2π divided by 2π and we have taken the dot product of the two REAL vectors. Each component of the dot product has a term that is proportional to:

$$\frac{|\mathbf{E}_i|^2}{2\pi} \int_0^{2\pi} \cos^2(\phi_i + \omega t) d(\omega t) = \frac{|\mathbf{E}_i|^2}{2} = \frac{\mathbf{E}_i \mathbf{E}_i^*}{2} \quad (6-20)$$

where * indicates the complex conjugate for each vector component i. Thus the RMS time average of a complex vector is simply obtained as:

$$E_{average} = \frac{(\bar{\mathbf{E}} \cdot \bar{\mathbf{E}}^*)^{1/2}}{\sqrt{2}} \quad (6-21)$$

where we recognize that $\sqrt{1/2} = 0.707$ is the root mean square (rms) average of a sinusoidal varying quantity that has a unity peak value.

While the above discussion was for arbitrary complex vectors, we now review the specific vectors required in this work. They are the incident field \mathbf{E}^i , the scattered field \mathbf{E}^s , and the total field \mathbf{E}^t .

The incident field is specified by a plane wave with polarization, wavelength, and direction of propagation:

$$\bar{\mathbf{E}}^{inc} = \hat{\mathbf{u}}^0 \text{ or } \mathbf{E}_0 e^{-j\mathbf{k} \cdot \mathbf{R}} \quad (6-22)$$

where \mathbf{u} is the polarization unit vector, \mathbf{k} is the direction of propagation, and \mathbf{E}_0 is the scalar amplitude. In MOM3D we take $\mathbf{E}_0 = 377$ which represents a unity value for the associated magnetic field \mathbf{H}_0 . This is done so that the currents are then normalized to \mathbf{H}_0 for comparison to Physical Optics values, $2\pi\mathbf{H}^i$.

The scattered field E^s is that due to currents on the scattering surfaces given by the previously derived expressions.

The total field E^t is the vector sum of the incident and scattered fields, $E^t = E^i + E^s$.

Near the scattering body, we mostly are interested in the total field since that is what a measurement probe (either dynamic or average) would measure. In the far field, a measurement probe, e.g., a radar receiver, would still measure the total field, but since the transmitted field has been turned off (and is in the opposite direction) when the scattered energy arrives back from the target, the measured quantity is just the scattered field E^s .

Formulation When the Field Point is Near Surface: When the field point for computing the scattered field is within one triangle dimension of the surface, the centroid approximation breaks down due to the $1/R$ and $1/R^2$ singularities in the formulation. The physical field is of course finite being due chiefly to the surface perpendicular field from the surface charge density σ . This section discusses the analytical approach used for computing the scattered field when the field point is very near the surface.

Several approaches could be developed. One could better approximate the singular integral with either a closed form analytical integration (if it could be derived!) or develop a surface numerical integration scheme. But, since only those few field points very near the body surface are affected by the singularity, it is not worth while to develop elaborate schemes to "fix" the problem. Thus the following approximation is used.

When the field point is on the surface with $R = 0$, the singular self patch field is its perpendicular value. This same vector value is then used to approximate the near surface self field as the field point moves away from the surface to a distance no greater than a triangle dimension.

Electromagnetic theory and boundary conditions tell us that the surface parallel and perpendicular fields are (for a general surface):

$$\vec{E}_\perp^{s, self} = \frac{\sigma}{2\epsilon_0} \hat{n} \quad \vec{E}_\parallel^{s, self} = -\frac{\vec{M} \times \hat{n}}{2}$$

(6-23)

$$\vec{H}_\perp^{s, self} = \frac{\sigma^*}{2\mu} \hat{n} \quad \vec{H}_\parallel^{s, self} = \frac{\vec{J} \times \hat{n}}{2} \quad (\text{Physical Optics Assumption})$$

where (σ, \mathbf{J}) and (σ^*, \mathbf{M}) are the local surface electric and magnetic charge density and current. For our MOM3D analysis, we have only resistive and perfect electric conductor boundary conditions, therefore equivalent magnetic sources do not exist, thus:

$$\vec{E}_\perp^{s, self} = \frac{\sigma}{2\epsilon_0} \hat{n} \quad \text{and} \quad \vec{E}_\parallel^{s, self} = 0$$

(6-24)

We thus make the assumption that very near the surface, the fields are the same as on the surface. We will approximate the self field with the above expression whenever $R = R_t - r$, is less than approximately one linear triangle dimension and use the centroid approach whenever $R > d$.

The self patch parallel field is zero. The perpendicular component is developed by expressing the surface charge density in terms of the surface divergence of current:

$$\vec{E}_\perp^{\text{scat, self}} = \frac{\sigma}{2\epsilon_0} \hat{n} = \frac{j\eta \nabla \cdot \vec{J}}{2k} \hat{n}$$

where $\nabla \cdot \vec{J} = -j\omega\sigma$, and $\omega \in -k/\eta$ (6-25)

Dimensional Check : $\frac{\text{ohm}}{1/m} \frac{\text{amps/m}}{m} = \frac{\text{volts}}{\text{meter}}$

In MOM3D, the triangle couple basis functions result in the following expression for the surface divergence:

$$\nabla \cdot \vec{J}_i = +\frac{l_i}{A_i^+} \text{ or } -\frac{l_i}{A_i^-} \quad (6-26)$$

The resulting expression for the i th self patch perpendicular field is thus:

$$E_{i,\perp}^{\text{scat, self}} = \pm \frac{j\eta l_i}{2k A_i^\pm} j_i \quad (6-27)$$

This expression is used for evaluating near surface patch fields where the $1/R$ singularities dominate. For field points further away, the previous approach using the centroid approximation to the integral is used.

SECTION 7

MONOSTATIC and BISTATIC RADAR CROSS SECTION

Monostatic (backscatter) and bistatic radar cross section may be computed in MOM3D. The body is excited via a plane wave from a specified direction in space, \mathbf{k}^{inc} , and the resulting body currents are computed. The far field radiation resulting from these currents is then computed. For backscatter RCS, the scattered field is computed at the same angular location as the source radiation. For bistatic RCS the scattered field is computed at angle cuts specified by the user. The required theory for computing radar cross section is presented.

Polarization Scattering Matrix: A complete electromagnetic scattering description is contained in the polarization scattering matrix that relates the two possible transverse incident field vectors to the two possible scattered field vectors. Only two components of \mathbf{E} are allowed since Maxwell's equations require that the \mathbf{E} field be transverse to the direction of propagation. The polarization scattering matrix relates the incident field vector to the scattered field vector:

$$\vec{E}^{\text{scat}} = \tilde{S} \vec{E}^{\text{inc}} \quad (7-1)$$

where S is a 2 by 2 dyadic (tensor) that relates the components of \mathbf{E}^{scat} to \mathbf{E}^{inc} :

$$\begin{bmatrix} E^{\text{scat},\theta} \\ E^{\text{scat},\phi} \end{bmatrix} = \begin{bmatrix} S^{\theta,\theta} & S^{\theta,\phi} \\ S^{\phi,\theta} & S^{\phi,\phi} \end{bmatrix} \begin{bmatrix} E^{\text{inc},\theta} \\ E^{\text{inc},\phi} \end{bmatrix} \quad (7-2)$$

The diagonal terms are the two independent co-polarized scattering elements while the off diagonal terms are the two cross polarized scattering terms. The scattering matrix completely represents the scattering properties of a target. The four terms of S are complex, each with amplitude and phase. The elements of S are related to RCS:

$$S_{ij} = \sqrt{\frac{\sigma_{ij}}{4\pi r^2}} \quad (7-3)$$

E^{inc} and E^{scat} are independent functions of angle, thus the elements of S become functions of the source and receiver angular coordinates,

$$S_{ij} = S_{ij}(\theta^{scat}, \phi^{scat}; \theta^{inc}, \phi^{inc}) \quad (7-4)$$

All possible electromagnetic scattering information is contained in the polarization scattering matrix. Huynen [15] and others have attempted to characterize (and therefore identify) target properties such as size, orientation, symmetry, de-polarization, and characteristic angles, etc. from the information contained in S.

MOM3D has the potential to compute the complete scattering matrix for both linear and circular polarization.

Radar Cross Section Definition: We generally do not work directly with the polarization scattering matrix S, we deal with the components of S as expressed by the co- and cross-polarized radar cross section. Radar Cross Section (RCS) is a measure of the power scattered by a target normalized to the power density incident on a target. Except for incident and received polarization, RCS is defined to be independent of specific radar system parameters such as transmitter power, receiver sensitivity, range to target, etc..

The definition of RCS assumes an incident plane wave on the target (which physically does not exist!). The scattered field is then computed or measured far from the target to avoid near field effects. Radar cross section is formally defined as the far field scattered power density normalized to the incident power density at the target:

$$\sigma^{\alpha,\beta} = \lim_{r \rightarrow \infty} 4\pi r^2 \frac{P^{\text{scat},\alpha}}{P^{\text{inc},\beta}} ; \quad P \propto E^2 \text{ or } H^2 \quad (7-5)$$

where α and β represent the polarization (θ or ϕ) of the scattered and incident radiation. RCS, while independent of specific radar system parameters, is a function of: target geometry; frequency (or wavelength); incident polarization; received polarization; and the angular position of the source and receiver:

$$\sigma^{\alpha,\beta} = \sigma^{\alpha,\beta}(\theta^{\text{scat}}, \phi^{\text{scat}}; \theta^{\text{inc}}, \phi^{\text{inc}}) \quad (7-6)$$

The power density for an electromagnetic wave is the sum of the E and H field components. For plane waves the E and H fields are related via wave impedance. Thus wave power density can be expressed entirely in terms of either E or H. Once the body currents are obtained, RCS may be computed via either E or H since in the far field they are related by $\eta = E / H$. Typically we compute the scattered E field assuming E^{inc} is unity. However, it is of more interest to have $H^{\text{inc}} = 1$ so that we may compare resulting currents to normalized physical optics values, $J = 2n \times H^{\text{inc}}$.

Radar cross section computation requires a scattered field, which in turn requires a body current distribution as excited by an incident plane wave. The formal theory for the plane wave voltage vector was presented in Section 2 and 3. Once a body impedance matrix has been computed and LU decomposed (or the inverse found), body currents corresponding

to the voltage vector are determined. The field radiated by these currents is computed using the row measurement vector (Sections 2 & 3).

The voltage vector used to compute the body currents is a function of the angular coordinates and polarization of the illumination source while the row measurement vector is a function of the angular coordinates and polarization of the receiver:

$$\bar{R}^a = \bar{R}^a(\theta^{scat}, \phi^{scat}) ; \quad \bar{V}^b = \bar{V}^b(\theta^{inc}, \phi^{inc}) \quad (7-7)$$

Radar cross section can then be defined in terms of the row measurement vector and body currents:

$$\sigma^{\alpha, \beta} = \frac{k^2}{4\pi} |\bar{R}^a \cdot \bar{j}^b|^2 \quad (7-8)$$

where we have assumed $E^{inc} = \eta = 377$. For the co-polarized case, $\alpha = \beta = \theta$ or ϕ . The current vector j is formally expressed as the inverse of the system impedance matrix times the excitation voltage vector:

$$\bar{j}^b = [\bar{Z}]^{-1} \bar{V}^b \quad (7-9)$$

Monostatic Case: Backscatter RCS is computed by evaluating the row measurement vector at the angular location of the plane wave source illumination. Our Galerkin weight function approach yields the same computation form for the voltage and row measurement vectors. Thus the backscatter row vector is equal to the voltage excitation vector used to compute

the body currents, $R^*(\theta^{rec}, \phi^{rec}) = V^*(\theta^{inc}, \phi^{inc})$. Therefore the backscatter RCS subroutine does not need to compute the R row vector for the co-polarized case.

Bistatic Case: Bistatic RCS is the case where one is interested in the scattered radiation at angular locations that are not the same as the illumination source. Bistatic RCS requires specification for both illumination and receiver angles. Two cases arise:

- 1) The illumination angle is fixed relative to the body while the receiver location is moved (angle "cut"); and
- 2) The illumination source and receiver are fixed relative to each other while the body is rotated.

In case 1) only one set of currents is computed for the body and the bistatic RCS is computed by re-evaluating the row measurement vector for each receiver angle of interest. This is the most common "analytical" case and is implemented in MOM3D.

In case 2) the body currents must be computed for each new illumination angle. For this case, a new voltage and row measurement vector must be computed for each angle and V is no longer equal to R . This is the most common "experimental" case and corresponds to rotating a target with fixed illumination and receiver angular locations (with constant angle between). This case is not presently implemented.

In each case the row measurement vector must be computed at the new receiver angle. This is done in MOM3D using the subroutine that computes the voltage vector V .

SECTION 8

CURRENT COMPUTATION

In efforts to understand the radiation and scattering mechanisms it is often desirable to display the current distribution on the body as caused by either an incident plane wave (as in a scattering case) or by local surface "port" excitation (as in an antenna problem). This section discusses a few of the issues required to compute the currents, spatial and temporal average values, and the two independent time values. Current "modes" of interest might be those corresponding to: physical optics; surface traveling waves; creeping waves; edge waves; leading edge diffraction; trailing edge diffraction; and multiple bounce.

Once the body impedance matrix is computed and solved and the voltage vector specified (either as an incident plane wave or as "port" excitation), the unknown current vector \mathbf{j} is formally computed as:

$$\bar{\mathbf{j}}^p = [\bar{Z}]^{-1} \bar{\mathbf{v}}^p \quad (8-1)$$

The complex vector body currents are then given by the surface basis function expansion:

$$\bar{\mathbf{J}}^p(\bar{r}) = \sum_{i=1}^N j_i^p \bar{f}_i = \sum_{i=1}^N j_i^p \frac{l_i}{2} \left(\frac{\bar{\rho}_i^+}{A_i^+} - \frac{\bar{\rho}_i^-}{A_i^-} \right) \quad (8-2)$$

Couple Spatial Averaged Current: The basis functions are functions of position ρ within each triangle. The triangle hat basis functions can be averaged over the couple (two triangles) as suggested by the results of Section 2. On a couple basis, the current average is given by:

$$\bar{J}_q^{\text{average}} = j_q \bar{f}_q^{\text{average}} = j_q \frac{l_q (\bar{r}_q^{c+} - \bar{r}_q^{c-})}{A_q^+ + A_q^-} \quad (8-3)$$

where $r^{c\pm}$ is the centroid location of the + and - triangles of each couple. This is the quantity that should be considered as representing the surface currents. The location of this averaged vector can be taken to be either end of the vector, i.e., triangle centroids, or the midpoint location, $0.5 * (\rho^{c+} + \rho^{c-})$. If the two triangles making up the couple are not co-planar, the midpoint is not in the plane of either triangle.

Triangle Currents: The number of triangles making up the geometry is not equal to the number of current couples. Often for ease of display it is convenient to show currents at the centroid of each triangle. This can be done simply by performing a vector sum of the current couples associated with each triangle,

Figure 8-1. This sum is over one, two, or three couples depending the number of common neighbor edges. Edge triangles have one free side (two couples) while a tip triangle has two free sides (1 couple). The triangle spatial average complex vector current is thus:

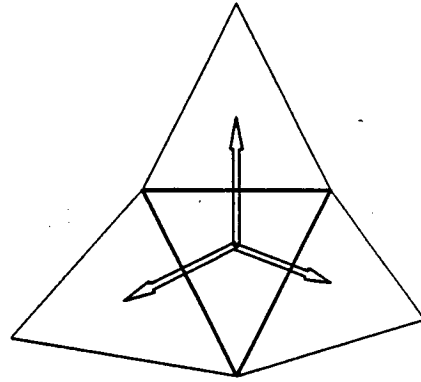


Figure 8-1 Triangle current can be considered as the sum of couple currents

$$\bar{J}_{i \text{ th triangle}}^{\text{ave}} = \sum_{q=1}^{1,2,\text{or}3} \bar{J}_q^{\text{ave}} \quad (8-4)$$

where \bar{J}_q^{ave} is computed from the previous expression.

Time Varying Vectors and Surface Current Animation: Surface currents are time varying vectors. The physical quantity is obtained by taking the real part *after* multiplying by the time phasor $e^{j\omega t}$. At each couple location the current vector sweeps out a trajectory on the surface as ωt varies between 0 and 2π . Two principal vector directions (basis vectors) from which all other values can be represented are the vectors at $\omega t = 0$ and $\omega t = -\pi/2$. These two vectors are the REAL and IMAG parts of \mathbf{J} :

$$\bar{J}_q^{\text{ave}}(\omega t = 0) = \Re \bar{J}_q^{\text{ave}} = \bar{J}_{\text{real},q}^{\text{ave}} \quad (8-5)$$

$$\bar{J}_q^{\text{ave}}(\omega t = -\pi/2) = \Im \bar{J}_q^{\text{ave}} = \bar{J}_{\text{imag},q}^{\text{ave}}$$

The surface current vector as a function of time is a linear combination of the real and imag basis vectors:

$$\bar{J}_q(\omega t) = \cos(\omega t) \bar{J}_{\text{real},q}^{\text{ave}} - \sin(\omega t) \bar{J}_{\text{imag},q}^{\text{ave}} \quad (8-6)$$

A dynamic graphical display of currents would simply vary ωt over $[0, 2\pi]$. One could display the dynamic vectors with magnitude shown as relative vector length or color. Or one could display the magnitude using a color scale without showing the vector direction. These displays would represent the dynamic currents induced on the body due either to an incident plane wave (as for RCS problems) or to local surface port excitation (as for antenna problems). For plane wave excitation one also could display the incident wave (forcing function) as it passes over the geometry.

Time Average Currents: Besides a spatial average, there is also a time average to consider. The time average is a stationary scalar quantity (not a vector) obtained by averaging the

REAL part of { $\mathbf{J} e^{j\omega t}$ } over the interval $[0, 2\pi]$. The root mean square (RMS) time average is computed in the same manner as discussed in Section 6 for near fields:

$$J_q^{\text{time ave}} = \frac{(\bar{\mathbf{J}} \cdot \bar{\mathbf{J}}^*)^{1/2}}{\sqrt{2}} \quad (8-7)$$

This stationary scalar quantity could be graphically displayed using a color magnitude scale for either the couple currents or the triangle based currents.

SECTION 9

ANTENNA FORMULATION

MOM3D can be used to compute antenna gain patterns. Since the impedance matrix represents the electrical interaction of the body with itself, independent of the excitation voltage vector, we can use a voltage vector corresponding to a local surface "port" excitation to excite body currents. Radiation from these currents is the antenna pattern. This section will discuss the voltage vector, antenna gain, radiated power density, power input, and input impedance.

Geometries operated as antennas have voltage forcing functions that are local. These can take the form of a coax feed from a transmitter or simply an open ended waveguide terminated on the surface over which there is an E field. The antenna problem does not depend on the nature of the transmitter, it depends on how the structure is excited: voltage magnitude, phase, and vector direction. This excitation induces currents on the body according to Maxwell's equations and boundary conditions.

Voltage Vector: For the antenna problem, the local surface voltage excitation occurs at any one of the surface couple basis functions. Each excited location is called a "port." For most antenna problems only one port is excited. But there may be multiple excitation ports on a body, each with its own magnitude, phase, and direction. The voltage vector forcing function takes a simple form:

$$\vec{V} = \begin{bmatrix} 0 \\ 0 \\ V_i \\ 0 \\ \vdots \\ \vdots \end{bmatrix} \quad (9-1)$$

Each excited port element of \mathbf{V} is computed as before with $\mathbf{W} = \mathbf{f}$:

$$\begin{aligned}
 V_i &= \langle \vec{W}_i, \vec{E}^a \rangle \\
 &= \vec{E}^a \cdot \vec{f}_i^{ave} (\int dS^+ + \int dS^-) \\
 &= (\vec{E}^a \cdot \Delta \vec{R}_i^{c,\pm}) l_i \\
 &= V_{term} l_i \quad \text{volt-meter}
 \end{aligned} \tag{9-2}$$

where we have assumed the applied port electric field \mathbf{E}^a is constant over the couple (two triangles), the expression for \mathbf{f}^{ave} has been used, and $\Delta \mathbf{r}^{c,\pm}$ is the vector from the + to - triangle centroid. In MOM3D we take \mathbf{E} to be in the same direction as $\Delta \mathbf{r}$ so that the applied voltage across the couple V_{term} is:

$$V_{term} = \int \vec{E}^a \cdot d\vec{l} \approx E^a \Delta r \tag{9-3}$$

In MOM3D we input the value of V_i directly so that the terminal voltage is expressed as:

$$V_{term} = \frac{V_i}{l_i} \tag{9-4}$$

Once V_i has been input for one or more excited ports, the body currents are computed in the normal manner:

$$\vec{j} = [\bar{\mathbf{Z}}]^{-1} \vec{v} \tag{9-5}$$

The far field radiation at specified angular direction and polarization $\alpha = \theta$ or ϕ is computed in the usual fashion in terms of the row measurement vector for the desired polarization:

$$E^{\text{scat},\alpha}(\theta, \phi) = -jk\eta \frac{e^{-jkR_0}}{4\pi R_0} [\vec{R}^\alpha(\theta, \phi) \cdot \vec{j}] \quad (9-6)$$

Antenna Gain: The antenna pattern or gain is computed in terms of the far field radiation power density normalized to the input power to the antenna (assuming the input power is radiated isotropically and that we have unity efficiency):

$$G(\theta, \phi) = \frac{P^{\text{rad}}(\theta, \phi)}{\left(\frac{P^{\text{input}}}{4\pi R^2} \right)} = 4\pi R^2 \frac{P^{\text{rad}}(\theta, \phi)}{P^{\text{input}}} \quad (9-7)$$

where P^{input} has units of watts while P^{rad} has units of power density, watts/meter², i.e., is the Poynting vector of the far field radiation. The astute reader will notice the similarity of this definition to that for radar cross section.

In the far field where $E / H = \eta = 377$, the power density is the REAL part of the Poynting vector:

$$P^{\text{rad}} = 0.5 \Re(\vec{E} \times \vec{H}^*) = \frac{|\vec{E}^{\text{scat},\alpha}|^2}{2\eta} \quad (9-8)$$

where * represents the complex conjugate and the factor of 1/2 results from using the root mean square value for the field quantities.

The power input to the antenna is the sum of input powers (real part) of all the excited ports:

$$P^{\text{input}} = 0.5 \sum_{i=\text{port}=1}^{N\text{ports}} \Re(V_{term} I_{term}^*) \quad (9-9)$$

The current at each port is the computed current density j (amps/meter) times the common edge length:

$$I_{term} = j_i l_i \quad (9-10)$$

The terminal voltage was previously given in terms of the port voltage vector so that the input power to the antenna is computed in terms of the input voltage port value V_i and resulting current coefficient j_i :

$$P^{\text{input}} = 0.5 \sum_{i=\text{port}=1}^{N\text{ports}} \Re(V_i j_i^*) \quad (9-11)$$

The final expression for antenna gain relative to isotropic is then

$$G^\alpha(\theta, \phi) = \frac{k^2 \eta}{8\pi} \frac{|\vec{R}^\alpha \cdot \vec{j}|^2}{P^{\text{input}}} \quad (9-12)$$

This is the antenna pattern for polarization $\alpha = \theta$ or ϕ . When expressed in decibels it is known as dBi, i.e., dB relative to isotropic. A half wave dipole has a figure eight gain pattern with broadside maximum of approximately 2.1 dBi.

Input Impedance and Admittance: Another quantity that is often of interest is the input impedance of the antenna at each excited port. This is obtained directly from the definition as the ratio of port voltage to current:

$$Z_{\text{input}} = \frac{V_{\text{term}}}{I_{\text{term}}} = \frac{V_i}{j_i l_i^2} \quad (9-13)$$

Z has both amplitude and phase. The real part is the radiation resistance while the imaginary part represents energy storage, either capacitive or inductive (current lagging or leading). A half wave dipole at resonance has an approximate input impedance of 72 ohms. At resonance, Z is often completely real, i.e., zero degrees phase.

The input admittance is just the reciprocal of input impedance:

$$Y_{\text{input}} = \frac{1}{Z_{\text{input}}} = \frac{I_{\text{term}}}{V_{\text{term}}} \quad (9-14)$$

SECTION 10

RESISTIVE BOUNDARY CONDITIONS

Resistive Boundary Conditions (RBC) have been implemented in MOM3D. This section describes the ohms per square concept for thin resistive materials and its extension to the more general case of thin dielectric material. Resistive Boundary Condition (RBC) is then presented followed by the more involved theory for Impedance Boundary Conditions (IBC) and the approximate IBC case. This is shown to be the same as the RBC case, therefore the present RBC MOM3D can be used where the approximate IBC hold.

Resistive Sheet Concepts: Resistive Boundary Conditions (RBC) are typically used to model thin sheets whose impedance does not change with angle of incidence. Such sheets typically are thin resistive layers, usually frequency independent, or thin dielectric layers (which are frequency dependent). Thin layers are characterized by a complex sheet impedance known as Ohms per Square (OPS) that has magnitude and phase, i.e., characterized by energy dissipation and reactive storage.

Ohms per square characterization of thin resistive layers is derived directly from bulk material resistivity characterizations when the thickness τ is allowed to become a thin layer. The resistance of many materials is characterized by resistivity ρ ohm-meters or by its inverse, conductivity $\sigma = 1/\rho$, whose SI units are Siemens per meter, S/m, or mhos/m (mhos = 1/ohms).

The OPS concept is derived by considering a rectangular block of resistive material. The resistance between parallel faces of the block, R_{term} , increases with spacing l , and decreases with area A , Figure 10-1,:

$$R_{\text{term}} = \frac{\rho l}{A} = \frac{\rho l}{\tau w} = \frac{l}{\sigma \tau w} \quad (10-1)$$

where τ is material thickness and w is width.

When thickness τ becomes small, as for a thin sheet, then the resistance between terminals is expressed in terms of R_{ops} ,

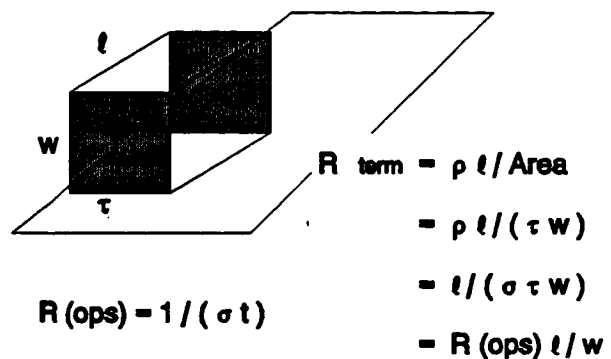


Figure 10-1 Ohms per square concept

$$R_{term} = R_{\Omega/\square} \frac{l}{w} \quad (10-2)$$

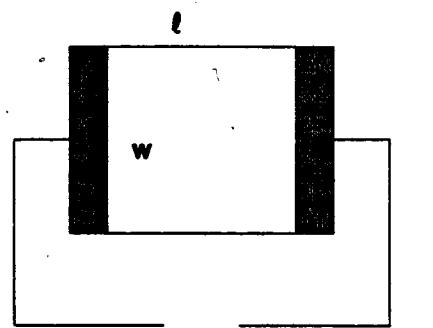
where R_{ops} has the definition

$$R_{\Omega/\square} = (\sigma \tau)^{-1} \quad (10-3)$$

R_{ops} then becomes the electrical characterization of the material rather than specifying conductivity σ and thickness τ . The resistance R_{term} between sheet ends becomes, Figure 10-2,

$$R_{term} = R_{\Omega/\square} \frac{l}{w} \quad (10-4)$$

If one measured R_{term} between the ends of a square sheet, where $t = w$, then $R_{term} = R_{ops}$ therefore the name Ohms per Square. While we generally are interested in the values of R_{ops} at microwave frequencies, experience has shown that conductivity is usually frequency insensitive, therefore a DC measurement of R_{ops} is representative even at microwave frequencies. Typical values range from 0 (conducting surface) to several thousand ohms per square. A unique value is $\eta/2 = 377/2 = 188.5$ ops where Physical Optics currents are 1/2 that on a PEC surface.



$$R_{term} = R_{(ops)} t / w$$

Figure 10-2 Ohms per square (OPS)

Dielectric Thin Sheet Impedance Concepts: The generalization of thin resistive sheets, i.e., sheets characterized only by dissipation characteristics can be extended to thin sheets that also may have energy storage characteristics, such as thin dielectric material, e.g., fiberglass sheets. The concept of thin means that the electrical thickness is small compared to a free space wavelength:

$$\sqrt{\epsilon_r \mu_r} d < \lambda_0 \quad (10-5)$$

When this holds, the dielectric polarization currents perpendicular to the sheet direction are very small compared to the "in plane" currents. In plane energy storage and dissipation can then be characterized as ohms per square that is complex, i.e., amplitude and phase.

A general thin sheet expression is given by [16]:

$$R_{\Omega/\square} = \frac{-j\eta}{k(\epsilon_r - 1)\tau} = \frac{-j60\lambda}{(\epsilon_r - 1)\tau} \quad (10-6)$$

where η is the impedance of free space, $(\mu_0/\epsilon_0)^{1/2} \approx 120\pi \approx 377$ ohms, k is the wave number $2\pi/\lambda$, λ is the wavelength, and $\epsilon_r = \epsilon' - j\epsilon''$ is the relative dielectric constant. The loss part of ϵ_r is ϵ'' and when conductivity is the principal loss mechanism, which is the case for most materials of interest, it is

$$\epsilon'' = \frac{\sigma}{\omega \epsilon_0} \quad (10-7)$$

where ω is the radian frequency, σ the material conductivity, and ϵ_0 is the permittivity of free space. When ϵ'' dominates the relative dielectric constant, as it does for resistive materials, then the thin dielectric sheet impedance reduces to the resistive sheet expression (using $\omega\epsilon_0 = k/\eta$),

$$R_{\Omega/\square} \approx \frac{-j\eta}{k \left(\frac{-j\sigma}{\omega \epsilon_0} \right) \tau} = (\sigma \tau)^{-1} \quad (10-8)$$

Thin dielectric layers, at high frequencies, can have low impedances. This must be considered when backing thin R card material with dielectric support surfaces such as fiberglass ($R_{\Omega/\square} \approx 600$ ohms at 10 GHz for $\epsilon_r=4$, and $\tau = 0.040$ ns).

Resistive Boundary Conditions: In the original MOM3D code, perfect electric conductor (PEC) boundary conditions were imposed, i.e., the total tangential electric field was set to zero,

$$\vec{E}_{\text{tan}}^{\text{Tot}} = [\vec{E}^{\text{inc}} + \vec{E}^{\text{scat}}]_{\text{tan}} = 0 \quad (10-9)$$

where \vec{E}^{inc} is the incident electric field and \vec{E}^{s} is the field scattered by the body. \vec{E}^{s} scattered is an integral over the surface currents and is written in operator form as $\vec{E}^{\text{s}} = -L(\vec{J})$. The PEC boundary conditions then take the form

$$-\vec{E}_{\text{tan}}^{\text{scat}} = L(\vec{J}) = \vec{E}_{\text{tan}}^{\text{inc}} \quad (10-10)$$

A solution is obtained by taking the inner product with a set of weight functions and expanding the current density \vec{J} with a set of sub-wavelength basis functions. A matrix equation results for unknown current coefficients with the incident wave voltage vector being the solution forcing function.

Resistive Boundary Conditions for thin materials follows Ohms law, namely that the total tangential electric field is equal to the current density \vec{J} times the resistance R ,

$$\vec{E}_{\text{tan}}^{\text{Tot}} = [\vec{E}^{\text{inc}} + \vec{E}^{\text{scat}}]_{\text{tan}} = R_{\Omega/\square} \vec{J} \quad (10-11)$$

RBC boundary conditions for the EFIE take the form

$$[-\vec{E}^{\text{scat}} + R_{\Omega/\square} \vec{J}]_{\text{tan}} = [L(\vec{J}) + R_{\Omega/\square} \vec{J}]_{\text{tan}} = \vec{E}_{\text{tan}}^{\text{inc}} \quad (10-12)$$

As with the PEC approach, a solution is obtained by taking the inner product of each side with a surface vector weight function \mathbf{W} ,

$$\langle \vec{W}_q, L(\vec{J}_p) \rangle + \langle \vec{W}_q, R_{ops} \vec{J}_q \rangle = \langle \vec{W}_q, \vec{E}^{inc} \rangle \quad (10-13)$$

We see that the RBC differs from the PEC only by the term $Z_{ops} = \langle \mathbf{W}, \mathbf{R} \mathbf{J} \rangle$ that is added to the diagonal elements of the PEC body impedance matrix.

The explicit expression for Z_{ops} is obtained by using the triangle couple expansion functions defined in Section 3. The Galerkin weight functions require $\mathbf{W} = \mathbf{f}$. We then use \mathbf{f}^{ave} to compute Z_{ops} :

$$\begin{aligned} Z_{qq,ops} &\approx \langle \vec{f}_q^{ave}, R_{ops} \vec{f}_q^{ave} \rangle \\ &= \frac{l_q^2 | \vec{r}_q^{c+} - \vec{r}_q^{c-} |^2}{A_q^+ + A_q^-} \left\{ \frac{R_{ops}^+ A_q^+ + R_{ops}^- A_q^-}{A_q^+ + A_q^-} \right\} \text{ ohm-m}^2 \end{aligned} \quad (10-14)$$

where R_{ops} is the average of the value assigned to the + and - triangles of the couple.

Impedance Boundary Condition Theory: This section outlines the more general Impedance Boundary Condition (IBC) and its approximate form that reduces to the RBC.

Interest in the IBC is for application to perfectly conducting surfaces coated with a thin layer of magnetic (mag) radar absorbing material (RAM). Mag RAM differs from thin resistive layers in that performance is due to phasor cancellation as well as energy dissipation. A mag RAM coated plate is a Dallenbach layer, Figure 10-3.

IBC apply only for high index of refraction materials where the path length inside the material is always normal to the surface. When this occurs, the path length does not change with incidence angle, Figure 10-3.

In the most general case, Maxwell's equations must be solved for both electric and magnetic currents, J and M . The standard definitions for these currents are in terms of tangential surface magnetic field H and electric field E ,

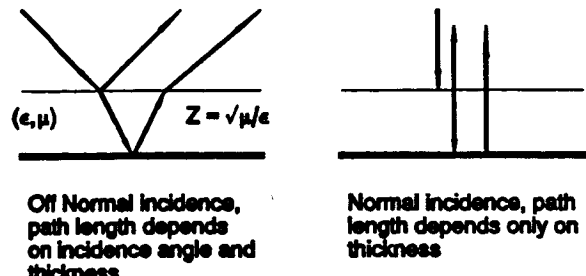


Figure 10-3 Dallenbach layer

$$\begin{aligned}\bar{J} &= + \hat{n} \times \bar{H}^{Tot} \\ \bar{M} &= - \hat{n} \times \bar{E}^{Tot}\end{aligned}\tag{10-15}$$

where \hat{n} is the local surface normal. For PEC surfaces there are no magnetic currents since $E_{tan}^{Tot} = 0$. For general impedance surfaces both H and E tangential fields can exist and we must solve for each.

Maxwells' equations in the Stratton Chu integral form for closed surfaces express the scattered E^s and H^s fields in terms of J and M source currents. The EFIE takes the form [7]:

$$\bar{E}^{scat} = - \int [j\omega \mu \bar{J}g + \bar{M} \times \nabla g - (\hat{n} \cdot \bar{E}) \nabla g] dS\tag{10-16}$$

where g is the Green's function, $\exp(-jk \cdot R) / (4\pi R)$. The corresponding MFIE is [7]:

$$\vec{H}^{scat} = \int [-j\omega \epsilon \vec{M} g + \vec{J} \times \nabla g + (\hat{n} \cdot \vec{H}) \nabla g] dS \quad (10-17)$$

It is customary [17] to express the boundary conditions in terms of L and K integral operators:

$$\begin{aligned} \vec{E}^{Tot} &= \vec{E}^{inc} - L(\vec{J}) + K(\vec{M}) \quad \text{and} \\ \vec{H}^{Tot} &= \vec{H}^{inc} - K(\vec{J}) - L(\vec{M}) / \eta_0^2 \end{aligned} \quad (10-18)$$

where $\eta_0 = 377$. The operators L and K have the definition [17]:

$$\begin{aligned} L(\vec{X}) &= j\omega \mu \int [\vec{X} + \left(\frac{\nabla \nabla \cdot \vec{X}}{\omega^2 \mu \epsilon} \right)] g \, dS \\ K(\vec{X}) &= \int \vec{X} \times \nabla g \, dS \end{aligned} \quad (10-19)$$

where X is either J or M.

From this general formulation, we see that an arbitrary impedance surface requires solving for magnetic and electric currents.

When one assumes that the surface impedance does not change with viewing angle, i.e., that the index of refraction is $n \gg 1$ such that phasor cancellation path lengths do not depend on look angle, then one can apply the impedance boundary condition.

The impedance boundary condition relates the magnetic current M to electric current J via the surface impedance Z_s ,

$$\bar{E}_{\text{tan}}^{\text{Tot}} = Z_s \bar{J} \quad (10-20)$$

which implies that [17]

$$\bar{M} = -\hat{n} \times \bar{E}^{\text{Tot}} = -Z_s \hat{n} \times \bar{J} \quad (10-21)$$

When IBC conditions apply, it reduces the unknowns from both J and M to only J . This is a very significant reduction in the complexity of the analysis and computer algorithm.

As indicated in [17], the IBC approach leads to physically correct solutions at interfaces where the refractive index of the surface layer is much greater than unity, $n = (\epsilon \mu_r)^{1/2} \gg 1$, and where the surface impedance can be expressed in terms of the surface material ϵ , μ , and thickness.

Surface impedance is constant with viewing angle if and only if the index of refraction is much greater than unity, $n \gg 1$ (see Figure 10-3). When this is the case, specular energy incident on the layer travels perpendicular to the surface when inside the material layer.

Using the IBC to eliminate the magnetic current M , reference [17] obtains:

$$\vec{E}_{\text{tan}}^{\text{inc}} - Z_s \hat{n} \times \vec{H}^{\text{inc}} = L(\vec{J})|_{\text{tan}} + Z_s K(\hat{n} \times \vec{J})|_{\text{tan}} \\ - Z_s \hat{n} \times K(\vec{J}) + Z_s^2 \hat{n} \times L(\hat{n} \times \vec{J}) / \eta_0^2$$
(10-22)

Reference [17] solved this equation for Bodies of Revolution (BOR's) by computing the L() and K() operators for the BOR coordinate system and Fourier modal basis functions.

A similar approach could be done for the MOM3D code coordinate system and basis functions if we computed the K operator in addition to the L operator matrix elements presently computed. Such a solution is clearly a large undertaking and is beyond the scope of the present effort. Several concerns, however, are the requirements for closed surfaces required for the MFIE and the vector representation of $\hat{n} \times \mathbf{J}$ for the triangular patch basis vectors.

Approximate Impedance Boundary Condition Theory: If we require that $Z_s \ll 377$ and if we approximate the K operator (which is a Fredholm integral equation of the second kind) to just its self term, then we can obtain the approximate IBC equation that has the same form as the RBC case. The K(X) operator is approximated as:

$$K(\vec{X})|_{\text{tan}} = \frac{\vec{X}}{2} + \int_{PV} \vec{X} \times \nabla g \, dS \approx \frac{\vec{X}}{2}$$
(10-23)

This approximation is the tangent plane approximation, valid for surfaces whose radii of curvature are large compared to λ , or is valid for planar surfaces away from edges. This is identical with the Physical Optics approximation where the surface field is due only to local sources and does not have contributions from other surface regions. When this approximation is made with the requirement that $Z_s \ll \eta_0 = 377$, the approximate IBC equation is obtained

$$L(\vec{J}) + Z_s \vec{J} = E_{\text{tan}}^{\text{IBC}} \quad (10-24)$$

This is the same form as the RBC. Thus the approximate IBC is the same as the RBC that has been implemented in MOM3D.

Summary: The resistive boundary condition expressions have been derived. The RBC can be applied to thin resistive or dielectric sheets whose surface impedance is not a function of illumination angle or polarization.

Impedance boundary conditions were reviewed. The material coating requirement to apply the IBC is that the index of refraction in the coating be $n >> 1$ so that the surface impedance is not a function of illumination angle.

An approximate form of IBC was developed that required that the surface impedance be $Z_{\text{surf}} \ll 377$. For this case, the approximate IBC formulation is the same as the RBC formulation.

SECTION 11

SYSTEM MATRIX SOLUTION

The motivation for this section is to remind ourselves of matrix solution considerations that are a fundamental requirement for method of moments solutions. Topics discussed are the system matrix, its dependence on linear body size, factors leading to matrix ill conditioning, and a discussion of the matrix condition number.

System Matrix: The impedance matrix represents the electrical interaction of the body with itself at the specified frequency (wavelength) according to Maxwell's equations and boundary conditions. All electromagnetic interactions are accounted for: physical optics (specular, i.e., angle of incidence = angle of reflection and end region), leading and trailing edge diffraction, shadowing of one surface by another, surface traveling, creeping, and edge wave phenomenon, multiple bounce(s), etc..

The system matrix is a powerful representation of the EM body response since *it is independent of the nature of body excitation*. Once the matrix is computed and solved via LU decomposition or inverse, we then obtain surface currents for any type of excitation, e.g., RCS scattering or antenna gain patterns. RCS scattering problems can specify polarization and angle of illumination for plane waves, or for spherical or even cylindrical waves provided one uses the corresponding voltage vector. Or the same matrix can be used to obtain antenna patterns with one or more localized regions of the body excited, each with user specified amplitude and phase. Once the system matrix is computed and solved, we can save the matrix for re-use for any type of EM problem.

The method of moments approach with excitation independence is contrasted to the differential equation approach to solving EM problems such as the Finite Difference Time Domain (FDTD) method. The FDTD, while in principle solves for all frequencies at once if an impulse excitation is applied, must be *re-solved for each excitation*. Thus to obtain an RCS backscatter plot at 1 degree increments, 360 new and different FDTD solutions must

be computed. This is in sharp contrast to the MOM approach where one does not compute a new Z but only a new voltage vector and currents.

The limitation of any MOM code, however, is the memory storage required for the matrix elements and the solution time to solve. The number of unknowns for 3-D surface problems is proportional to linear body size squared ($L^2 \sim \text{area}$). Memory requirements vary as the fourth power of body size, $N^2 \propto L^4$, while solution time increase as the sixth power of body size, $N^3 \propto L^6$.

We have been able to increase body size as computer resource capabilities have grown. The L^6 increase in CPU time implies that for every factor of ten increase in computer speed, the corresponding body size capability grows by 47 percent ($10^{1/6} = 1.47$). Similarly, every factor of 10 increase in memory increases body size by 78 percent ($10^{1/4} = 1.78$). Continued growth of serial computer architecture will not translate into appreciable growth in body size. For present architecture one must wring out all possible efficiencies such has been done in MOM3D by using matrix and body symmetries to reduce memory and CPU times.

Significant increases in body size will most likely require parallel computer architecture with vastly improved throughput, *or we will need a revised formulation of the problem to reduce significantly the number of unknowns.*

MOM3D has treated the actual matrix solution as a black box operation by using the LINPAK library of matrix algorithms [9]. Other libraries are available and a motivated user should feel free to implement.

The practicality issues and virtues of LINPAK are:

- * Routines for matrices that are complex;
- * Routines for symmetric matrices with reduction in run time and storage;

- * Routines that compute the matrix condition number to check the "quality" of the solution;
- * Routines written in FORTRAN transportable code without common blocks (data is passed via subroutine arguments);
- * Routines which build on the optimized low level Basic Linear Algebra Subroutines (the BLAS) as fundamental building blocks; and
- * LINPAK is in the public domain.

Matrix Condition Number: The concept of matrix inverse implies that the matrix is not singular, i.e., the matrix determinant is non zero. Matrix singularity implies that the set of equations is not linearly independent. The method of moments matrix formulation arises by expanding the unknown currents with a set of N basis functions with unknown coefficients. The boundary conditions are then applied to N independent locations on the body. The solution of this coupled set of equations is then obtained. Except for internal resonances, the matrix is never singular (in theory). While the matrix determinant may never be identically zero, it may be numerically small enough to cause unstable solutions. Thus it almost becomes mandatory to obtain a quality check of the solution. This can be done by choosing LINPAK routines that compute the matrix condition number (which typically requires a 10% overhead in computation time).

Factors which can lead to numerically singular matrices are:

- * Too many samples per wavelength such that the body becomes over sampled with each resulting equation becoming less unique (independent). This can occur when one tries to sample geometry variations on a finer scale than $\lambda/10$. Electrically small bodies suffer from this effect;

- * Interior body resonances that occur at specific frequencies. This can be overcome by using a combined field formulation but at the expense of more complexity with many additional unknowns. Since this effect is always narrowed banded in frequency, it makes more sense just to be alert to this possibility and not to attempt computation near these few frequency locations.
- * The number of unknowns is large and the precision of the computer arithmetic insufficient;

The matrix condition number κ is a measure of the sensitivity of the solution to errors in the matrix and/or the right hand side forcing function. The following discussion is adapted from the LINPAK Users' Guide [9] with the notation changed to that of our MOM code problem. The general MOM matrix equation and solution is:

$$\bar{Z} \bar{J} = \bar{V} ; \quad \bar{J} = \bar{Z}^{-1} \bar{V} \quad (11-1)$$

Errors in the matrix Z due to numerical round off or formulation and/or in voltage vector V of magnitude ϵ

$$\epsilon = \frac{\Delta Z}{Z} \text{ or } \frac{\Delta V}{V} \quad (11-2)$$

may lead to possible relative error in the current solution J of

$$\frac{\Delta J}{J} = \kappa \epsilon \quad (11-3)$$

The LINPAK routine for obtaining the LU decomposition of the complex symmetric matrices is CSPCO. This routine computes a parameter RCOND that is an estimate of the reciprocal of the matrix condition number, $1/\kappa$. If RCOND is approximately 10^{-d} then the elements of J can usually be expected to have d fewer significant figures of accuracy than the elements of Z. If RCOND is so small that in floating point arithmetic it is negligible compared to 1.0, then J may have no significant figures. On most computers this condition may be tested by the logical expression

$$[(1.0 + \text{RCOND}) .\text{EQ.} 1.0]$$

When this expression is true, the matrix is considered to be "singular to working precision." As a special case, if exact singularity is detected, RCOND may be set to 0.0, Reference [9].

MOM3D computes the condition number as $\kappa = \text{COND} = 1 / (\text{RCOND} + 10^{-30})$. Low values of COND suggests a reasonable non singular solution while a value of 10^{+30} shows a useless singular solution. While we do not have definitive threshold values for poor solutions, if COND is large and the resulting current solution looks suspicious, then the solution most likely is not correct. If the computer has 6 digits of precision, and COND is greater than 10^{+6} , i.e., $\text{RCOND} < 10^{-6}$, then the solution for J may not have any significant figures.

Matrix solution algorithms usually produce a result. It is up to the user to figure out if the result is garbage or is a good solution.

SECTION 12

MODELING ISSUES

The objective of this section is to introduce several modeling related issues inherent when using the triangle basis functions introduced by [1], particularly the ZIG-ZAG nature of the basis function representation and lack of symmetry.

The method of moments approach to modeling electromagnetic current behavior requires two critical steps. First one must choose basis functions that can adequately represent currents and charges on the geometry for the specified excitation. Second, the analyst must develop an algorithm that adequately models the body-body interactions using the chosen basis function representation. If either of these steps are not adequate, then the computation model will not produce physically correct results. The quest for correct results however, often times leads to inordinate computation complexity and/or computer resources. Thus we need to decide when our modeling process is good enough to answer the questions we pose.

Balance in the modeling processes is required. The basis function choice and sample density is inherently an approximation to the surface currents. Since we need both adequate basis function representation and an EM prescription, we cannot make up for poor basis function choice and density by developing a precise EM prescription. Still, sometimes a higher density of basis functions can compensate for a poor EM prescription.

Surface Current Characteristics: Surface current spatial variation inherently is scaled to the free space wave length. It is vector in nature, i.e., has directional characteristics. The spatial variation λ sets the sampling requirements necessary to model a continuum with a set of discrete basis functions. Typically we choose 7 to 10 samples per λ as sufficient to model this spatial change, i.e., 98 to 200 samples per λ^2 of surface area (2 basis vectors required for surface). But sometimes the geometry or electrical characteristics change faster than

the wave length scale and we model this behavior. Current variation near edges, depending on the voltage vector forcing function, may have a square root singularity in its behavior.

Current vector direction depends strongly on excitation, i.e., current flows in the direction of the applied electric field. Yet, structure also influences direction. For example, edge diffraction behavior usually involves currents either parallel or perpendicular to the edge. Surface wave reflection (traveling and edge wave) and how we model the edge or tip can influence the current direction and magnitude. Edge wave currents are coupled strongly to the edge and "reflect" from the tip. Thus a vector basis function representation that is completely general to allow for any type of surface current flow for any possible excitation function must allow for many directional possibilities.

Triangle Basis Function Considerations: The surface triangle couple basis functions introduced by [1] and used in MOM3D have certain desirable characteristics. The triangle nature allows for modeling doubly curved surfaces in a smoother fashion than rectangular or square patches. They model currents in a piece-wise linear manner and charge density in a pulse doublet manner. They do not introduce extraneous line charges since the current from one triangle must flow completely to the second.

The fundamental vector direction of these basis functions is from the centroid of one triangle to the centroid of the adjacent triangle forming the couple. *This leads to a ZIG ZAG representation of current direction on a body.* Consider the plate geometry shown in figure 12-1 modeled with triangle couples. The triangles are shown with dashed lines while the current basis functions are shown in solid arrows from centroid to centroid. We see the inherent

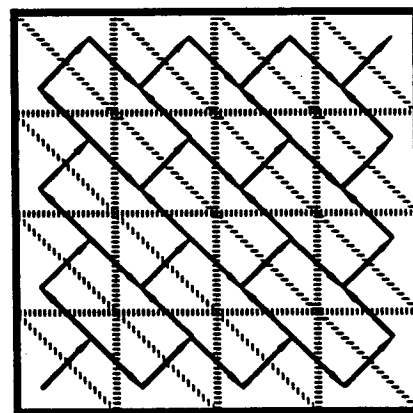


Figure 12-1 Basis function currents are from triangle centroid to centroid (zig-zag)

change of vector direction from one couple to the next, interior to the plate and along its edges.

Also note that the basis function direction on each corner tip is different for adjacent corners and is a function of body symmetry. Referring to Figure 12-2, the plate with no symmetry has all corner couple directions parallel which makes the basis function direction parallel or perpendicular to the diagonal for adjacent tips. For the plate with symmetry the basis function vector directions are no longer all parallel and is different for each pair of tips. *The symmetric plate has a basis function representation that is not symmetric.*

The ZIG ZAG nature of the triangle couple basis functions will change if one invokes model symmetry. Figure 12-2 shows a typical triangle modeling scheme with and without symmetry. Note that the corner tip couple vector direction is different for each of these plates.

This ZIG ZAG nature of the vector direction is inherent in the triangle basis functions introduced by [1].

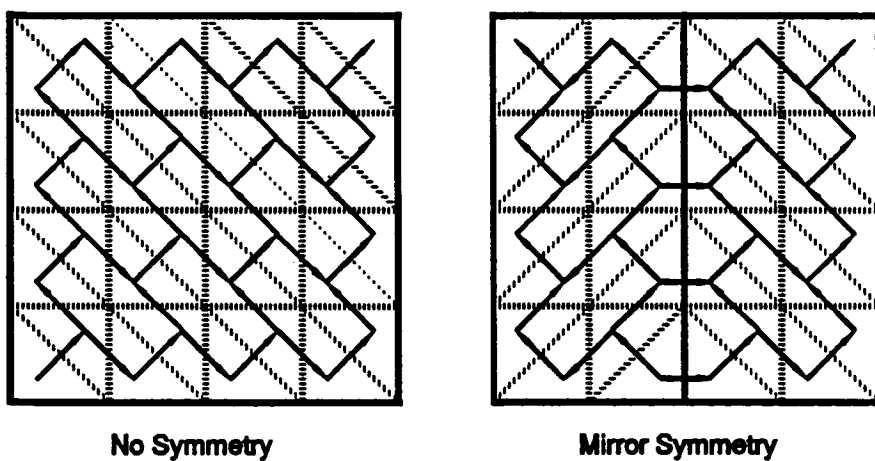


Figure 12-2 Geometry symmetry alters basis vector orientation

Physical currents do not have this ZIG ZAG characteristic. *Triangle couple representation of physical surface currents introduces a modeling artifact.* The consequence of the ZIG-ZAG representation is usually minor, yet, on occasion it will introduce minor asymmetric results in radiation patterns. This often times is seen in edge wave scattering from a square plate where the computed results do not have complete symmetry as one would expect. This is due to the tip basis functions not being the same direction on all four corners.

SECTION 13

EXAMPLE RESULTS

This section presents sample MOM3D results for backscatter RCS, bistatic RCS, current distributions, downrange images, down/cross range images, near zone field maps, and antenna gain patterns. These results were computed on a personal computer with a 486 processor operating at 33 MHz.

Coordinate System: The coordinate system is the standard spherical system with the azimuth angle ϕ measured from the X axis and the elevation angle measured up from the X-Y plane, Figure 13-1. The polar angle θ is the 90° complement of elevation and is measured down from the Z axis. The two fundamental polarization unit vectors are u^{θ} and u^{ϕ} that are in the "direction" of the corresponding angle θ and ϕ . The xyz rectangular representation of these vectors become functions of (θ, ϕ) .

Model Geometry: The model geometry was a 5.5 inch square plate at a frequency of 3 GHz. The side length and area were 1.4λ and $1.95 \lambda^2$ respectively. The plate was centered in the X-Y plane and was modeled with 200 triangles with mirror symmetry about the Y axis, Figure 13-2. This resulted in 280 unknown current couples. The symmetric geometry resulted in an "even" matrix rank of 145 and an odd matrix rank of 135. There were 10 current couples on the spine. The normalized sample density was 143 current couples per square wavelength, which is over-sampled. The plate was a perfect conductor.

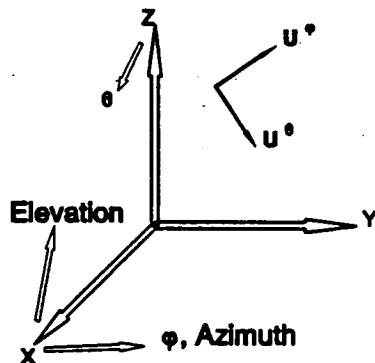


Figure 13-1 MOM3D coordinate system is the standard spherical system

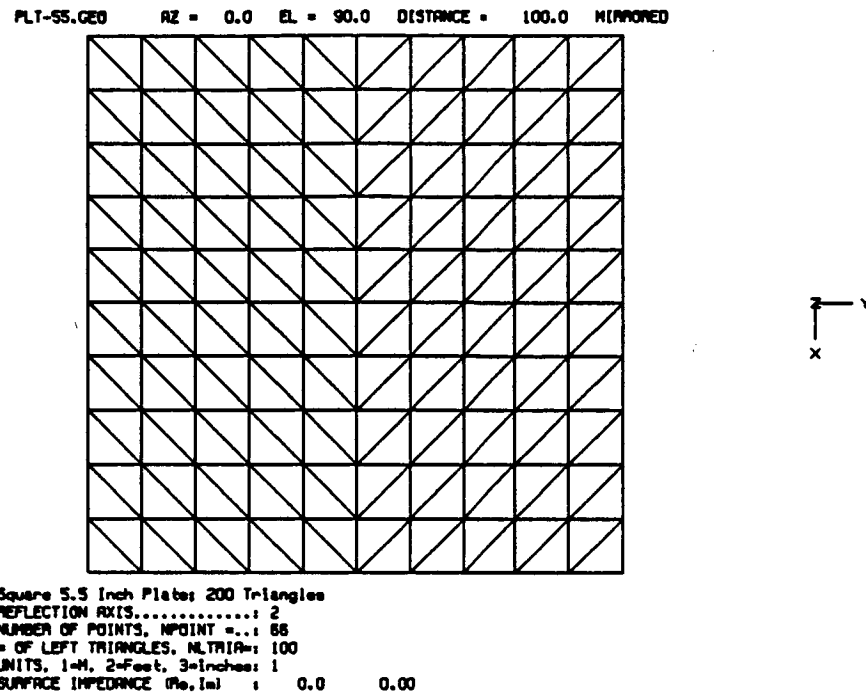


Figure 13-2 PLT-55.GEO Mesh Model, Symmetric about Y = 0 (X-Z) plane.

Backscatter RCS: The backscatter RCS is shown in Figure 13-3. An elevation cut is shown for both θ (solid line) and ϕ (dashed line) polarizations. We see that the RCS is the same for both polarizations when perpendicular to the plate, i.e., the "specular flash" where the angle of reflection is equal to the angle of incidence. This flash has a value of -4 dBsm that compares to the high frequency physical optics value of $\sigma_{po} = 4\pi A^2 / \lambda^2 = -3.2$ dBsm. Thus even for this electrically small plate we obtain optics results for the specular return. For θ polarization at 0° incidence the electric field is perpendicular to the plate so that no currents are induced (no tangential E field), and therefore no scattered electric field.

The θ polarization lobe at 40° is the surface traveling wave (TW) lobe. The location compares well to the hip pocket standard location given by $\theta = 49 (\lambda / L)^{0.5} = 41^\circ$. The TW magnitude is -14 dBsm, which compares to the hip pocket estimate that the TW return be less than $3\lambda^2 = -15$ dBsm.

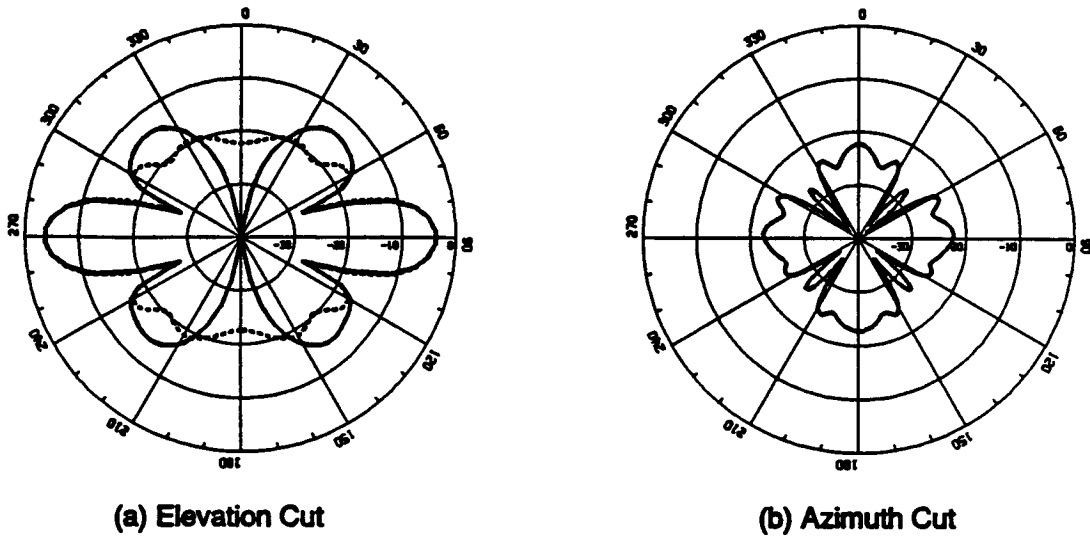
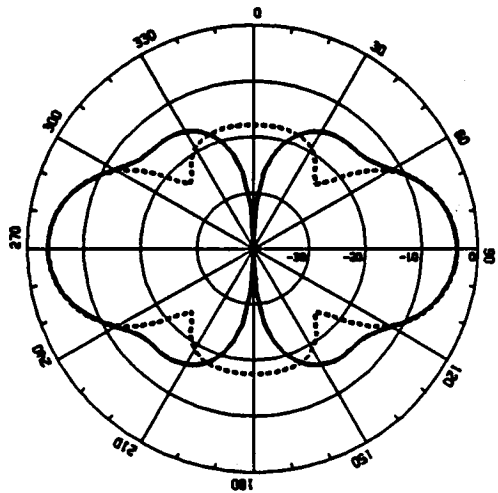


Figure 13-3 Backscatter RCS

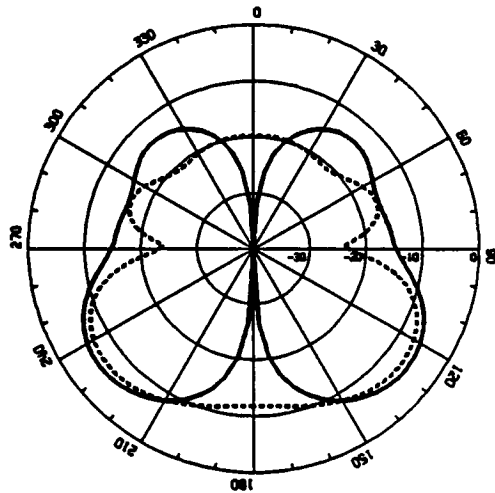
For ϕ polarization at 0° , the RCS is due to edge currents, - 22 dBsm, which corresponds to the standard edge optical return of $\sigma_{\text{edge}} = L^2 / \pi = -22$ dBsm.

The azimuth cut, Figure 13-3(b), is for ϕ polarization and is typically called the edge wave cut since the RCS is dominated by specular edges and edge traveling waves. The edge specular is the same as the previous edge value, -22 dBsm. The edge traveling wave here is not particularly dominant. The slight asymmetry in this result is due to the ZIG-ZAG basis function representation and the effect of model symmetry that causes asymmetric basis functions (see Section 12).

Bistatic RCS: Bistatic RCS is shown in Figure 13-4 for θ and ϕ polarizations (solid and dashed lines respectively) for an elevation cut. In (a) the plate is illuminated at 90° . The backscatter RCS at 90° is -4 dBsm. This is the optics specular flash and corresponds to $\sigma_{p0} = -3$ dBsm. The forward scattered field at 270° has the same amplitude as the backscatter value. This forward scattered field, when added to the incident field (in a vector phasor



(a) 90 deg incidence



(b) 45 deg incidence

Figure 13-4 Bistatic RCS

manor) forms the shadow behind the plate. At edge viewing angles of 0° and 180° there is no scattered field for θ polarization (perpendicular to plate) but there is a finite ϕ polarized scattered field due to edge induced currents.

The bistatic result for 45° incidence is shown in (b). The specular flash here, where angle of refection is equal to angle of incidence, is at 135° . The specular value is -7 dBsm and compares to the physical optics value of $\sigma_{po} = \cos^2\alpha \cdot 4\pi A^2 / \lambda^2 = -6$ dBsm that is down by 3 dB over the 90° specular result due to the $\cos^2(45^\circ) = 0.5$ factor. The forward scatter lobe at 225° , ($= 45^\circ + 180^\circ$), forms the shadow behind the plate when added to the incident field. For edge viewing angles, as before, there is a ϕ component of scattered field, but no θ component.

Square 5.5 Inch Plate; 200 Triangles
CURRENT MOM3D COMPUTATION

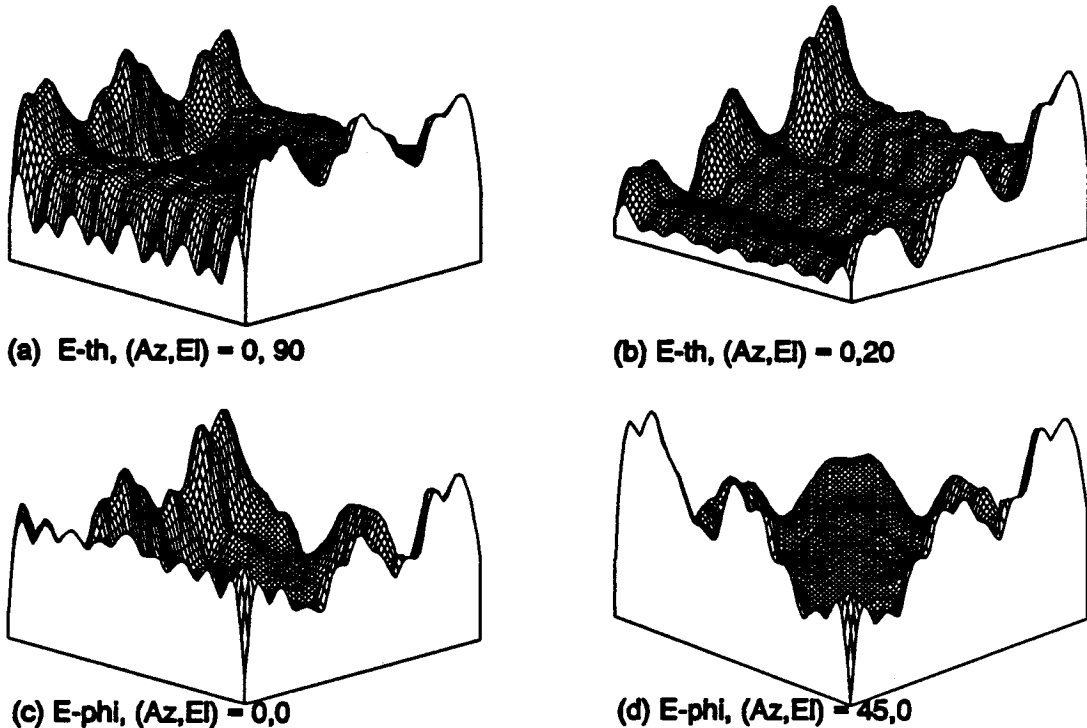


Figure 13-5 Current examples

Current Computation: Plate currents are shown in Figure 13-5 for the RMS (root mean square) average for four excitation angles. In (a), the excitation is perpendicular to the plate for E^θ polarization. We see that the current peaks along the pair of edges parallel to the incident field and tends toward zero for the edges perpendicular to the incident field. Currents in the center of the plate correspond to physical optics levels. We note that the edge parallel currents show a 3 peak standing wave pattern corresponding to energy flashing between the vertices (recall that the plate edge length was approximately 1.4λ that would create 3 standing wave peaks, one every half wavelength). The current along the edge perpendicular to the incident E field, while tending to zero, show an oscillatory pattern. Recall that triangle currents are the vector sum of the common (couple) edge currents. Thus referring to Figure 13-2, we see that edge triangles alternate between having two or three common edges. Those with three will have higher currents.

Figure 13-5 (b) shows the RMS induced currents for the surface traveling wave excitation case, E^θ polarization at 20° elevation and 0° azimuth (looking perpendicular to edges). The

results show low levels of currents near the front edge that build in intensity going toward the rear edge. A three peak current standing wave pattern is evident, one every $\lambda/2$. This is caused by the forward current phasor adding with the current reflected by the rear edge. We also see two pronounced edge current peaks along each plate side, again showing a standing wave pattern due to forward and reflected edge currents.

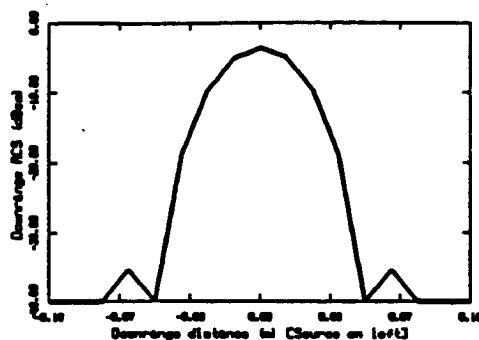
Figure 13-5 (c) shows the RMS currents for parallel edge on excitation. The incident field is ϕ polarized. We see a dominant leading edge current at the plate front edge. The side edges show the edge standing wave caused by the forward and reflected edge energy. The currents in the plate center tend to be small. The rear edge current show a small peak, probably due to diffraction energy flashing between the two back vertices.

Figure 13-5 (d) shows the RMS currents for the edge wave excitation at 45° azimuth for ϕ polarization. We see two symmetric edge standing wave currents, again with a peak every $\lambda/2$. These build in amplitude as the wave travels toward the aft vertices where they diffract energy toward the front and rear corner vertices. The rear corner vertex current also peaks. Currents in the center of the plate are small since this is an edge wave dominated excitation.

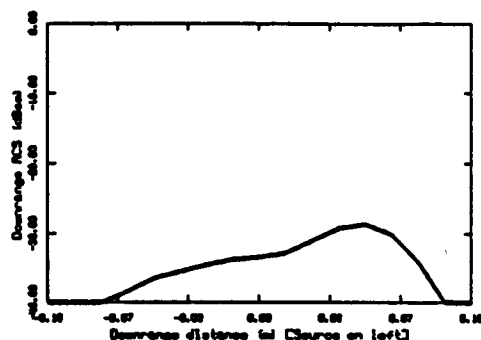
Downrange Images: Downrange images are shown in Figure 13-6. The images presented here correspond to co-polarized backscatter energy (recall that the method described in Section 5 also could compute a bistatic and/or a cross polarized image).

Case (a) is for illumination perpendicular to the plate such that the backscatter is the specular flash, -4 dBsm. This orientation shows all energy originating from a single downrange location.

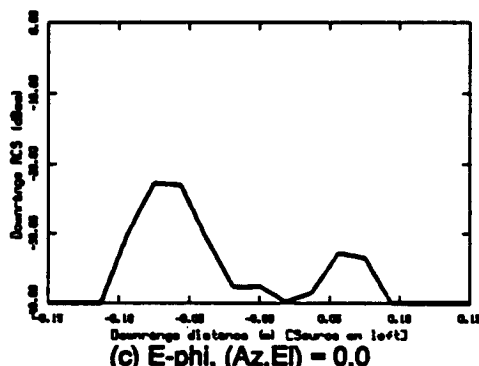
Case (b) is for the traveling wave excitation, E^0 polarization at 20° elevation. We clearly see the return as originating from the aft edge of the plate. This is due to the reflection of the "forward" currents at the aft discontinuity. When these surface currents reflect and travel toward the plate front edge they reduce in intensity as they radiate energy back toward the illuminating source that causes the image level to decay going toward the front



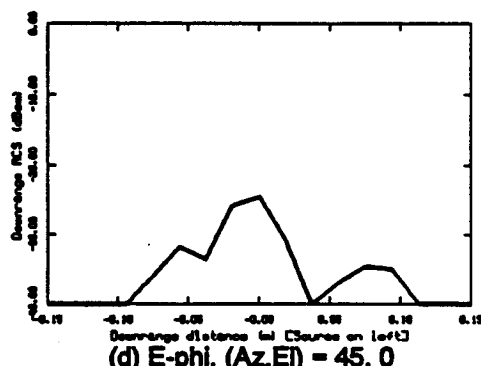
(a) E-th, $(Az, El) = 0, 90$



(b) E-th, $(Az, El) = 0, 20$



(c) E-phi, $(Az, El) = 0, 0$



(d) E-phi, $(Az, El) = 45, 0$

Figure 13-6 Down range image of plate edge of the plate.

Case (c) is for E^* front edge parallel polarization for 0° azimuth and elevation. The image shows the scattered energy as originating from the front edge currents and corresponds to the physical optics edge value of $\sigma_{po} = 1^2 / \pi = -22$ dBsm. We also see a return from the aft end of the plate due to reflected edge wave energy.

Case (d) is for E^* polarization at 45° azimuth that is the edge wave illumination case. We see a peak return corresponding to edge wave reflected energy from the corner vertices and a smaller return from the front vertex and the extreme aft vertex due to multiple diffraction.

Cross Range Images: Two dimensional cross range images are shown in Figure 13-7. The 5.5" plate dimension corresponds to ± 0.07 m for cross and downrange. These images are co-polarized in the backscatter direction. The cross range direction, Figure 5-1, is in the ϕ

direction that corresponds to a "rotation" about the Z axis. The images are shown as contour plots using PLOT 88 FORTRAN graphics. The contour lines are spaced in 2 dB increments. The cases presented here are the same illumination excitation as shown for the downrange examples, Figure 13-6, and the induced current plots, Figure 13-5.

Case (a) is for E^* illumination perpendicular to plate, $(Az, El) = 0^\circ, 90^\circ$. The backscatter return here is the "specular" flash where the plate currents have mostly the same phase and when radiating, phasor add to form the "flash." The two dimensional image shows radiation as originating at a constant downrange distance distributed over the cross range dimension of the plate. Recall that the specular flash had a value of -4 dBsm while the image shows a maximum contour of between -14 and -12 dBsm. Two dimensional images thus show distributed levels.

Case (b) is for the surface traveling wave illumination, E^* polarization at 20° elevation and 0° azimuth (perpendicular to edges). As expected, the image shows the major scattering as originating from the surface traveling wave reflecting from the aft plate edge. Note that the intensity then falls off as this reflected energy decays as it flows back toward the front edge (Figure 13-6b). The intensity is slightly higher along the downrange edges.

Case (c) is for parallel edge illumination, E^* polarization at 0° azimuth and elevation. The image clearly shows the leading edge as the dominant scattering source due to leading edge induced currents. The two rear vertices are lesser scattering centers due to energy flowing down each downrange edge. The source at the center of the rear edge is probably due to multiple diffraction from the rear vertices.

Case (d) is the edge wave illumination example, E^* polarization at 45° azimuth and 0° elevation. The major scattering centers are the two vertices that reflect the edge waves. The far rear vertex also is a major scattering center due to multiple vertex diffraction of the edge traveling waves. The forward vertex is not a significant scattering center. Compare to the downrange result, Figure 13-6d.

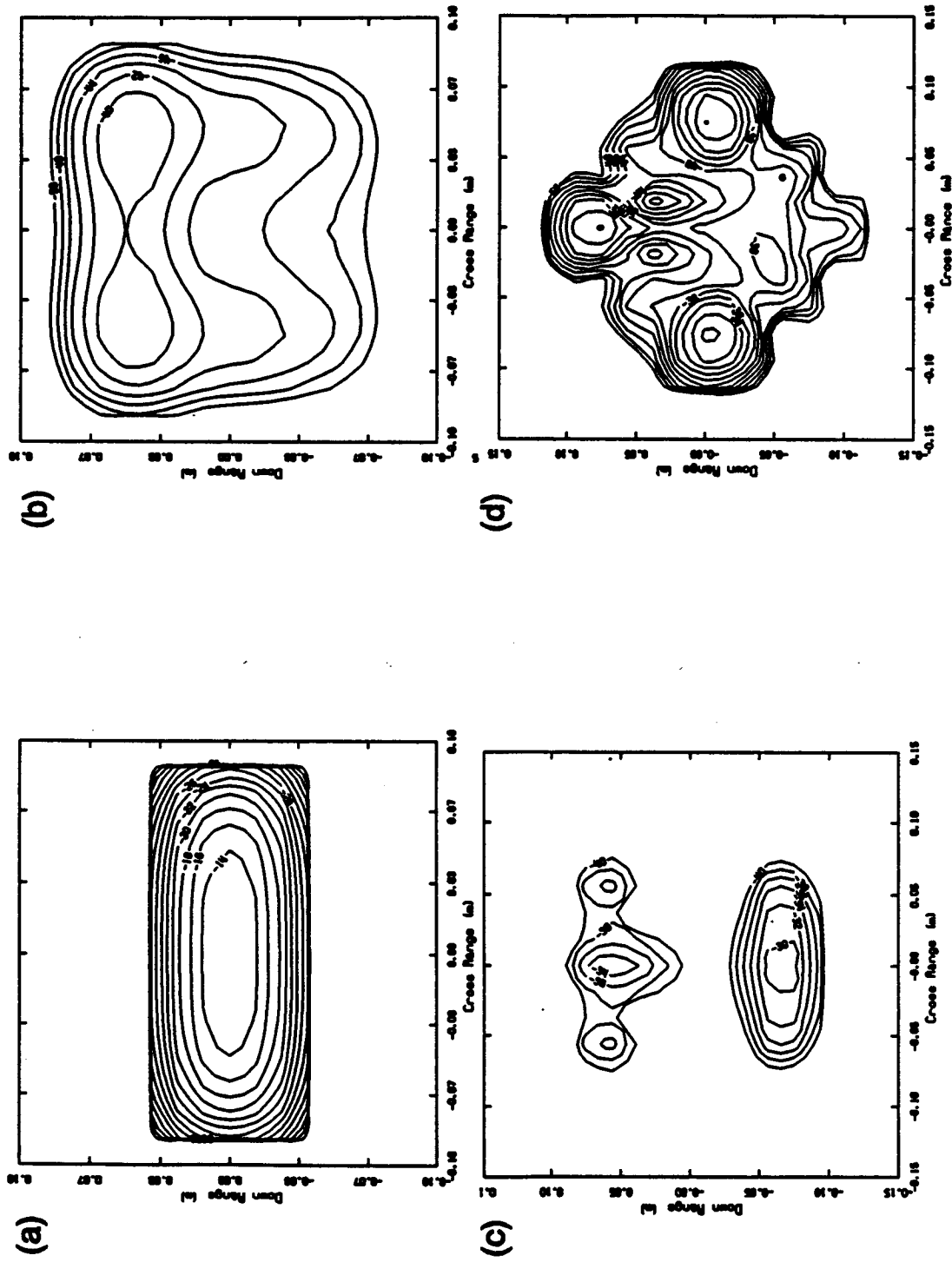


Figure 13-7 Two dimensional range / cross range images

Near Field Examples: Near field computations for E^{total} and E^{scat} are shown in Figures 13-9 and 13-10. The plate excitation was E^{θ} perpendicular to the plate, 90° elevation, 0° azimuth. The near zone fields were computed over a 6λ square grid centered in the X-Z plane, Figure 13-8, with computation points spaced every 0.1λ . Two vector fields were computed, E total and E scattered. For each, the root mean square (RMS) scalar time average was computed along with the two principal time values, one for $\omega t = 0^\circ$ (the REAL part), and the second for $\omega t = -90^\circ$ (the IMAG part). The results displayed are for contours of intensity, not vector direction.

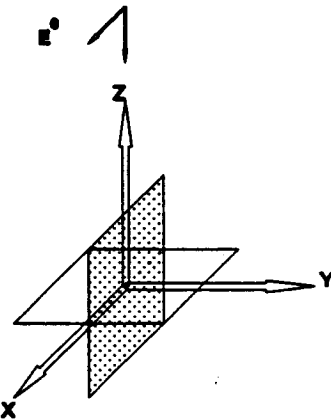


Figure 13-8 Near field computation grid

E Total Field: The total electric field, Figure 13-9, is the vector sum of the incident and scattered field, $E^{\text{tot}} = E^{\text{inc}} + E^{\text{scat}}$. The incident field for this case is a plane wave propagating down the Z axis.

Case (a) is the RMS average. Beneath the plate the incident and scattered fields are out of phase to form a shadow region. Above the plate is a standing wave pattern every $\lambda/2$. The peaks of the standing wave occur when the scattered and incident fields are in phase while the nulls occur when the two fields are out of phase. The first peak occurs at a height above the plate of $\lambda/4$.

Case (b) is the IMAG value of the field. This is an instantaneous snap shot in time corresponding to $\omega t = -90^\circ$. The alternating intensity of the incident plane wave is clearly seen. Above the plate the reflected (scattered) field causes an interference pattern (standing wave) with the incident field. Beneath the plate the interference pattern forms the shadow region.

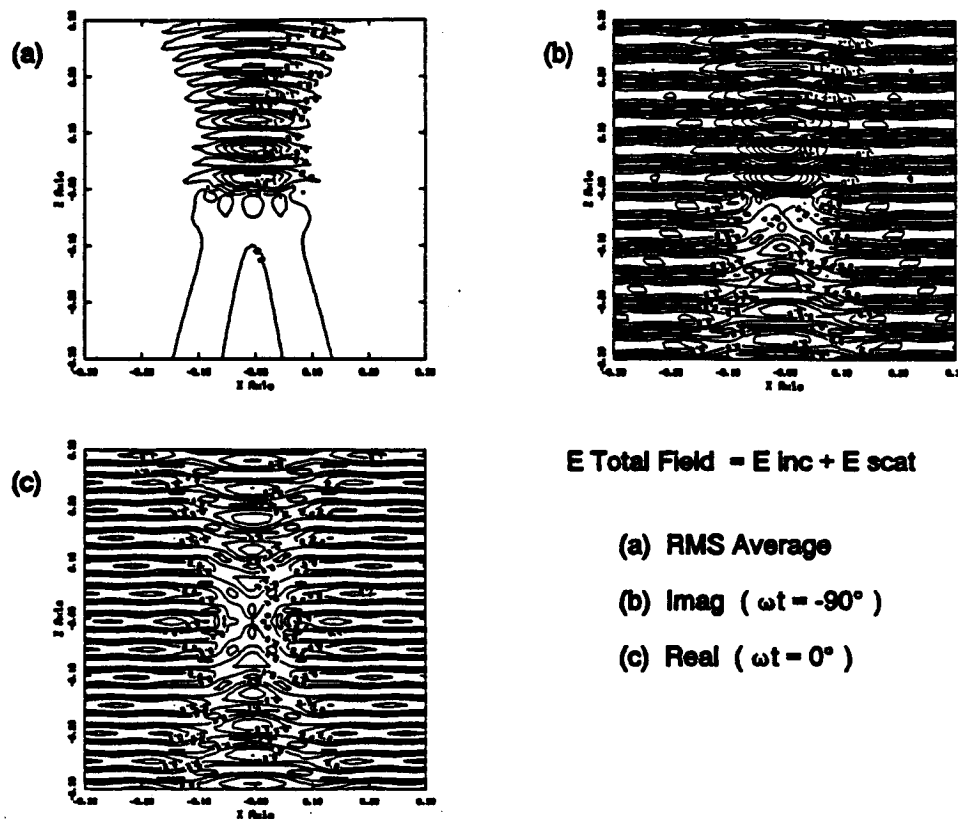


Figure 13-9 Total field

Case (c) is the REAL value of the field. This corresponds to a snap-shot in time of $\omega t = 0^\circ$. The incident wave for this case has moved $\lambda/4$, i.e., 90° , relative to case (b). Thus the peaks of the incident field for (c) are located where the nulls in (b) are located.

E Scattered Field: The scattered field \mathbf{E}^{scat} is shown in Figure 13-10. The equivalent far field RCS pattern for this case is the bistatic result shown in Figure 13-4a. The backscatter direction (reflected) is above the plate while the forward scattered field, which forms the shadow region beneath the plate by phasor subtraction with the incident field, is beneath the plate. The back and forward scattered fields are symmetric above and below the plate.

Case (a) shows the RMS average intensity contours. The four lobes at 45° intervals are also seen in the bistatic result, Figure 13-4a, at 45° , 135° , 225° , and 315° . The field is most intense near the plate.

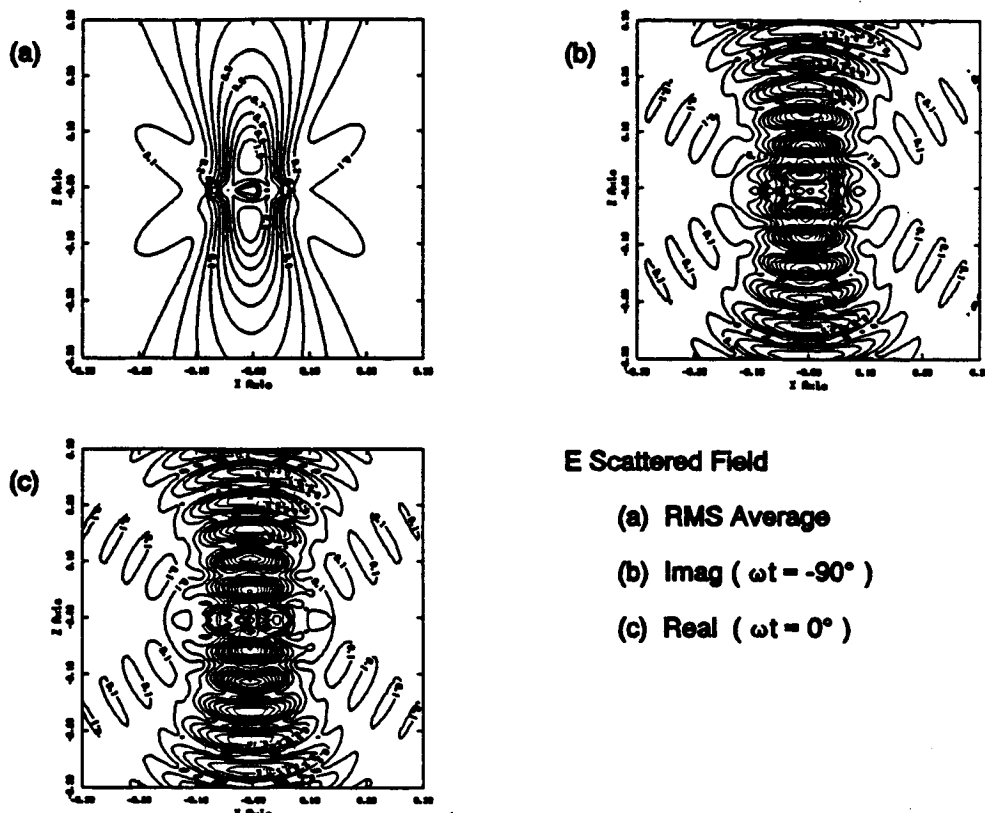


Figure 13-10 Scattered field

Case (b) and (c) show the two instantaneous snap-shots of the scattered field. The two are separated by 90° phase, i.e., $\lambda/4$, such that in (b) the peaks occur where the nulls occur in (c). Far from the plate the field lines close back on themselves, i.e., the field is solenoidal. Near the plate the field lines terminate on the induced charges.

Antenna Example: MOM3D also may be used for antenna analysis. This example shows the computed gain pattern for a half wave dipole modeled as a thin strip, Figure 13-11. The dipole is centered along the Y axis in the X-Y plane. The center port (couple) is the feed location, 8. The computed gain pattern, Figure 13-12, shows the typical half wave dipole figure eight pattern

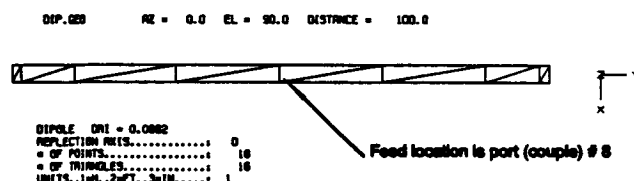
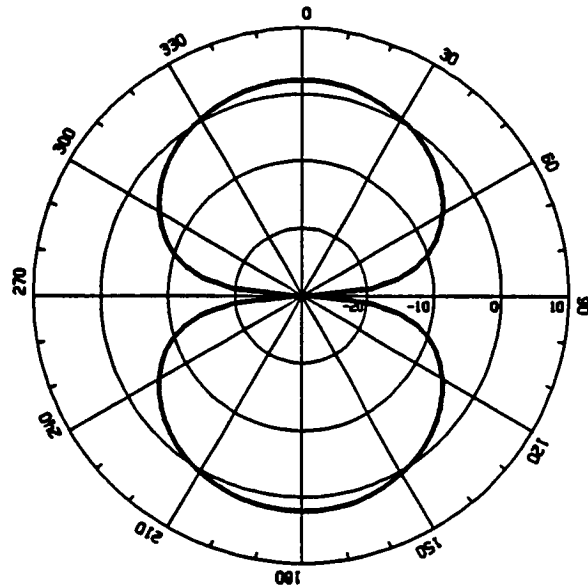


Figure 13-11 Half wave dipole strip antenna geometry

DIPOLE DRI = 0.0882

ANTENNA MOM3D COMPUTATION
Azimuth Cut: Fixed Elevation = 0.0 ; E-Phi Pol



DIP.GEO : Zin = 72.26 6.46; Iport(1) = 8
Wavelength: 0.1887 m; 1589.8 MHz; Epsilon: 1.0; Tau: 0.0000; Izsurf: 0.
LU Cond. #: 1953.7 0.0 0.0

Figure 13-12 Half wave dipole antenna gain pattern

with peak gain of 2.1 dbi. The computed input impedance was $Z = 72 + j 6$ ohms that corresponds to a resonant half wave dipole operated slightly above resonance since the reactive component is inductive.

REFERENCES

- 1 S. M. Rao, D. R. Wilton, and A. W. Glisson; "Electromagnetic Scattering by Surfaces of Arbitrary Shape" IEEE Trans. Antennas Propagat., vol. AP-30, no. 3, pp. 409-418, May 1982.
- 2 E. K. Miller; "A Selective Survey of Computational Electromagnetics", IEEE Trans. Antennas Propagat., vol. AP-36, no. 9, pp. 1281-1305, Sept. 1988.
- 3 J. F. Shaeffer and L. N. Medgyesi-Mitschang, "Radiation from Wire Antennas Attached to Bodies of Revolution: The Junction Problem", IEEE Trans. Antennas Propagat., vol. AP-29, no. 3, pp. 479-487, May 1981.
- 4 J. F. Shaeffer, "EM Scattering from Bodies of Revolution with Attached Wires", IEEE Trans. Antennas Propagat., vol. AP-30, no. 3, pp. 426-431, May 1982.
- 5 J. R. Mautz and R. F. Harrington, "Radiation and Scattering from Bodies of Revolution", Appl. Sci. Res., vol. 20, p. 405, 1969.
- 6 R. F. Harrington, "Field Computation by Moment Methods", New York: Macmillan, 1968.
- 7 A. J. Poggio and E. K. Miller, "Integral Equation Solutions of Three Dimensional Scattering Problems", in Numerical and Asymptotic Techniques in Electromagnetics, R. Mittra, Ed. New York: Hemisphere Publishing Corp., 1973.
- 8 W. H. Press, B. P Flannery, S. A. Teukolsky, and W. T. Vettering, Numerical Recipes: The Art of Scientific Computing, Cambridge University Press, Cambridge., 1986.

- 9 J.J. Dongarra, C.B. Moler, J.R. Bunch and G.W. Stewart, "LINPACK USERS' GUIDE", SIAM, Philadelphia, 1979.
- 10 J.J. Dongarra, I.S. Duff, D.C. Sorensen and H.A. van der Vorst, Solving Linear Systems on Vector and Shared Memory Computers", SIAM, Philadelphia, 1991
- 11 E.H. Newman and D.M. Pozar, "Electromagnetic Modeling of Composite Wire and Surface Geometries", IEEE Trans, Antennas and Propagat., AP-26, 784, 1978.
- 12 D.L. Mensa, High Resolution Radar Imaging, Artech House, Norwood, MA, 1981.
- 13 N.C. Currie editor, "Radar Reflectivity Measurement: Techniques and Applications", Artech House, Norwood, MA, 1989.
- 14 E.O. Brigham, The Fast Fourier Transform and its Applications, Prentice Hall, 1988
- 15 J.H. Huynen, "Phenomenological Theory of Radar Targets," Electromagnetic Scattering, L.E. Uslenghi, ed., New York, Academic Press, 1978.
- 16 R. Haupt and V. Liepa, "Synthesis of Tapered Resistive Strips," IEEE Trans. Antennas Propagat., vol. AP-35, No. 11, November 1987.
- 17 L.N. Medgyesi-Mitschang and J.M. Putnam, "Integral Equation Formulations for Imperfectly Conducting Scatters," IEEE Trans. Antennas Propagat., vol. AP-33, No. 2, February 1985.
- 18 M.M. Horst and J.F. Shaeffer, Chapter 8, Radar Reflectivity Measurements: Techniques Applications, N. Currie Editor, Artech House, Norwood, MA, 1989.

- 19 PLOT88 Software Library Reference Manual, Third Edition, Version 19, Plotworks,
Inc., 16440 Eagles Crest Road, Ramona, CA 92065, (619) 457-5090, (These are
FORTRAN callable plotting routines for the PC-DOS operating system)

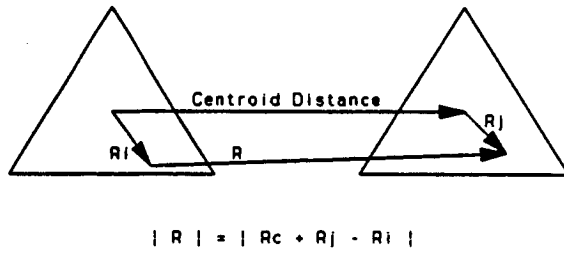
APPENDIX A

NUMERICAL and ANALYTICAL MATRIX ELEMENT INTEGRATION

The approach and theory used to compute the Green's function integrals in a less approximate or more exact manner than the centroid approach is presented. MOM3D uses the centroid approximation for all triangle interactions greater than approximately ten triangle spacings apart. For closer interaction distances, as specified by the user, one may choose from three approaches for computing matrix elements: the centroid approximation; or a combination analytical / numerical approach where the numerical integration may use a single point (centroid) or may use three points.

Theory is presented for: numerical quadrature formulas for surfaces; singular removal; and an analytical formula for the $1/R$ integration (point in space integrated over a triangular area).

Overview: The initial development of MOM3D used a centroid approximation when computing triangle to triangle matrix element interactions, Figure A-1. This results in a considerable reduction in complexity and in the computer time required to fill the impedance matrix. This technique is reasonable when the mesh triangles are greater than one characteristic mesh length apart. Early work showed that the approach was still viable even for touching co-planar triangles. But, the centroid approximation becomes less reasonable when two triangles become very close to each other, such as when one triangle bends back



$$| R | = | R_c + R_j - R_i |$$

Distance between source and field points written in terms of the centroid distance.

Figure A-1 Interaction distance R

on the second, as in modeling a small angle wedge, or when modeling two parallel surfaces with separation less than a characteristic dimension L . The fundamental difficulty is with the $1/R$ integrand. When R is greater than L , the centroid approximation is reasonable, but when the distance between triangles is less than L , then the centroid approximation over estimates the $1/R$ interaction. Early studies showed that the centroid approximation was a good approximation when triangle spacing was greater than one characteristic dimension L apart, i.e., depends on mesh size and not on wavelength. Further, the centroid approximation was adequate for two triangles with a common edge whenever the included angle between was greater than 50 degrees, i.e., valid for planar surfaces and those with not too rapidly varying curvature.

The basic current unknown is two adjacent triangles with a common side, which forms a *couple*. The matrix element interaction is between pairs of couples, Figure A-2, and involves interaction between four triangles. The impedance matrix element between the i th and j th couples is a sum of four terms accounting for the interaction between the four triangles making up the two couples:

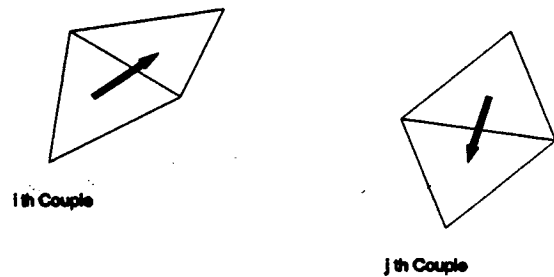


Figure A-2 Matrix elements involve 4 triangle interactions

$$\begin{aligned}
 Z_{ij} &= \langle \vec{W}_i, L(\vec{f}_j) \rangle \\
 &= jk\eta \sum_{p=1}^2 \sum_{q=1}^2 l_i l_j S_{ip} S_{jq} \left[\frac{G_{ipjq}^{(1)}}{4} - \frac{G_{ipjq}^{(0)}}{k^2} \right]
 \end{aligned} \tag{A-1}$$

This expression is exact in the sense that no approximations have been made other than the fundamental choice of basis and weight functions. The terms $G^{(1)}$ and $G^{(0)}$ involve integration of the Green's function between pairs of triangles,

$$G_y^0 = \frac{1}{A_i A_j} \int \int \frac{\exp(-jk(\vec{r}_i - \vec{r}_j))}{4\pi |\vec{r}_i - \vec{r}_j|} dS_i dS_j$$

and (A-2)

$$G_y^1 = \frac{1}{A_i A_j} \int \int (\vec{p}_i \cdot \vec{p}_j) \frac{\exp(-jk(\vec{r}_i - \vec{r}_j))}{4\pi |\vec{r}_i - \vec{r}_j|} dS_i dS_j$$

These are four fold integrals that express the electrical interaction of one surface patch with another.

The centroid approximation for G^0 and G^1 is:

$$G_y^{0c} = \frac{e^{-jk\vec{r}^c}}{4\pi |\vec{r}^c|}, \text{ where } \vec{r}^c = \vec{r}_i^c - \vec{r}_j^c, \text{ and}$$

(A-3)

$$G_y^{1c} = (\vec{p}_i^c \cdot \vec{p}_j^c) G_y^{0c}$$

where r_{ij}^c is the distance between the centroid of the i th and j th triangles. This approach is computationally simple and fast, which is important when solving large geometries. This approximation begins to fail when the triangle interaction distance becomes less than a characteristic dimension such as for very close parallel surfaces or for knife edges where one triangle folds back sharply on another.

Numerical Triangle Integration Formulas: An integration scheme similar to one dimensional Gaussian quadrature, but for triangular surfaces and tetrahedron volumes is discussed by Hammer, Marlowe, and Stroud [A1]. They derive general surface and volume numerical integration formulas of the form

$$\int f(\xi) dV \approx \sum_{j=1}^k a_j f(\xi_j) \quad (\text{A-4})$$

where the numbers a_j are constants (weights) ($j=1$ to k), ξ_j are points in the domain of f , and R is the bounded closure of an open set in E_n where n is the dimensionality of the space. Their goal was to obtain numerical integration formulas for the n -simplex to hold exactly for polynomial functions f of at most degree k .

Hammer et. al. [A1] give weight sets, a_j , and function evaluation points, ξ_j , for 1, 3, 4, and 7 function evaluation points over a triangle. The three point formula is said to hold exactly for quadratic functions, the four point formula for cubic functions, and the seven point formula for quintic functions.

It is interesting that reference [A1] specifies the centroid as the first affine invariant formula for the triangle as the sole evaluation point with the weight equal to the area. This of course is our centroid approach.

Application of reference [A1] results requires us to represent the function evaluation points as vectors. Writing the vertices of a triangle as V_1, V_2, V_3 and the centroid as $C = 1/3 \sum V_i$, the function evaluation points r_i (inside the triangle) are specified as

$$\vec{r}_i = r \vec{V}_i + (1 - r) \vec{C} \quad \text{where } i = 1, 2, 3. \quad (\text{A-5})$$

where r is a constant specified by [A1] for the various orders of numerical integration. The function evaluation points inside the triangle can be rewritten in terms of the triangle centroid \mathbf{C} as

$$\vec{r}_i = \vec{C} - r(\vec{C} - \vec{v}_i) \quad (\text{A-6})$$

where we recognize that the vector ($\mathbf{C} - \mathbf{v}_i$) is from the i th triangle vertex to the centroid, Figure A-3.

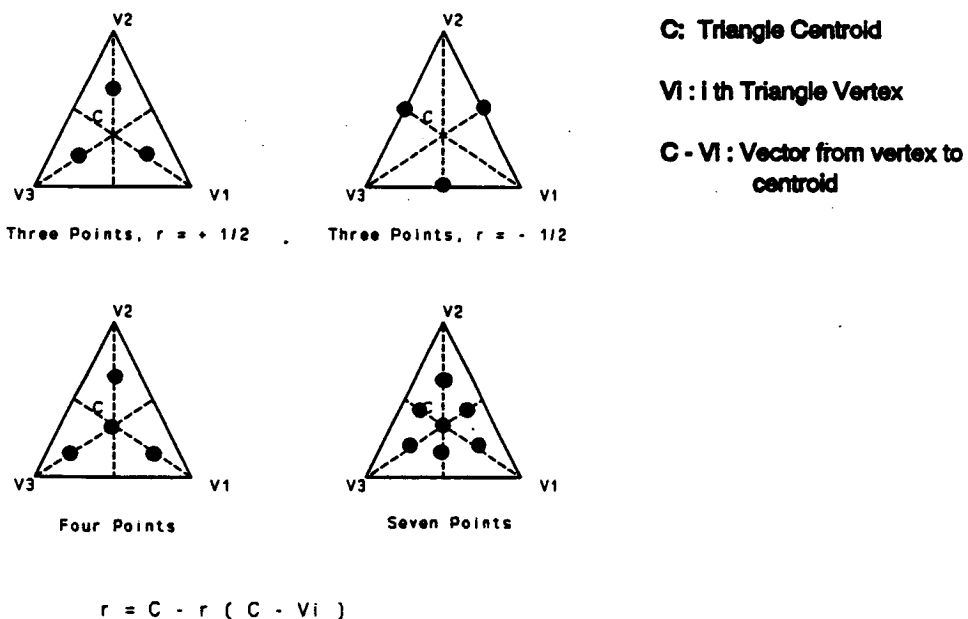


Figure A-3 Triangle function evaluation points

Three point surface integration is exact for quadratic functions (e.g., 2 terms of a Taylor series expansion) for $r = \pm 1/2$ with weights $W = 1/3 \Delta$ where Δ is the triangle area. For

$r = + 1/2$, the evaluation points are the distinct trisection of the median chords and for $r = - 1/2$, the evaluation points are the midpoints of the sides.

Four point surface integration is exact for a cubic polynomial for $r = 2/5$ with weights $25/48 \Delta$ for each of the three median chords and the centroid, $r = 0$, with weight $(-9/16) \Delta$.

Seven point surface integration is exact for a quintic polynomial for function evaluations at the centroid with weight $(9/40) \Delta$ and by two points on each median chord given by

$$r = (1 + \sqrt{15}) / 7 \quad \text{with weight } (155 - \sqrt{15}) / 1200 \Delta$$

$$r = (1 - \sqrt{15}) / 7 \quad \text{with weight } (155 + \sqrt{15}) / 1200 \Delta$$

or approximately

$$r = +0.6961405 \quad \text{with weight } 0.1259392 \Delta$$

$$r = -0.4104262 \quad \text{with weight } 0.1323942 \Delta$$

The astute reader will recognize that the sum of the weights for the 3, 4, or 7 point formulas is just the area of the triangle Δ .

Figure A-3 shows the evaluation points within a triangle for the 3, 4, and 7 point integration formulas.

Application to the double surface integral of MOM3D requires triangle to triangle integration, i.e., a double sum. Thus the 3 point formulas will require 9 function evaluations, the 4 point formula 16 evaluations and the 7 point formula 49 evaluations.

Analytical Point to Plane Line Integral Approach: Another method of computing surface integrals is to use Stoke's theorem to reduce an area integration to a peripheral line integral. If we let f represent the function to be integrated over a surface then:

$$I = \int f \cdot \hat{n} dS = \int \nabla_x \vec{H} \cdot \hat{n} dS = \oint \vec{H} \cdot d\vec{l} \quad (A-7)$$

where the function f must be represented by the curl of the vector \vec{H} (vector potential). Stoke's theorem transforms the surface area integration to a closed perimeter line integral.

This technique has been discussed by Baker and Copson [A2] in terms of diffraction of light by apertures in terms of the Maggi transformation, and by Gordon [A3] who applied the technique to Physical Optics scattering by replacing a surface integration with the equivalent peripheral line integral.

The resulting line integral can then be integrated analytically, as done by Gordon [A3] for PO scattering by triangles or numerically, e.g., by Gaussian quadrature.

The key to applying this technique is to find the vector function \vec{H} for a given integrand f . This is not trivial. We would need a vector \vec{H} corresponding to $f = e^{jr}/r$. An alternative approach is to remove the $1/r$ singularity and develop a vector \vec{H} corresponding to $f = 1/r$.

Singularity Removal and 1/R Formulas: The main difficulty in the centroid approximation is the dominance of the $1/R$ singularity of the Green's function. Several authors have subtracted out this singularity and split the Green's function integration into two terms, one with only the $1/R$ singular part and the other with the singularity removed. The benefit of this approach is that the term with the singularity removed is a very well behaved function with a defined limiting value when R goes to zero. This well behaved function can be numerically integrated while the singular part is dealt with separately. The following approach follows that by Rao [A4] who developed an analytical formula for triangles for the $1/R$ singular integration.

The starting point is to subtract and add $1/R$ to the Green's function resulting in

$$\frac{e^{-jkR}}{R} = \frac{e^{-jkR} - 1}{R} + \frac{1}{R} \quad (\text{A-8})$$

We will loosely call the first non singular term the phase. We note that this term has the finite value of $-jk$ when $R = 0$ as can readily be determined from its series expansion. Thus the phase term is well behaved at $R = 0$ and can readily be integrated using any desired numerical scheme.

The goal now is to integrate the singular $1/R$ term. Following [A4], a unique cylindrical

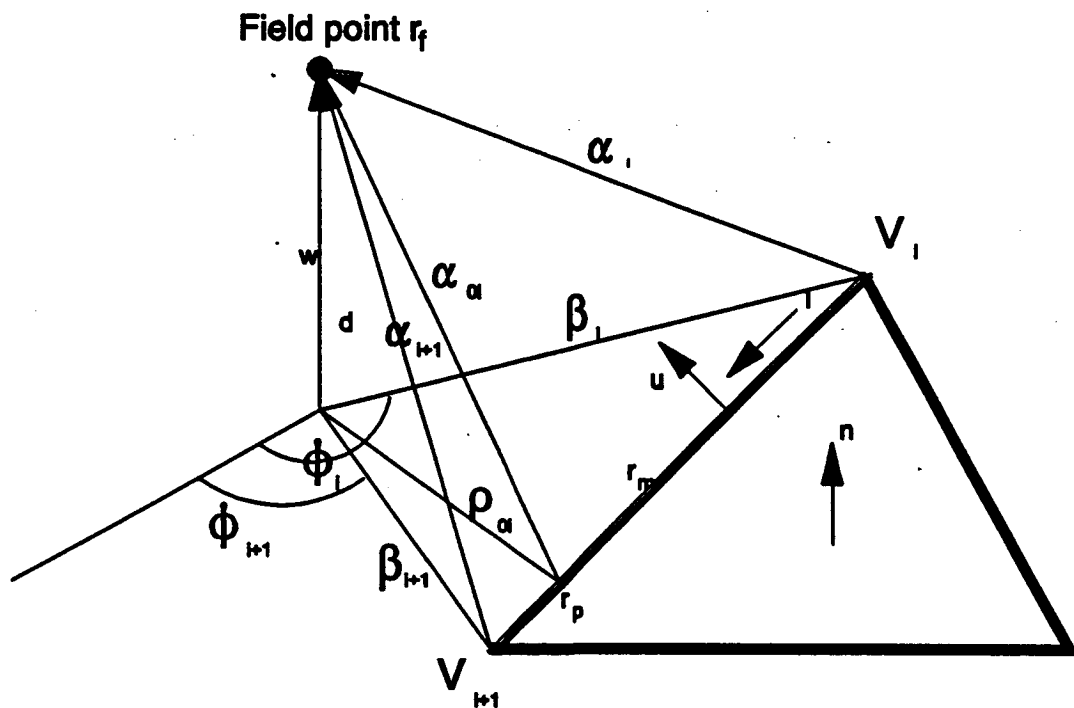


Figure A-4 Coordinate system for $1/R$ triangle integration

coordinate system (ρ, ϕ, w) is introduced, Figure A-4, where the polar axis w is through the field point r_f and is parallel to n , the unit normal to the plane of the triangle. The $w = 0$

plane is coincident with the plane of the triangle. The field point \mathbf{r}_f is at $w = \pm d$ (d assumed positive) along the w axis. The singular integral is written, using $w \cdot \mathbf{n} = 1$, as

$$\begin{aligned}
 I &= \int \frac{1}{|\vec{r}_f - \vec{r}|} dS \\
 &= \int \frac{\vec{w} \cdot \hat{n}}{|\vec{r}_f - \vec{r}|} dS \\
 &= \int \frac{\vec{w} \cdot \hat{n}}{\sqrt{d^2 + \rho^2}} dS
 \end{aligned} \tag{A-9}$$

where ρ is the radial distance to \mathbf{r}' in the triangle. This area integral is then converted to line integral using Stoke's theorem,

$$\int \nabla \times \vec{\Pi} \cdot \hat{n} dS = \oint \vec{\Pi} \cdot d\vec{l} \tag{A-10}$$

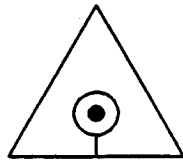
where the line integral is completely around the triangle. The vector $\vec{\Pi}$ is chosen to have only a ϕ component (in the plane of the triangle), thus

$$\nabla \times \vec{\Pi} \cdot \hat{n} = \frac{1}{\rho} \frac{\partial(\rho \Pi_\phi)}{\partial \rho} = \frac{1}{\sqrt{d^2 + \rho^2}} \tag{A-11}$$

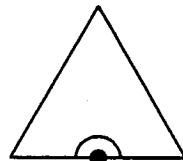
Integrating, [A4] obtains

$$\vec{\Pi} = \Pi_\phi \hat{\phi} = \frac{\sqrt{\rho^2 + d^2}}{\rho} \hat{\phi} \quad (\text{A-12})$$

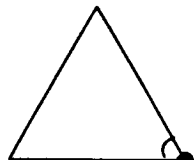
where $\hat{\phi}$ is the unit vector in the ϕ direction (right hand rule applies). This function is singular when $\rho = 0$ is included in the integration, which happens whenever the field point r_f is on or inside the parallel projection of the triangle parallel to n or w .



Singularity when Field Point is inside projection of triangle



Singularity when Field Point is on edge projection of triangle



Singularity when Field Point is on vertex projection of triangle

Figure A-5 Singularity removal depends on projection of field point r_f

The singularity is excluded by not including it in the integration, Figure A-5,

$$I = I_c - I_c' \quad (\text{A-13})$$

where

$$I_c = \int \frac{\sqrt{\rho^2 + d^2}}{\rho} \hat{\phi} \cdot d\vec{l} \quad (A-14)$$

The singularity integration, where $\rho = \epsilon \Rightarrow 0$, is

$$I_c = \lim \int \sqrt{\epsilon^2 + d^2} d\phi = \gamma d \quad (A-15)$$

where γ is the amount of polar angle required to integrate around the singularity.

If the field point r_f lies outside the projection of the triangle, no singularity exists and $\gamma = 0$. If r_f lies interior to the projection of the triangle, $\gamma = 2\pi$; if r_f lies on one line of the triangle, $\gamma = \pi$; and if r_f lies on two lines of the projected triangle (i.e., a vertex), then $\gamma =$ the included angle of the two lines forming the vertex, Figure A-5.

We are now left with performing the integration of

$$\begin{aligned} I_c &= \int \frac{\sqrt{\rho^2 + d^2}}{\rho} \hat{\phi} \cdot d\vec{l} \\ &= \int \sqrt{\rho^2 + d^2} d\phi \end{aligned} \quad (A-16)$$

where we note that $\hat{\phi} \cdot d\vec{l} = \rho d\phi$. This line integral could be integrated numerically, e.g., Gaussian quadrature. However, Rao [A4] has analytically performed the integration for the case of a triangle. The integration is along each side of the triangle from ϕ_i to ϕ_{i+1} , which are the polar angles corresponding to the end points (triangle vertices) of each line segment. The interested reader is directed to [A4] for the details.

Before presenting the result, we define the relevant parameters according to Figure A-4, which differs slightly from that used in [A4]. Let α_i be the out of plane vector from each vertex to the field point r_f . Let β_i be the in (triangle) plane distance from each vertex to the w axis ($\rho=0$). Let ρ_0 be the in plane perpendicular distance of closest approach from the w axis to the line segment i to $i+1$. Let r_{oi} be the location on each line segment where ρ_0 intercepts the line segment i to $i+1$ (Note that this point can be outside the triangle on the line extension). Let ℓ_i , u_i be the unit vector along and in plane perpendicular to the i th edge. Referring to Figure A-4, the following definitions should be evident:

$$\begin{aligned}
 d &= |\hat{n} \cdot \vec{\alpha}_i| \quad \text{where } i = 1, 2, \text{ or } 3 \\
 r_{pd} &= -\vec{l}_i \cdot \vec{\alpha}_{i+1} \\
 r_{mi} &= -\vec{l}_i \cdot \vec{\alpha}_i \\
 \rho_{oi} &= -\hat{u}_i \cdot \vec{\alpha}_i \\
 \alpha_{oi} &= \sqrt{\rho_{oi}^2 + d^2} \\
 \beta_{oi} &= \sqrt{\alpha_i^2 - d^2}
 \end{aligned} \tag{A-17}$$

The final analytical formula for the singular function $1/R$ over a triangle is:

$$\begin{aligned}
 \Psi_1(\vec{r}_f) &= \frac{1}{A_1} \int \frac{1}{|\vec{r}_f - \vec{r}_1|} dS_1 = \frac{1}{A_1} \oint \vec{n} \cdot d\vec{l} \\
 &= \frac{1}{A_1} \sum_{i=1}^3 \frac{\rho_\alpha}{2} \ln \left[\frac{(\alpha_{i+1} + r_{pi})(\alpha_i - r_{mi})}{(\alpha_{i+1} - r_{pi})(\alpha_i + r_{mi})} \right] \\
 &\quad + \frac{d}{A_1} \left\{ \sum_{i=1}^3 \left[\arcsin \left(\frac{dr_{pi}}{\alpha_\alpha \beta_{i+1}} \right) - \arcsin \left(\frac{dr_{mi}}{\alpha_\alpha \beta_i} \right) \right] - \gamma \right\}
 \end{aligned} \tag{A-18}$$

where the singularity removal is

$$\gamma = 0, 2\pi, \pi, \text{ or } \alpha \tag{A-19}$$

This analytical result enables us to compute the singular portion of the integral.

When the field point \vec{r}_f is far from the source triangle, this formula should not be used since it contains the difference of large quantities. However, at large distances, we will simply use the centroid approach.

Combined Numerical and Analytical Result: MOM3D has used these results by using the 1 and 3 point numerical integration formulas with the singular $1/R$ analytical formula to compute G^0_i . Higher order numerical integration could have been implemented at the expense of additional matrix fill time. It was decided to start simple and implement better formulas only if required.

The single point formula uses the triangle centroid as the numerical integration function evaluation point, as specified by [A1], for the non singular "phase" term and the 1/R analytical formula:

$$G_y^{0,1pt} = \frac{e^{-jk\vec{r}_y^c} - 1}{|\vec{r}_y^c|} + \frac{\Psi_j(\vec{r}_i^c) + \Psi_i(\vec{r}_j^c)}{2} \quad (A-20)$$

where $\vec{r}_{ij}^c = \vec{r}_i^c - \vec{r}_j^c$.

The three point formula uses the 3 interior points specified by [A1] for integration. The "phase" term is a double numerical integration while the singular term is a single numerical integration that is averaged to enforce symmetry:

$$\begin{aligned} G_y^{0,3pt} &= \frac{1}{3} \sum_{p=1}^3 \frac{1}{3} \sum_{q=1}^3 \frac{e^{(-jk\vec{r}_p^q - \vec{r}_q^p))} - 1}{|\vec{r}_p^q - \vec{r}_q^p|} \\ &+ \frac{1}{2} \left[\frac{1}{3} \sum_{q=1}^3 \Psi_i(\vec{r}_q) + \frac{1}{3} \sum_{p=1}^3 \Psi_j(\vec{r}_p) \right] \end{aligned} \quad (A-21)$$

APPENDIX A REFERENCES

- 1 P. C. Hammer, O. P. Marlow, and A. H. Stroud, "Numerical Integration Over Simplexes and Cones , Math Tables Aids Comp., 10, pp. 130-137, 1956.**
- 2 B. B. Baker and E. T. Copson, The Mathematical Theory of Huygens' Principle, Chelsea Publishing Co., New York, Third edition, 1987.**
- 3 W. B. Gordon, "Far-Field Approximation to the Kirchhoff-Helmholtz Representation of Scattered Fields", IEEE Trans. Antennas Propagat., July 1975, pp. 590-592.**
- 4 S. M. Rao, "Electromagnetic Scattering and Radiation of Arbitrarily-Shaped Surface by Triangular Patch Modeling , Dissertation, University of Mississippi, August, 1980.**

REPORT DOCUMENTATION PAGE			Form Approved OMB No. 0704-0188
<p>Public reporting burden for this collection of information is estimated to average 1 hour per response, including the time for reviewing instructions, searching existing data sources, gathering and maintaining the data needed, and completing and reviewing the collection of information. Send comments regarding this burden estimate or any other aspect of this collection of information, including suggestions for reducing this burden, to Washington Headquarters Services, Directorate for Information Operations and Reports, 1215 Jefferson Davis Highway, Suite 1204, Arlington, VA 22202-4302, and to the Office of Management and Budget, Paperwork Reduction Project (0704-0188), Washington, DC 20503.</p>			
1. AGENCY USE ONLY (Leave blank)	2. REPORT DATE	3. REPORT TYPE AND DATES COVERED	
	March 1992	Contractor Report - Final	
4. TITLE AND SUBTITLE		5. FUNDING NUMBERS	
MOM3D Method of Moments Code Theory Manual		C NAS1-18603	TA 18
6. AUTHOR(S)		WU 505-69-30-01	
John F. Shaeffer			
7. PERFORMING ORGANIZATION NAME(S) AND ADDRESS(ES)		8. PERFORMING ORGANIZATION REPORT NUMBER	
Lockheed Advanced Development Company P. O. Box 250 Sunland, CA 91041-7287			
9. SPONSORING/MONITORING AGENCY NAME(S) AND ADDRESS(ES)		10. SPONSORING/MONITORING AGENCY REPORT NUMBER	
National Aeronautics and Space Administration Langley Research Center Hampton, VA 23665-5225		NASA CR-189594	
11. SUPPLEMENTARY NOTES			
John F. Shaeffer: DENMAR, Inc., 3278 Hunterdon Way, Marietta, GA 30067 This report was prepared by DENMAR, Inc., for Lockheed Advanced Development Company Langley Technical Monitor: Noel A. Talcott, Jr.			
12a. DISTRIBUTION/AVAILABILITY STATEMENT		12b. DISTRIBUTION CODE	
FEDD Subject Category 32			
13. ABSTRACT (Maximum 200 words)			
<p>MOM3D is a FORTRAN algorithm that solves Maxwell's equations as expressed via the electric field integral equation for the electromagnetic response of open or closed three dimensional surfaces modeled with triangle patches. Two joined triangles (couples) form the vector current unknowns for the surface. Boundary conditions are for perfectly conducting or resistive surfaces. The impedance matrix represents the fundamental electromagnetic interaction of the body with itself. A variety of electromagnetic analysis options are possible once the impedance matrix is computed:</p> <ol style="list-style-type: none"> 1) Backscatter radar cross section (RCS); 2) Bistatic radar cross section; 3) Antenna pattern prediction for user specified body voltage excitation ports; 4) RCS image prediction showing RCS scattering center locations (mechanisms). <p>Either down range or 2D range / cross range images may be specified; 5) Surface currents excited on the body as induced by specified plane wave excitation;</p> <ol style="list-style-type: none"> 6) Near field computation for the electric field on or near the body 			
14. SUBJECT TERMS			15. NUMBER OF PAGES
Method of Moments; Electromagnetics; Radar Cross Section; Antennas; Integral Equations			132
			16. PRICE CODE
17. SECURITY CLASSIFICATION OF REPORT	18. SECURITY CLASSIFICATION OF THIS PAGE	19. SECURITY CLASSIFICATION OF ABSTRACT	20. LIMITATION OF ABSTRACT
Unclassified	Unclassified	Unclassified	